Synthesis and Characterization of Polysaccharide Based Hydrogels for removal of Mercury Ion from Aqueous Solution

Samaneh Saber Samandari

Submitted to the
Institute of Graduate Studies and Research
in partial fulfillment of the requirements for the Degree of

Doctor of Philosophy
in
Chemistry

Eastern Mediterranean University
February 2015
Gazimağusa, North Cyprus

Approval of the Institute of Graduate Studies and Research

Prof. Dr. Serhan Ciftcioglu
Director

I certify that this thesis satisfies the requirements as a thesis for the degree of Doctor of Philosophy in Chemistry.

Prof. Dr. Mustafa Halilsoy
Chair, Department of Chemistry

I certify that I have read this thesis and that in our opinion it is fully adequate in scope and quality as a thesis for the degree of Doctor of Philosophy in Chemistry.

Assoc. Prof. Dr. Mustafa Gazi
Supervisor

Examining Committee

1. Prof. Dr. Niyazi Bicak
2. Prof. Dr. Hayal Bulbul Sonmez
3. Prof. Dr. Osman Yilmaz
4. Assoc. Prof. Dr. Mustafa Gazi
5. Assoc. Prof. Dr. Rana Kidak

ABSTRACT

Production of major industrial products may degrade the environment. It can result in water pollution since it produces pollutants such as water-coloring agents and toxic heavy metals that are extremely harmful and impair the environment even at low concentrations. To reduce the risk of environmental pollution from these wastes, it is necessary to treat them prior to discharging into the environment. The adsorption process onto solid substrate and natural polymeric materials especially polysaccharides is considered superior to other removal techniques.

Mercury deserves special attention among heavy metals such as cadmium, cobalt, chromium, copper, lead, nickel, and zinc, which are highly toxic and dangerous. Mercury spillage is highly dangerous because it destroys brain tissue, lungs, and has the ability to distort protein leading to toxic effects; it mainly affects the kidney and nerve system and may cause some disorders and diseases. Therefore, the removal of mercury from aqueous solutions, especially drinking water, is very important in hydrometallurgical and wastewater treatment. The main aim of this thesis is to investigate the mercury ion removal ability of different natural polymers, cellulose, chitosan, and pullulan.

For this purpose, acrylamide monomer has been grafted to chitosan, cellulose, and pullulan and three different hydrogels were synthesized. In addition, the cellulose-graft-polyacrylamide/nano-hydroxyapatite composite hydrogel and pullulan-graft-polyacrylamide porous hydrogels were prepared and characterized using FTIR and SEM. Then, the effects of several variables such as time, temperature, and pH on the

swelling behavior of the hydrogels were examined. The results showed that the cellulose-graft-polyacrylamide hydrogel with 5170 % has the maximum and pullulan-graft-polyacrylamide hydrogel with 1554 % has the minimum swelling amount. In addition, the swelling amount of all hydrogels significantly changed with temperature and pH and the kinetics of swelling of hydrogels were best fitted with the second-order model.

Finally, the adsorption studies of the mercury (II) ions on synthesized hydrogels were performed to investigate their uptake performances. The results showed that the maximum mercury ion adsorption by cellulose-graft-polyacrylamide hydrogel (1.93 $g.g^{-1}$), cellulose-graft-polyacrylamide/hydroxyapatite composite hydrogel (1.99 $g.g^{-1}$), chitosan-graft-polyacrylamide hydrogel (1.87 $g.g^{-1}$), pullulan-graft-polyacrylamide hydrogel (1.75 $g.g^{-1}$), and pullulan-graft-polyacrylamide porous hydrogel (1.78 $g.g^{-1}$) were attained after 24 h. In addition, batch adsorption experiments in different conditions such as temperature, pH, mercury solution concentration, with different amount of adsorbent were performed. According to the results, all synthesized hydrogels are temperature, pH and concentration sensitive. In addition, the kinetic, isotherm, and the thermodynamic parameters of adsorption were calculated. The results indicated that adsorption of mercury ions on all hydrogels followed pseudo-second-order kinetics and best fitted with Langmuir adsorption isotherm with the highest maximum adsorption (q_{max}) of Hg(II) ions for composite hydrogel and the lowest for pullulan based hydrogels. The negative value of free energy change (ΔG^o) and positive value of enthalpy change (ΔH^o) shows the adsorption process is spontaneous and endothermic. Finally, the regeneration ability of hydrogels through desorption of mercury ions for three adsorption/desorption

cycles were examined. It can be concluded that the synthesized hydrogels qualified for practical application since they can be used repeatedly with negligible loss of adsorption capacity for the mercury ions.

Keyword: Cellulose, chitosan, pullulan, hydroxyapatite, hydrogel, porous hydrogel, composite hydrogels, water treatment, mercury

ÖZ

Büyük sanayi ürünlerinin üretimi çevreyi olumsuz etkileyebilmektedir. Su renklendirici maddelerle son derece zararlı ve düşük konsantrasyonlarda bile çevreyi bozan zehirli ağır metaller gibi kirletici ürünler su kirliliğinin nedenidir. Bu atıklardan oluşan çevre kirliliği riskini azaltmak için,çevreye salınımları öncesi onları gidermek gerekir.Katı yüzey ve doğal polimerik malzemeler, özellikle polisakkaritler üzerine adsorpsiyon işlemi diğer giderim tekniklerine göre üstün kabul edilir.

Civanın son derece zehirli ve tehlikeli olan kadmiyum, kobalt, krom, bakır, kurşun, nikel, ve çinko gibi ağır metaller arasında dikkate değer bir yeri vardır. Civa beyin dokusu, akciğerleri tahrip ve protein bozucu toksik etkiye sahiptir, Ana etkisi ile ağırlıklı olarak böbrek ve sinir sistemini etkileyerek bazı bozukluklar ve hastalıklara neden olabilir. Bu nedenle, sulu çözeltilerden civa, özellikle içme suyu için, hidrometalurjik ve atık sulardan arıtımı son derece önemlidir. Bu tezin temel amacı, selüloz, kitosan ve pullulan gibi farklı doğal polimerlerin civa iyonu giderme yeteneği araştırmaktır.

Bu amaçla, akrilamid monomerin kitosan, selüloz ve pullulana aşılanarak ve üç farklı hidrojeller sentezlenmiştir. Buna ek olarak selüloz-aşı-poliakrilamid/nano-hidroksiapatat kmposit hidrojeli ve pullulan-aşı-poliakrilamid poroz hidrojelleri hazırlanarak FTIR v SEM kullanarak karakterize edilmişlerdir. Daha sonra, bu hidrojeller şişme davranışına karşın zaman, sıcaklık ve pH gibi çeşitli değişkenlerin etkileri incelenmiştir. Sonuçlar selüloz-greft-poliakrilamid hidrojelinin % 5170 şişme değeri ile maksimum, pululan-greft-poliakrilamid hidrojelinin ise %1554

değerle minimum şişme yüzdesi değerine sahip olduğunu göstermiştir. Buna ek olarak, tüm hidrojellerin şişme miktarı ısı ve pH ile önemli ölçüde değişimiş ve hidrojellerin şişme kinetiği ikinci dereceden modeline uygunluk göstermiştir.

Son olarak, sentezlenen jellerin cıva (II) iyonlarının adsorpsiyon çalışmaları onların tutma performanslarını araştırmak için yapılmıştır. Araştırma sonucunda, 24 saatlik etkileşim süresi sonucundaki maksimum civa tutma kapasiteleri selüloz-aşı-poliakrilamid hidrojeli (1.93g.g^{-1}), selüloz-aşı-poliakrilamid /hidroksiapatat kompozit hidrojeli (1.99 g.g^{-1}), kitosan-aşı-poliakrilamid hidrojeli (1.87 g.g^{-1}), pululan-aşı-poliakrilamid hidrojeli (1.75 g.g^{-1}), ve pululan-aşı-poliakrilamid poroz hidrojeli (1.78 g.g^{-1}) olarak belirlenmiştir. Buna ek olarak, batch adsorpsiyon deneyleri adsorbentin farklı bir miktarı ile, sıcaklık, pH, civa çözelti konsantrasyonlarının etkileşimleriyle gerçekleştirilmiştir.

The negative value of free energy change (ΔG^o) and positive value of enthalpy change (ΔH^o) shows the adsorption process is spontaneous and endothermic.

Elde edilen sonuçlara göre, tüm hidrojel sıcaklık, pH ve konsantrasyona duyarlıdır. Buna ek olarak,adsorpsiyonun, kinetik, izoterm ve termodinamiği hesaplandı. Sonuçlar tüm hidrojellerin üzerinde civa iyonların tutunmalarının yalancı-ikinci-dereceden kinetiği takip ettiğini ve Langmuir adsorpsiyon izotermiyle civa adsorpsiyonun (q_{max}) en yüksek değerinin kompozit hidrojeli ile en düşük değerinin pululan bazlı hidrojelle olduğu belirlenmiştir. Serbest enerji değişimi (ΔG^o) negatif ve entalpi değişimi (ΔH^o) pozitif değeri adsorpsiyon işleminin kendiliğinden ve endotermik olduğunu göstermektedir.

Son olarak, üç kez adsorpsiyon / desorpsiyon döngüsü ile civa iyonları desorpsiyon yoluyla hidrojellerin yenilenmesi yeteneği incelenmiştir. Bu da, civa iyonları için adsorpsiyon kapasitesinin göz ardı edilebilir kayıp değerinde olması nedeniyle tekrar tekrar kullanılabilmesi özelliğini ortaya çıkarmakta ve hidrojelin pratik uygulama için nitelikli olduğu sonucuna varılabilmektedir.

Anahtar Kelimeler: Selüloz, kitosan, pullulan, hidroksiapatat, hidrojel, poroz hidrojel, kompozit hidrojel, su iyleştirme, civa.

ACKNOWLEDGMENT

I would like to thank Assoc. Prof. Dr. Mustafa Gazi for his guidance and continual assistance through the course of preparation of this thesis. His support made the success of the work possible. Thanks are also due to Prof. Dr. Elvan Yilmaz and Prof. Dr. Osman Yilmaz who have provided direction for the project.

My education would not have been possible without the support of my mother Fatemeh Honaripanah, my father Mohammad Hossein Saber Samandari, my brother, and my sister. Their caring and love has allowed me to reach my aim in my education.

To My Lovely Parents

TABLE OF CONTENTS

LIST OF TABLES

LIST OF FIGURES

LIST OF SCHEMES

Chapter 1

INTRODUCTION

1.1 Water Pollution

Water pollution can be defined as contamination of water caused by human that decreases its efficacy for humans and other organisms in the world. Environmental pollution became more important due to the increase in development of industrial applications and the world population. Most of the water pollution comes from industrial production activities (e.g., dye, cosmetic, leather, paper, plastics, food, textile, planting, and mining), which include contaminants such as water-coloring agents and toxic heavy metals [1]. They are extremely harmful to people and degrade the environment even at low concentrations [2]. Industrial wastewaters, which contain organic and/or inorganic pollutants may be released into natural waterways and consequently into water supplies. In recent years, the presence of heavy metals such as Cu (Copper), Cd (Cadmium), Ni (Nickel), Pb (Lead), Zn (Zinc), Ag (Silver), Cr (III) (Chromium), Hg (Mercury), Fe (Iron), Co (Cobalt), As (Arsenic) and other pollutants, have reached the risky levels in nature for many countries in the world. In addition to the industrial and domestic wastes, the other important source of heavy metals can be acid rain, which breaks down soils and finds its way into groundwater, rivers, streams, and lakes.

Therefore, the considerable amount of heavy metals contained in industrial wastewaters which would endanger public health and the environment should be

discharged with adequate treatment, as their degradation products are toxic and carcinogenic, or they cannot be degraded or destroyed in the worst case [3]. Although, the trace amount of some heavy metals, which can enter to our bodies via drinking water, food, and air are essential for human body to maintain the metabolism, at higher levels can cause serious poisoning.

1.2 Health Risks of Heavy Metals

The persistence of heavy metals in the environment with documented potential for serious health and adverse health effects in human metabolism becomes obvious concerns. The heavy metal intoxications may harm central systems of human body such as nervous, gastrointestinal, and cardiovascular system. In addition, it can damage tissues like liver, lungs, bones, endocrine glands, and kidneys. Moreover, acute heavy metal exposures participate in several degenerative diseases and enhance the risk of some cancer disease. Among the wide range of heavy metals, only mercury has been chosen in this thesis.

Mercury deserves special attention among heavy metals such as cadmium, cobalt, chromium, copper, lead, nickel, and zinc, which are highly toxic and dangerous. Mercury spillage is highly dangerous because it destroys brain tissue, lungs, and has the ability to distort protein leading to toxic effects; it mainly affects the kidney and nervous system and may cause some disorders and diseases [4, 5]. In addition, mercury is a mutagen, teratogen, and carcinogen, causing embryocidal, cytochemical, and histopathological events [6]. Therefore, the removal of mercury from aqueous solutions, especially drinking water, is very important in hydrometallurgy and wastewater treatment.

1.3 Common Methods for Removal Heavy Metals from Water

A number of techniques have been developed in recent years both to improve the quality of the treated effluent and to decrease the amount of wastewater produced. These techniques with their inherent advantages and limitations in application are precipitation, reverse osmosis, coagulation–flocculation, electrodialysis, ultrafiltration, ion exchange, flotation, and adsorption as summarized in the following sections.

1.3.1 Chemical Precipitation

Chemical precipitation is employed for most of the metals. Chemical precipitation is based on the removal of dissolved and suspended solids which their physical state changed by addition of chemicals through sedimentation. Metals are precipitated by assistance of common precipitants including hydroxide and sulfides of metals through the addition of chemicals which are able to affect their solubility by changing the pH of solution. Despite, chemical precipitation has excessive sludge production that requires further costly treatment and also requires a large amount of chemicals to reduce metals [7]. The chemical precipitation is the slow procedure with long-term environmental impacts of sludge disposal [8].

1.3.2 Reverse Osmosis

Reverse osmosis is based on the theory of osmotic pressure. The pressure differences of two solutions with different solute concentrations across the semipermeable membrane will be balanced by diffusing of water through the semipermeable membrane from the higher concentration side to the lower concentration, if a pressure gradient greater than the osmotic pressure and opposite in direction imposed across the membrane [9]. It is worth to mention that the reverse osmosis is usually applied for the removal of dissolved chemicals or metals from wastewater remaining

after advanced treatment. The solute characteristics, concentration and temperature of a finite volume solution can affect the performance of reverse osmosis. Therefore, prior to the reverse osmosis some pretreatment is needed like pH adjustment, anti-precipitant additions, media filtration, and equalization. Although, reverse osmosis is very effective but it is a costly method as the membranes get easily damaged requiring replacement.

1.3.3 Coagulation–Flocculation

The coagulation–flocculation method consists of coagulation and flocculation procedures. First, a coagulant (usually, ferric/alum salts) will be added to overcome the repulsive forces between particles and destabilize and increase the particle size of colloidal particles which leads to sedimentation and then the unstable particles will convert to the bulky floccules by flocculation procedure [10]. The pH adjustment requirement and high operational cost due to chemical consumption limited the usage of this method for water treatment.

1.3.4 Electrodialysis

In the electrodialysis, semipermeable ion-selective membrane has the main role while the ionic components of a solution will be separated through this membrane. The drawback of this method stems from the chemical precipitation of salts with low solubility on the membrane surface.

1.3.5 Ultrafiltration

Ultrafiltration is a type of membrane filtration technologies. In this method, water and low molecular weight solutes can pass through the membrane by applying forces like pressure or concentration gradients, while retentate (suspended solids and solutes of high molecular weight) will be retained. Although, it has some advantages like the

use of small amount of treatment chemicals, smaller space, and labor requirements, it needs more electricity, pretreatment, and replacement of membranes.

1.3.6 Ion Exchange

Ion exchange, a costly process, is based on the replacing the ions of a given species by an insoluble exchange material, which commonly are zeolites, weak and strong anion and cation resins and chelating resins. pH of the solution has a significant influence on the interaction between exchanging ions and the resin.

1.3.7 Flotation

Flotation technique, a physical separation process, is based on bubble attachment to separate solids from a liquid phase. The attached particles-bubble rise up and will be separated from the bulk water or suspension of heavy metal in a foaming phase. Flotation can be classified as: (1) dissolved-air flotation, (2) dispersed-air flotation, (3) electro-flotation, (4) biological flotation, and (5) vacuum air flotation [11]. Flotation especially dispersed-air flotation with some advantages such as low cost, better removal of small particles, and shorter hydraulic retention times, is one of the most useful method for the removal of heavy metals from wastewater.

1.3.8 Adsorption

The process of adsorption that is based on the transfer of substance from the liquid phase to the surface of a solid through physical and/or chemical interactions is the preferred method for the removal of toxic contaminants from water. Adsorption technique is cost effective, efficient, energy economical, simple, and does not generate toxic sludge or other waste by-products [1, 12]. The adsorption process onto solid substrate such as industrial by-products, agricultural wastes, biomass and natural polymeric materials especially polysaccharides is considered superior to other

removal techniques [13]. In this thesis, natural polymers were applied as an adsorbent of heavy metal for water treatment.

1.4 Scope of the Thesis

The aim of this thesis was the preparation and characterization of grafted biopolymers by using chitosan, cellulose, and pullulan as adsorbent materials for water treatment. As a monomer, acrylamide has been chosen for grafting to the mentioned polysaccharides. Then, the ability of the synthesized grafted polymers for adsorption of mercury (Hg (II)) ion was examined. For better understanding adsorption mechanisms, the porous pullulan grafted hydrogel and cellulose composite polymer using hydroxyapatite were prepared. The effects of time, adsorbent amount, adsorbate concentration, pH, and temperature on adsorption efficiency for all kinds of synthesized hydrogels were studied. In Chapter 2, all natural polymers and applied materials were introduced extensively.

1.5 Literature Review

Up to now, the ability of natural polymers to remove mercury (II) ions from wastewater has been demonstrated in many articles. The mercury (II) ions sorption properties and capacity by using adsorption technique in these articles has been investigated. Examples include cellulose, chitin, chitosan, pullulan, etc. However, the adsorption capacity of pure natural polymers for heavy metals including mercury ions was not considerable (Table 1).

Therefore, chemical modification and specially graft polymerization of natural polymers by different monomers with the aim of improving its properties and following its applications has attracted interest among scientists. Among the diffrent existing monomers, hydrophilic non-ionic monomers such as acrylic acid,

acrylamide, acrylic acid-co-acrylamide, acrylic acid/acrylamide/2-acrylamido-2-methyl-1-propanesulfonicacid, hydroxylethyl methacrylate, methacrylic acid, and vinyl alcohol are widly apllied for grafting onto natural polymers. The product of the mentioned graft polymerization normally is superabsorbent hydrogels, which they have amazing ability of swelling in aqueous solution with variaty of applications including water treatment. In many studies, the authors reported the successful removal of heavy metals and dyes using superabsorbent hydrogels. A large proportion of these literatures contained results of batch experiments for the following parameters; contact times, pH, metal solution concentrations, adsorbent amounts and temperature. Most of these superabsorbent hydrogels based on cellulose, chitosan, and pullulan, which are candidate natural polymers in this thesis are listed in Table 1 and their maximum adsorption capacity for mercury (II) ions were compared.

However, we couldn't find any literature which compare the adsorption efficiency of at least three natural polymers. Therefore, we decided to synthesis and characterize hydrogels based on three diffrent natural polymers grafted with polyacrylamide. Then, their Hg(II) adsorption capacity was investigated in diffrent conditions.

It is worth mentioning that many parameters were taken into consideration in the thesis for the synthesis of hydrogels with very similar physical and chemical properties to find the exact influence of natural polymers on adsorption but it cannot be said with total certainty that the conclusion of this thesis is very general for all kind of hydrogels based on these candidate natural polymers.

Table 1. Comparison of mercury sorption capacities on several synthesized materials

Materials	**Maximum adsorption capacity ($mmol.g^{-1}$)**	**References**
Chitosan and its derivatives		
Commercial CTS	5.62	[14]
Commercial CTS	2.59	[15]
CTS bead	0.90	[16]
Aminated CTS bead	2.24	[17]
Magnetic CTS	0.75	[18]
CTS/GLA	3.30	[19]
CTS/ECH	3.50	[19]
CTS/GLA	1.05×10^{-4}	[20]
CTS/ barbital-GLA	3.11×10^{-4}	[20]
GLA-CCTS	4.42	[21]
Aminated GLA- CCTS	2.30	[22]
GLA-CCTS immobilized in PVA	9.44	[23]
CTS/CNTs bead	0.91	[24]
CTS-*graft*-PVA	2.92	[25]
CTS-*graft*-PAAm	1.60	[16]
CTS-*graft*-PAA	3.91	[26]
CTS-*graft*-Poly(ethyleneimine)	2.2	[27]
CTS NH_2-*graft*-azacrown ether	0.71	[28]
EDGE-CCTS-*graft*-PAAm	1.60	[29]
GLA- CCTS-*graft*-thiourea	3.25	[30]
Cellulose and its derivatives		

CE-*graft*-PAAm	3.55	[31]
Porous CE-PEI	1.43	[32]
O-benzenedithiol-modified CE	0.11	[33]
Cross-linked CE beads-ferric oxide	0.09	[34]
Sulfonamide containing CE	1.95	[35]
Polyacrylamide and its derivatives		
P4-VP-*graft*-PAAm	3.36	[36]
N-chlorosulfonamidated PS-*graft*-PAAm	4.35	[37]
Coconut husk-*graft*-PAAm	0.06	[38]
(PS-DVB) based resin-*graft*- PAAm	5.75	[39]

CTS: chitosan; ECL: epichlorohydrin; CCTS: crosslinked chitosan; EDGE: ethylene glycol diglycidyle Ether; PAAm: polyacrylamide; PAA: polyacrylic acid; GLA; glutaraldehyde; P4-VP: polyvinyl pyridine; PS: polystyrene; PEI: polyaminated; PVA: polyvinyl alcohol; CE: cellulose; PEI: polyethyleneimine

Chapter 2

PROPERTIES, CHARACTERIZATION AND APPLICATION AREAS OF APPLIED CHEMICALS

2.1 Cellulose

Cellulose, the most abundant organic polymer on earth, is a polysaccharide which has the formula $(CH_{10}O_5)_n$. Several hundred to many thousands D-glucose units with β(1→4) linkage designed the linear chain of cellulose. The most important constituent in the cell wall structure of green plants, algae and the oomycetes is cellulose. According to the location of hydrogen bonds between and inside of cellulose, a number of different crystalline structures exists like cellulose I, II, III, and IV. Normally cellulose of plants and cellulose produced by bacteria and algae is type I and cellulose II exist in regenerated cellulose fibers. While, cellulose II is metastable and cellulose I is stable, the conversion of cellulose I to cellulose II is irreversible. Cellulose III and cellulose IV can be produced by various chemical treatments.

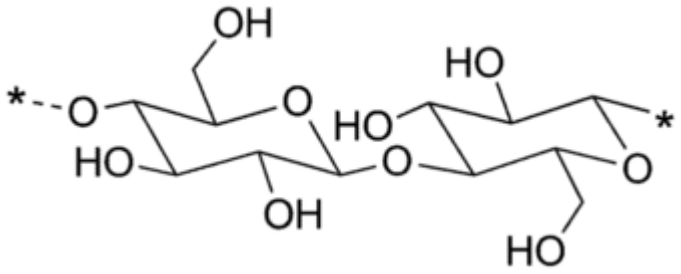

Scheme 1. Chemical Structure of cellulose

2.1.1 Properties of Cellulose

Cellulose is a hydrophilic, odorless, and biodegradable polymer with the contact angle of 20–30 degrees. Cellulose can have several different properties depending on the number of glucose units, degree of polymerization or its chain length. However, cellulose cannot dissolve in water and most organic solvents, it is soluble in Schweizer's reagent, cadmium ethylene diamine, cupriethylene diamine, lithium chloride/dimethyl acetamide, and N-methyl morpholine N-oxide. The linear chain of cellulose can be broken down by treating it with concentrated acids at high temperature and converted to its glucose units. Cellulose consists of crystalline and amorphous regions. The crystalline part can switch to amorphous shape when heated beyond 320 °C and a pressure of 25 MP. If amorphous regions treated with strong acid, it can be broken up, thus nanocrystalline cellulose will be produced. Nanocrystalline cellulose is a novel material with many desirable properties.

2.1.2 Applications of Cellulose

Cellulose is mainly applied in textiles industry in the form of linen, cotton, and other plant fibers. In addition, cellulose is used in production of cellophane, rayon, paperboard and paper. Cellulose in paper of thin layer as a stationary phase is used for chromatography in the laboratory. In addition, in pharmacy it has application as fillers in drug tablets. In food industry, cellulose is used as inactive stabilizers, and thickeners in processed foods. Hydrophilic and absorbent sponges can be made from cellulose. Cellulose is a promising natural biomaterial for biomedical applications including controlled drug release, wound dressing and micro-encapsulation owing to its non-toxic, renewable, biocompatible, biodegradable and readily modified properties. Cellulose is used to make water-soluble adhesives and binders such as methylcellulose and carboxymethyl cellulose, which are used in wallpaper paste.

2.2 Chitosan and Its Properties

Chitosan is a high molecular weight polysaccharide, which consists of mostly β-(1→4)-2-deoxy-2-amino-D-glucopyranose units and partially of β-(1→4)-2-deoxy-2-acetamido-D-glucopyranose (Scheme 1). Chitosan with average molecular weight ranging between 3,800 and 2,000,000 in the form of dry flakes, solution and fine powder, is a brittle material [40]. Despite the abundant availability of chitin (well-known biodegradable polymer), chitosan is naturally available only in small amounts in several kinds of mushrooms [41]. Therefore, chitosan is produced by deacetylation of chitin. Degree of deacetylation changes from 40% to 98% and its molecular weight can be between 5×10^4 Da and 2×10^6 Da [42]. The characteristics such as viscosity, density, particle size, molecular weight, and degree of deacetylation can influence its properties and applications.

Production of chitosan from chitin by removal of the acetyl group involves a harsh treatment with concentrated aqueous NaOH solution with care to protect reaction mixture from oxygen, with a nitrogen purge or by addition of sodium borohydride in order to avoid undesirable reactions such as depolymerization [42].

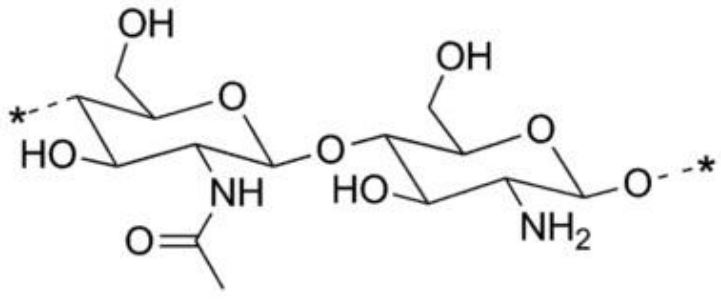

Scheme 2. Chemical structure of chitosan

2.2.1 Properties of Chitosan

Chitosan, being a poly amino saccharide, contains amino and hydroxyl reactive groups, which can react with other reagents under mild conditions. Because of the inter- and intra-molecular hydrogen bonding, chitosan can be dissolved only in dilute organic acids such as lactic acid, acetic acid, formic acid, maleic acid, and succinic acid. After dissolving, it becomes a cationic polymer because of the protonation of amino groups on the C2 position of pyranose rings [43, 44]. Therefore, it exhibits a pH responsive behavior due to the large numbers of amino groups on its backbone. It adsorbed attention of scientist, because it is a biodegradable, antimicrobial, biocompatible, non-allergenic, antibacterial, non-toxic, anticoagulant and immunologic polysaccharide [45, 46]. Recently, chemical modification of chitosan has been investigated to improve its properties and to expand its chemical, physical and biological applications. Graft copolymerization of monomers onto chitosan is an effective and promising method to incorporate desirable properties into chitosan without sacrificing its biodegradable nature [45, 47, 48].

2.2.2 Applications of Chitosan

Chitosan is a basic polymer with amine side groups and is of great interest with its wide application [49]. Chitosan and its derivatives especially hydrogel forms are widely applied in medicine and pharmaceutics, cosmetics, pulp and paper industry, agriculture, food industry, textile industry, and water treatment.

Chitosan is widely used in different methods of water treatment such as desalination, filtration, flocculation/coagulation, removal of color, detecting of trace and recovery of heavy metals from sea water or waste waters by the process of adsorption [40]. This biopolymer is a well-known sorbent and effective in the uptake of anionic or

reactive dyes; however, it has poor sorption capacity for basic dyes [13]. Therefore, to make it more suitable for adsorbing basic dyes, various functional groups, including carboxylate, sulfonate and phosphate groups have been used to modify chitosan [13, 50]. Chitosan is perfect for adsorption of transition metals and dyes since the amino groups on chitosan chains serve as coordination sites [13, 51, 52].

2.3 Pullulan

Pullulan is a polysaccharide polymer consisting of maltotriose units. It is also called α-1,4- ;α-1,6-glucan while consecutive glucose units are connected to each other by an α-1,6 glycosidic bond whereas each three glucose units are connected to each other by an α-1,4 glycosidic bond. Pullulan is abundant in nature, but normally it is produced from starch syrup by fermentation in industry.

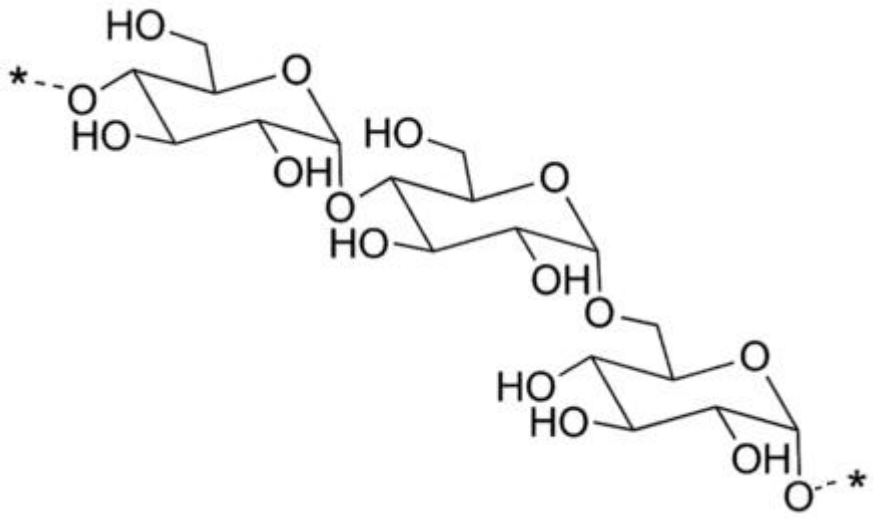

Scheme 3. Chemical structure of pullulan

2.3.1 Properties of Pullulan

Pullulan a white noncrystalline powder, naturally resourced with high water solubility is spinnable, adhesive, moldable, impermeable to oxygen, biodegradable, and non-hygroscopic and non-reducing tasteless polymer which is

edible [53]. The main specialty of pullulan is that it is polysaccharide, which is not ionic, also compatible with blood media, biodegradable, non-toxic, non-immunogenic, non-mutagenic and non-carcinogenic. It is easily soluble in water, since it is linear and not branched. It is a good biocompatible alternative for dextran solution which consist of several α-1, 6 glucose linkage and some α-1, 3 branching. Pullulan results in a viscous media while dissolving in warm or cold water. It has also high adhesion.

Pullulan with good adhesion properties has the ability to forming thermally stable films. Pullulan manifested anti-static and elastic properties. It can be developed into compression moldings. These properties of pullulan are attributed with its structure flexibility [53].

2.3.2 Applications of Pullulan

Pullulan is a promising material for various applications, including cosmetic, coating, food industry, packaging, emulsions, and biotechnological and biomedical uses [1, 54, 55]. These recent years there is increasing demand for it especially in pharmaceutical applications [53, 56]. It is an ideal material for tablet film coating and delivery systems in the form of films due to the excellent film-forming ability. Pullulan film with very low oxygen permeability is printable and heat sealable. However, pullulan is not suitable for water treatment applications due to its solubility in water [1].

2.4 Acrylamide

Acrylamide with the IUPAC name of 2-propenamide has the molecular formula C_3H_5NO (Scheme 4). Acrylamide is prepared in an industrial scale by the hydrolysis of acrylonitrile by nitrile hydratase [57].

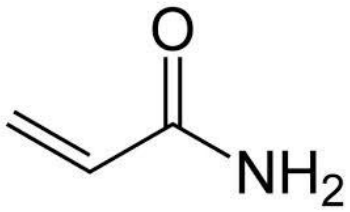

Scheme 4. Chemical structure of acrylamide

2.4.1 Properties of Acrylamide

It is a white odorless solid with flake like crystals, soluble in water, ethanol, ether, and acetone and slightly soluble in chloroform. Acrylamide reacts easily with hydroxyl-, amino-, and sulfhydryl- containing compounds. It is incompatible with acids, bases, oxidizing agents, iron, and iron salts. Due to the thermal decomposition, it can produce carbon monoxide, carbon dioxide, and oxides of nitrogen. It decomposes non-thermally to form ammonia.

2.4.2 Applications of Acrylamide

Acrylamide is produced industrially for use in products such as plastics, chemical grouting materials, soil conditioners, cosmetics, flocculants, fiber modifiers, adhesives, binders for seed coatings and foundry sand, thickening agents for agricultural sprays, printing ink emulsion stabilizers, latex dispersions, and textile printing paste [58]. The most important and primary application of acrylamide is the production of polyacrylamide polymers, which are well-known superabsorbents. This property can be useful to apply in wastewater treatment, gel electrophoresis, paper-making, and manufacture of permanent press fabrics. [59]. Acrylamide monomer with some other monomers such as vinyl acetate, styrene, vinyl chloride, ethylene fork dichloride, and acrylonitrile produced copolymers, which access to a variety of uses of polymer. Meanwhile, polyacrylamide with its hydrophilic nature,

relatively non-toxicity and simplicity for preparation has good potential for application in drug delivery studies [45, 60, 61]

2.5 Hydroxyapatite

Bone and other calcified tissues are natural anisotropic composites consisting of biominerals embedded in a protein matrix, other organic materials, and water [62]. Calcium phosphates (CaPs), which is the major biomineral constituent, constitutes 65-70 % of vertebrate bone and tooth. CaPs have excellent bioactivity and biodegradability and are relatively insoluble at physiological pH of 7.4. However, they have increasingly high solubility in acidic environments, i.e., below pH 6.5 [63]. CaPs can exist in different phases (such as amorphous calcium phosphate, biphasic calcium phosphate, carbonated apatite, calcium deficient hydroxyapatite, Dicalcium phosphate anhydrous, etc.) depending on temperature, impurities, and the presence of water. Among the various types of CaP salts, HAP is the most thermodynamically stable crystalline phase in body fluid and possesses the greatest similarity to the mineral part of bone [64].

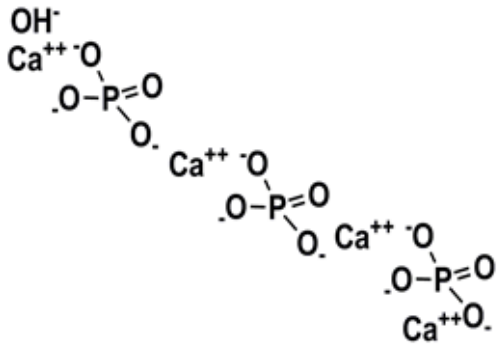

Scheme 5. Chemical structure of hydroxyapatite

LeGeros demonstrated for the first time that biologic apatite (e.g., from coral, bovine bone or marine algae) is not pure HAP but is a carbonate apatite similar to synthetic apatite with the CO_3^{2-} substituting for the PO_4^{3-} groups [65]. Subsequent studies on synthetic HAP and other CaPs that started in the late 1970s were motivated by the

need to develop synthetic biomaterials for bone repair, substitution, and augmentation [66]. Synthetic HAP and substituted apatites (e.g., Sr^{2+}, Mg^{2+}, and Fe^{2+} for Ca^{2+}, F^-, Cl^-, and CO_3^- for OH^-, and CO_3^{2-} for PO_4^{3-}) can be prepared by solid-state reactions, hydrothermal reactions, compacting and sintering, precipitation, hydrolysis reactions, sol–gel, micro emulsion techniques, and biomimetic methods. Commercial HAP is often prepared by compacting and sintering apatite powder prepared by precipitation reactions between calcium nitrate and ammonium phosphate solution [67]. Synthetic HAP can be produced as either dense or macroporous. Dense HAP is described as having a maximum micro-porosity of 5 % by volume and consisting of crystals with a size exceeding 2,000 Å. HAPs with different morphologies such as nano-rods, nano-tubes, plate-like nano-crystals, single crystal, nano-particles, and three-dimensional structures were also prepared. Pure HAP has a Ca/P=1.67 molar ratio and contains mainly of Ca^{2+} (40 wt%) and $PO4^{3-}$ (18.5 wt% as P) [68]. It shows only the O–H (for OH group) and P–O (for PO_4 groups) absorption bands in the FT-IR spectra (Figure 8). The chemical stability of apatites is influenced by the apatite composition and synthesis method, which also affects composition and crystal size. Solubility of apatite can be affected by substitution in its structure [69]. For example, strontium, magnesium, or carbonate substitution of apatite compared with unsubstituted apatites prepared by precipitation or hydrolysis methods, causes an increase in solubility [70]. In addition, the physical properties of the apatite powder, macro-porosity, micro-porosity, compression and sintering conditions, and the differences in the preparation methods affect the mechanical properties of the dense HAP. Increasing amounts of micro-porosity decreases various mechanical properties (e.g., compressive strength).

2.5.1 Application of Hydroxyapatite

Currently, HAP is the material of choice for various bone repair and tissue engineering applications (i.e., bone deformities, bone filling cement, implants for immediate tooth root replacement, orthopedic metallic implants, and ear implants) [71, 72]. It has been well documented that HAP can promote new bone in-growth through osteoconduction mechanisms and accelerates the augmentation of the materials by bone tissue [73, 74]. In addition, HAP is becoming increasingly popular for drug delivery because it overcomes many of the inherent problems associated with systemic administration of drugs or other therapeutic agents including proteins, antibiotics, anticancer drugs (to delay the recurrence of cancer cells), radioisotopes, genes, and even antigens for vaccines [75].

The first reports on the use of hydroxyapatite for the capture of heavy metal ions, such as lead, copper, and cadmium ions by exchange with calcium ions were generated by Suzuki and collaborators in 1981 [76-78]. To date, a synthetic hydroxyapatite has been widely used as an adsorbent for the removal of heavy metals such as Pb^{2}+, Cr^{2+}, Zn^{2+}, Cu^{2+}, Cd^{2+}, Co^{2+}, V^{5+}, Ni^{2+} and Sb^{3+} from contaminated soil and water due to its high specific surface area, low cost, high stability under reducing and oxidizing conditions, low water solubility, and availability [77, 79, 80]. In addition, a large number of substitutions can be made into the flexible and highly stable hydroxyapatite lattice due to increasing its ligand binding affinity using a large number of anions, cations and functional groups such as F^{-}, $Fe^{2+/3+}$, Mn^{2+} and CO_3^{2-} [1, 81].

2.6 Mercury

Mercury, silvery-white metal, has a freezing point of −38.83 °C and a boiling point of 356.73 °C. In comparison with the other metals, both its freezing and boiling points are very low. Mercury is a fair conductor of electricity but poor conductor of heat. However, mercury cannot react with most acids and oxidizing acids, like sulfuric and nitric acid, it can be dissolve to give sulfate, nitrate, and chloride salts.

Figure 1. Image of mercury element (left) and mercury chloride powder (right), adopted from [82]

As explained extensively in the Section 1.1, the presence of mercury ions in drinking water can be very harmful, thus the removal of mercury from aqueous solutions is very important in wastewater treatment. Removing mercury by adsorption needs an efficient sorbent to bind and form complexes like thioether, thiol, and amide groups [5, 24]. Because, thiol and thioether also react with other metal ions, the best choice for binding mercury ion is the amide group [36]. Therefore, the acrylamide has been chosen as a suitable monomer in this thesis.

2.6.1 Mechanism of Mercury Ion Adsorption

Mercuric ions can be extracted by many chelating polymers and ion exchangers, but its selective extraction has a special attraction due to its exceptional affinity towards some functional groups (i.e. thiol, thioether, and amide). The selectivity decreses greatly in the thioether and thiol groups because of their reaction with other metals

ions as well [83-85]. Therefore, mercury ion selectively binds to the amide groups [5, 36]. The chemistry of mercury–amide interactions has been known for about 100 years. Amide compounds readily react with mercuric ions, under ordinary conditions, to give monoamido–mercury or diamido–mercury compounds (Scheme 6). The mercury–amide linkage is believed to be covalent rather than coordinative. The amide group, however, is a weak donor because of an electron-withdrawing carbonyl group [86]. Therefore, it shows very little tendency for coordination with transition-metal ions. This makes amide groups unique in mercury binding with extremely high selectivity [87].

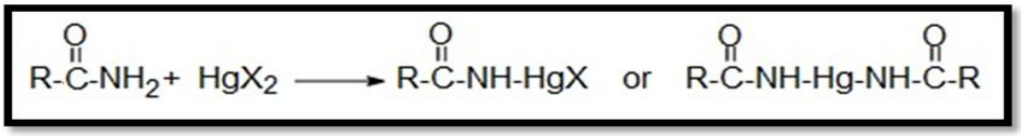

Scheme 6. Preparation of monoamido- or diamido–mercury compounds [86]

Chapter 3

EXPERIMENTAL

3.1 Materials

The synthesis of the hydrogel was achieved using natural polymers; medium molecular weight chitosan (4×10^5) with 200 mPa s viscosity (Aldrich), cellulose (microcrystalline, 20 μm with bulk density 0.5 $g.L^{-1}$ and 20 mPa s viscosity reported by the manufacturer, Aldrich), obtained from cotton linters and pullulan (Freda). Acrylamide (Aldrich) was used as a monomer without further purification. The crosslinker was N,N'-methylene-bis-acrylamide (Aldrich). Potassium persulfate (Aldrich) was used as an initiator. The progen for preparation of porous pullulan hydrogel was calcium carbonate (Aldrich). For synthesis of hydroxyapatite, disodium hydrogen phosphate (Analar) and calcium chloride (Aldrich) were used as received. The solvent of cellulose was prepared by mixing N,N-dimethylformamide (Merck) with lithium chloride (Sigma–Aldrich). The ethanol (Aklar Kimya) was used without further purification. The buffer solutions were prepared with, sodium chloride (Analar), sodium hydroxide (Aldrich), sodium hydrogen carbonate (Analar), sodium hydrogen orthophosphate (Analar), potassium chloride (Sigma Aldrich), potassium phosphate monobasic (Aldrich), potassium hydrogen phthalate (Analar), magnesium sulfate (Analar), acetic acid 100% (Riedel-de Haen), and hydrochloric acid 37% (Riedel-de Haen). Finally, mercury (II) chloride (Merck) and 1,5 diphenylcarbazide (Merck) were used for water treatment purposes as received.

3.2 Synthesis of Hydrogels

3.2.1 Chitosan-*graft*-polyacrylamide Hydrogel

A chitosan solution (1.6 % w/v) was prepared by dissolving chitosan powder (1 g) in 60 mL of acetic acid aqueous solution (1 % v/v) in a two-necked flask equipped with a mechanical stirrer and nitrogen gas inlet. Then, 0.1 g of potassium persulfate was added to the chitosan solution as an initiator and stirred at 65 °C. Ten minutes later, 1 g of acrylamide along with N,N-methylene-bis-acrylamide (4% w/w of monomer) was introduced into the flask as a monomer and crosslinker, respectively. The suspension was stirred at 600 rpm in a nitrogen atmosphere for 2 h. Then, the resulting hydrogel was kept in the same condition for completing gelation. Thereafter, the hydrogel were cut in desired shape and size and immersed in distilled water overnight to remove unreacted monomer and homopolymer. It should be noted that water is the best solvent for acrylamide and polyacrylamide, which had monopolar surface nature [88]. Finally, the hydrogel was allowed for drying in oven at 60 °C for a day.

3.2.1.1 Amine Content Analysis

The amine content of the sample was determined by the titration method [45]. Into 100 mL of a 0.1 mol.L^{-1} hydrochloric acid solution, 0.05 g of chitosan or grafted chitosan was added and dissolved. After adding 2–3 drops of phenolphthalein indicator, the solution was titrated with 0.1 mol.L^{-1} sodium hydroxide. The NH_2 (%) content was calculated as follows:

$$\mathbf{NH_2}(\%) = \frac{(\mathbf{C_1V_1 - C_2V_2})\mathbf{0.016}}{\mathbf{W}} \times \mathbf{100} \qquad (1)$$

Where C_1 and V_1 are concentration (mol.L^{-1}) and volume (mL) of sodium hydroxide, respectively and C_2 and V_2 are concentration (mol.L^{-1}) and volume (mL) of

hydrochloric acid, respectively. W is sample weight (g), (C_1 V_1- C_2 V_2) is moles of amine in mL, and 0.016 is molar mass of NH_2 ($g.mmol^{-1}$).

3.2.2 Cellulose-*graft*-polyacrylamide Hydrogel

Cellulose solution (1.6 % w/v) was prepared by dissolving cellulose powder in fresh lithium chloride/N,N-dimethylformamide (8% w/v) with continuous stirring [78]. Then, the hydrogel was prepared using radical polymerization methods. 80 mL of acrylamide (5.68 g) solution consisting of N,N-methylene-bis-acrylamide (4% w/w), were added to the cellulose solution which contained potassium persulfate (0.024 g) in a three-neck round bottom flask, fitted with a condenser and nitrogen gas inlet, with vigorous stirring at 65 °C for 2 hours. Finally, the hydrogel was cut in desired shapes and immersed in 500-mL water to remove any unreacted monomer and homopolymer, which shows distinct solubility in water. The synthesized hydrogel was dried at 50 °C in oven for 24 h.

3.2.3 Pullulan-*graft*-polyacrylamide Hydrogel

A pullulan-*graft*-polyacrylamide hydrogel was prepared by free radical polymerization. Briefly, potassium persulfate (0.01 $mol.L^{-1}$) was added to the pullulan solution (1.66 %w/v) in a two-necked round-bottom flask fitted with an argon gas inlet in a water bath at 60 °C with continuous stirring. After 10 min, acrylamide (0.37 $mol.L^{-1}$), and N,N′-methylene-bis-acrylamide (0.02 $mol.L^{-1}$) were added to the above solution and the mixture was continuously stirred for 1 h. Then, the synthesized hydrogel was cut in to several pieces and each piece was immersed in water for a day at room temperature, which resulted in unreacted monomer and homopolymer dissolution. Finally, they were dried at 60 °C in an oven overnight to constant weight.

3.2.4 Pullulan-*graft*-polyacrylamide Porous Hydrogel

First, a pullulan solution (1.6 % w/v) was prepared by dissolving pullulan powder (0.25 g) in distilled water (15 mL) [1]. Then it was placed in a round-bottom flask fitted with an argon gas inlet in a water bath at 60 °C with continuous stirring. The potassium persulfate (0.0123 $mol.L^{-1}$) as an initiator was dissolved in the pullulan solution and was allowed to stir for 10 minutes. During this time, the exact amount of calcium carbonate (0.666 $mol.L^{-1}$) as a porogen was added to the solution. Subsequently, acrylamide (0.2344 $mol.L^{-1}$) and N,N-methylene-bis-acrylamide (0.0108 $mol.L^{-1}$) were added to the above solution and the mixture was continuously stirred for 1 h. Finally, the obtained hydrogels were cut into several pieces and washed with distilled water. Then, the hydrogels were immersed in a 10 % wt hydrochloric acid solution for a day with stirring at room temperature. The newly formed CO_2 bubbles will rise up immediately through the porous medium. For removing the calcium chloride and the other remained substrates, like homo-polymer or unreacted acrylamide, the hydrogels were kept under distilled water overnight. After that, the hydrogels were immersed in 200 mL of ethanol with the aim of dewatering for 24 hours, and then dried in oven at 80 ºC for a day.

3.2.4.1 Porosity (%) Measurements

The porosity (%) of synthesized hydrogels was determined by using a liquid replacement method [89]. For this purpose, the ~0.05 g of dried porous hydrogel (W_1) was immersed in a graduated cylinder containing a known volume (V_1) of ethanol overnight until no air bubbles were seen emerging from the hydrogel. The new volume of cylinder called V_2 which containing ethanol and hydrogel. Therefore, the volume difference of cylinder (V_2-V_1) represented the primary volume of hydrogel. Then the ethanol-impregnated hydrogel was removed from the cylinder

and after removing the excess amount of ethanol from the surface of hydrogel by the filter paper, it was weighed (W_2). The volume of the cylinder after removing the hydrogel was recorded as (V_3). Therefore, the volume of porous hydrogel was calculated by a summation of the volume of ethanol held by the hydrogel (V_1-V_3) and the primary volume of the porous hydrogel (V_2-V_1). The porosity (%) of porous hydrogel was calculated using Equation 2:

$$\text{Porosity } (\%) = \frac{W_2-W_1}{\rho V_S} \quad (2)$$

where, ρ is the density of ethanol ($g.cm^{-3}$) and V_S is the volume of porous hydrogel (V_2-V_3).

3.2.5 Cellulose-*graft*-polyacrylamide/hydroxyapatite Composite Hydrogel

3.2.5.1 Synthesis of Nano-hydroxyapatite

The nano-hydroxyapatite powder was synthesized through micro-emulsion technique [60]. 80 mL of disodium hydrogen phosphate (0.18 $mol.L^{-1}$) was added drop-wise to 0.31 $mol.L^{-1}$ of calcium chloride solution (80 mL) with vigorous stirring at 65 ºC under an argon atmosphere. A molar ratio of Ca/P = 1.67 was kept constant in all reactions to produce nano-hydroxyapatite powder. It should be noted that the pH of the reaction was kept at 10±0.5 while the addition speed of disodium hydrogen orthophosphate was controlled at 2 $mL.min^{-1}$ using a tube pump. Then, the product was washed several times with distilled water then dried in a 60 ºC oven overnight and then weighed (Y_2). Finally, the yield % of synthesis of nano-hydroxyapatite was calculated according to the following reaction and Equation;

$$10CaCl_2 + 6Na_2HPO_4 + 2H_2O \rightarrow Ca_{10}(PO_4)_6(OH)_2 + 12NaCl + 8HCl$$

$$Yield\ (\%) = \frac{Y_2}{Y_1} \times 100 \quad (3)$$

where Y_1 and Y_2 (g) are the theoretical (1.7 g) and actual amount of reaction respectively.

3.2.5.2 Synthesis of Composite Hydrogel

Cellulose solution (2 % w/v) was prepared by dissolving cellulose powder in fresh lithium chloride/N,N-dimethylformamide (8 % w/v) with continuous stirring [78]. The cellulose-graft-polyacrylamide/nano-hydroxyapatite composite hydrogel was prepared using radical polymerization methods. 80 mL of acrylamide solution consisting of N,N-methylene-bis-acrylamide (4 % w/w), potassium persulfate (0.024 g) and a synthetic amount of nano-hydroxyapatite were added to the cellulose solution in a three neck round bottom flask, fitted with a condenser and an argon gas inlet, with vigorous stirring at 65 ºC. The mixture was placed in an 80 °C oven for completion of the reactions and aged overnight. Then, the milk-white composite hydrogel of cellulose-graft-polyacrylamide/nano-hydroxyapatite was cut from the upper soft polymer layer and immersed in 250 mL of distilled water for several days to remove the unreacted materials and residues (see Figure 2). The distilled water was changed several times each day. Finally, composite hydrogel was dried in an 80 °C oven for 1 day.

Figure 2. Image of composite hydrogel after synthesis

3.2.6 Grafting and Gelation (%) Measurements

After synthesis of all kinds of hydrogels in this thesis, grafting and gelation (%) was calculated using the following Equations:

$$\text{Grafting (\%)} = \frac{W_1 - W_3}{W_3} \times 100 \quad (4)$$

$$\text{Gelation (\%)} = \frac{W_1}{W_4} \times 100 \quad (5)$$

where W_1 (g) is the weight of the dried hydrogel, W_3 (g) is the weight of the natural polymers (i.e., chitosan, cellulose and pullulan), and W_4 is the combined weight of the natural polymers, acrylamide and crosslinker which were used during the synthesis of hydrogels.

3.3 Methods of Characterization of Synthesized Hydrogels

To verify the synthesis of natural polymers-graft-polyacrylamide hydrogels, FTIR spectra of samples were obtained (Perkin-Elmer Japan FTIR-140 8700 Fourier transform infrared spectrophotometer) in the range of 500–4000 cm^{-1}. The microstructure of the gold-coated hydrogels was observed using SEM (Stereoscan S-360 Cambridge) operated at the acceleration voltage of 15 kV. The size of synthesized nano-hydroxyapatite was measured by a Malvern Zetasizer Nanozs 3600 (Malvern Instruments Limited, UK). In addition, the morphology of the porous hydrogel surface was observed by an optical microscope (MT9000 Polarizing Microscope, Meiji Techno Co. Ltd., Japan with Invenio 3S, DeltaPix Camera).

3.4 Investigation of Swelling Properties of Synthesized Hydrogels

The swelling property of the hydrogels was investigated by immersing 0.05 g of hydrogel in 100 mL of distilled water at room temperature (~20 ºC) in atmospheric conditions, kept overnight until swelling equilibrium was reached. Then, the swelling capacity was calculated using Equation 6. In addition, for measuring the deswelling

behavior of the swollen hydrogel, the water retention capacity at a constant temperature (80 °C) was considered. First, the swollen and equilibrated hydrogel was weighed and then put into an oven, which passed a current of hot air at a constant temperature of 80 °C. The weight of the porous hydrogel was measured regularly for 24 hours. Then, the water retention capacity was calculated by using Equation 7:

$$\text{Swelling}\ (\%) = \frac{W_5 - W_1}{W_1} \times 100 \quad (6)$$

$$\text{Water retention capacity}(\%) = \frac{W_5 - W_6}{W_6} \times 100 \quad (7)$$

where W_1 (g), W_5 (g) and W_6 (g) are weights of the dried, swollen and deswelled hydrogels, respectively.

3.4.1 Effect of Several Variables on Swelling Behavior of Hydrogels

The swelling behavior of hydrogels is significantly influenced by both synthesis and swelling medium conditions such as time, temperature and pH. The individual effect of these variable conditions on the swelling behavior was also investigated.

3.4.2 Swelling Kinetics of Hydrogels

To evaluate the swelling mechanism of chitosan, cellulose and pullulan-*graft*-polyacrylamide hydrogels, Schott's first-order and second-order kinetic models were studied. As stated by Pourjavadi and Mahdavinia, in a first-order kinetic model, the rate of swelling at any time (t) is directly related to the water content that the hydrogel must take up prior to reaching the equilibrium stage [90]. The first and second-order models can be expressed as the following Equations:

$$\ln \frac{(W_e - W_t)}{W_e} = K_1 t \quad \text{(First-order)} \quad (8)$$

$$\frac{t}{W_t} = \frac{1}{K_2 W_e^2} + \frac{t}{W_e} \quad \text{(Second-order)} \quad (9)$$

Where K_1 ($hour^{-1}$) and K_2 ($g.g^{-1}.hour^{-1}$) are the rate constants for first and second order, W_t ($g.g^{-1}$) and W_e ($g.g^{-1}$) are water content at time t and equilibrium swelling ratio.

3.5 Mercury(II) Ion Adsorption Procedures by the Synthesized Hydrogels

The initial aqueous mercury solutions (1 $g.L^{-1}$) were prepared by dissolving mercury (II) chloride $HgCl_2$ in 100 mL deionized water. Then, the dried synthesized hydrogels (0.05 g) were immersed in the prepared mercury solution and shaken for a night at room temperature. Finally, the equilibrium amount of mercury ions was determined colorimetrically, using 1,5-diphenylcarbazide as indicator through UV-visible spectrophotometer (T80+ UV/VIS Spectrophotometer, Beijing PG Instrument Co. Ltd. China) at a wavelength of 532 nm. The mercury uptake (g per g of each synthesized hydrogels as an adsorbent) was calculated by the following Equation:

$$q_e = \frac{C_0 - C_t}{W_1} \times V \quad (10)$$

where V is the volume of mercury solution in L, and C_0 and C_t are the initial concentrations of mercury solution and concentration in specific time in $g.L^{-1}$, respectively [5].

3.5.1 Regeneration of Hydrogels

After adsorption of Hg(II) ions, the synthesized hydrogels were washed with distilled water, dried and prepared for desorption experiments. Regeneration was carried out through the batch technique using an HCl solution (0.1 $mol.L^{-1}$) as a desorbent solution. The dried adsorbed hydrogels (0.05 g) were immersed in 100 mL desorbent solution and the suspension was shaken for 24 hours at room temperature. After that, the concentration of desorbed Hg(II) ions in solution was analyzed by using UV–visible spectrophotometer as explained above. The amount of adsorbate, which was

desorbed in acidic solution, was determined spectrophotometrically and hydrogel regeneration efficiency was calculated by using the following Equation:

$$\text{Regeneration (\%)} = \frac{q_t}{\text{desorbed amount of adsorbate}} \times 100 \quad (11)$$

3.5.2 The Effects of Variable Conditions on Adsorption

In addition, the effects of variable conditions such as time, initial adsorbates concentration, adsorbent amounts, pH and temperature on the adsorption behavior of synthesized hydrogels were investigated. For each case, one parameter was changed and analyzed and the other factors were kept constant. For instance, the influence of time on adsorption was calculated by immersing 0.05 g of each synthesized hydrogels in 100 mL of each adsorbate solutions (1 $g.L^{-1}$) and then shaken at room temperature (20 °C) for 24 h. Then, in different time intervals, 2 mL of solution was taken out and the amount of remaining adsorbate in solution was determined by using UV-visible spectrophotometer, which was explained above.

3.5.3 Kinetics of Adsorption

The adsorption rate is an important factor for designing an appropriate adsorption system by choosing a better material as an adsorbent, which exhibits a large capacity and fast rate [91]. In order to determine the Hg(II) ions adsorption efficiency and the adsorption rate constant by the synthesized hydrogels, the three kinetic models pseudo-first-order, pseudo-second-order and intra-particle diffusion were considered. These models are given in Equations 12-14, respectively.

$$\log(q_e - q_t) = \log q_e - \frac{K_1}{2.303} t \quad (12)$$

$$\frac{t}{q_t} = \frac{1}{K_2 (q_e)^2} + \frac{t}{q_e} \quad (13)$$

$$q_t = K_3 (t)^{\frac{1}{2}} + C_i \quad (14)$$

In these Equations, t is the time, q_e, q_t, ($g.g^{-1}$) and $(q_e)^2$ are the amounts of Hg(II) ions adsorbed by the hydrogels at equilibrium, at time t and at maximum adsorption capacity, respectively. K_1 ($hours^{-1}$), K_2 ($g.g^{-1}.hours^{-1}$) and K_3 ($g.g^{-1}.hour^{-0.5}$) are the adsorption rate constants of the pseudo-first-order, pseudo-second-order and intra-particle diffusion models, respectively. In addition, C_i ($g.g^{-1}$) is the intra-particle diffusion constant, which is directly proportional to the boundary layer thickness.

3.5.4 Isotherms of Adsorption

In general, the adsorption isotherms indicate the interaction of the adsorbate with the adsorbent. In addition, these isotherms show the equilibrium that is established between the liquid phase (free adsorbate solution) concentrations and the solid phase (adsorbent-attached solute) concentrations at constant temperature and represents the adsorption capacity of the adsorbent [92]. Two isotherm models (i.e., Langmuir and Freundlich) were investigated to determine a more suitable model for the design process. The Langmuir model, which is the most popular, has been widely used to describe single-solute systems. The Langmuir model is based on the assumptions that adsorbate produces monolayer coverage on the outer surface with uniform energies of adsorption, which is structurally homogeneous, and the adsorbent-adsorbate intermolecular forces decrease rapidly with distance [93-95]. The theoretical Langmuir isotherm is represented by the following Equation:

$$\frac{C_e}{q_e} = \frac{1}{q_m K_L} + \frac{C_e}{q_m} \quad (15)$$

where q_e is the amount of mercury ions adsorbed at the equilibrium time ($g.g^{-1}$), C_e is the equilibrium Hg(II) concentration ($g.L^{-1}$), q_m is the maximum adsorption capacity ($g.g^{-1}$), and K_L is the Langmuir adsorption equilibrium constant ($L.g^{-1}$). In addition, the shape of the Langmuir isotherm was examined by the dimensionless constant called separation factor, R_L:

$$R_L = \frac{1}{1+K_L C_0} \quad (16)$$

R_L values indicate the type of isotherm to be linear (R_L=1), irreversible (R_L= 0), favorable ($0< R_L<1$) or unfavorable ($R_L>1$).

In the Freundlich model, the adsorption of the adsorbate occurs on a heterogeneous surface by multilayer sorption with non-uniform distribution of heat of adsorption and affinities over the heterogeneous surface. The Freundlich model can be expressed by the following Equation:

$$\log q_e = \log K_F + \frac{1}{n}\log C_e \quad (17)$$

where K_F is the equilibrium adsorption coefficient ($L.g^{-1}$) and 1/n is an empirical constant.

3.5.5 Thermodynamics of Adsorption

The effect of temperature can be further investigated by calculating thermodynamic parameters. In addition, to determine whether the adsorption of mercury ions by hydrogels is an exothermic or endothermic process, the thermodynamic parameters including standard enthalpy change (ΔHº), the Gibbs free energy change (ΔGº) and standard entropy change (ΔSº) have been determined using the following Equations:

$$\Delta G^0 = -RT \ln K_d \quad (18)$$

The distribution ratio (K_d), can be calculated using the following Equation:

$$K_d = \frac{q_e}{C_e} \quad (19)$$

Then, the relation between ΔG°, ΔH° and ΔS° can be expressed by the following Equation:

$$\Delta G° = \Delta H° - T\Delta S° \quad (20)$$

Standard enthalpy (ΔH°) and entropy (ΔS°) were determined from the slope and intercept of the plot of $\ln K_d$ vs 1/T, which came from the Van's Hoff Equation:

$$\ln K_d = \frac{\Delta S^\circ}{R} - \frac{\Delta H^\circ}{RT} \quad (21)$$

Chapter 4

RESULTS AND DISCUSSION

4.1 Synthesis of Hydrogels

4.1.1 Synthesis of Acrylamide Grafted Chitosan, Cellulose, and Pullulan Hydrogels

The hydrogels of natural polymers (i.e., chitosan, cellulose, pullulan)-graft-polyacrylamide were prepared according to the procedures which has been extensively explained in Chapter 3. Acrylamide, which was added to homogeneous natural polymer solutions containing an initiator, potassium persulfate, has been crosslinked and grafted simultaneously onto natural polymers using N,N-methylene-bis-acrylamide as a crosslinker. The graft polymerization of acrylamide onto natural polymers is shown in Scheme 6. The grafting and gelation (%) of chitosan, cellulose, and pulllulan-graft-polyacrylamide hydrogels are listed in Table 2. As explained in Chapter 3, the grafting (%) was calculated through Equation 4, and in this equation W_1 is the weight of hydrogels. In the synthesized hydrogels, the other chemicals such as hydroxyapatite, crosslinker and maybe homopolymer of our monomer can affect the weight of synthesized hydrogel to show them heavier. On the other hand, the porous hydrogel with low weight compared to its volume due to the several pores in the structure is the lightest. Hence, the Equation 4 (for calculating grafting %) cannot be reliable and also cannot explain the efficiency of hydrogels synthesis. Therefore, in this thesis, the gelation percent has been considered more. As can be seen in Table 2, the pullulan-graft-polyacrylamide hydrogels has the highest gelation (%)

compared to the other two natural polymer hydrogels due to its high amount of water solubility. While, the chitosan was dissolved in acetic acid solution and cellulose was dissolved in the mixture of lithium chloride/N,N-dimethylformamide solution, pullulan can directly be dissolved in water. Therefore, through synthesis of pullulan-graft-polyacrylamide hydrogel, the monomer was in contact with pullulan backbone and crosslinker directly and easily. Hence, its gelation (%) and simultaneously crosslinking was higher than other hydrogels.

Table 2. Grafting and gelation amounts (%) of synthesized hydrogels

Samples	Grafting %	Gelation %
Cellulose Grafted Hydrogel	145.3	77.1
Cellulose Grafted Composite Hydrogel	211.5	75.4
Chitosan Grafted Hydrogel	135.9	85.3
Pullulan Grafted Porous Hydrogel	74.3	96.5
Pullulan Grafted Hydrogel	152.8	97.2

4.1.1.1 Amine Contents of Hydrogels

It can be suggested that amine groups of chitosan backbone were not suitable grafting sites in this grafting polymerization. This fact was confirmed by measuring the amine contents in pure chitosan, acrylamide and chitosan-graft-polyacrylamide. The amine content analysis demonstrates that while parent chitosan has an amine content of 8.5% by weight, chitosan-graft-polyacrylamide is composed of 32.3% amine, whereas polyacrylamide has 24.1% amine groups. Hence, it can be concluded that amine groups do not act as grafting sites.

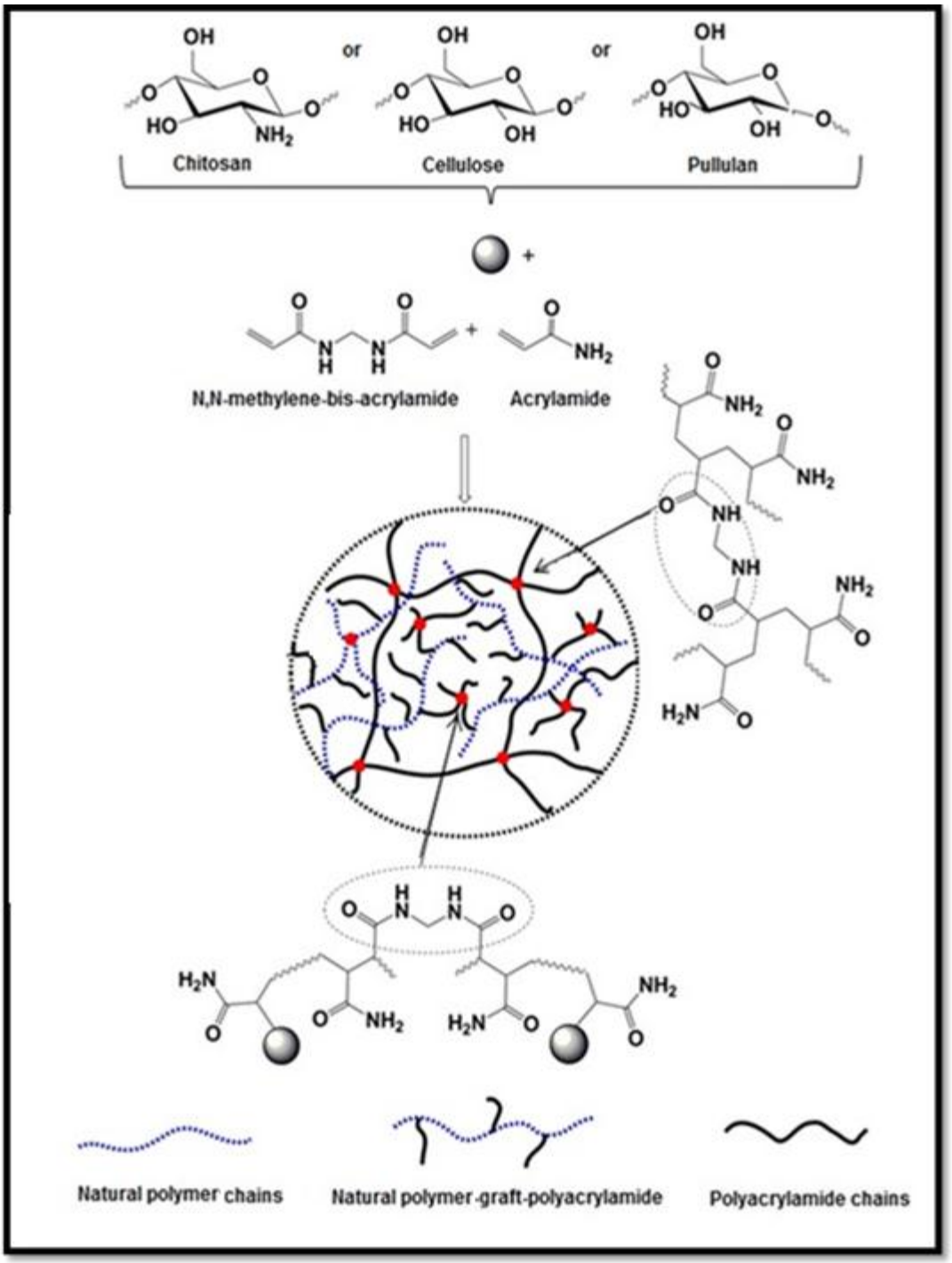

Scheme 7. Schematic illustration for the synthesis of cellulose, chitosan, and pullulan-graft-polyacrylamide hydrogels

4.1.2 Synthesis Mechanisms of Hydrogels

The natural polymer-graft-polyacrylamide hydrogels have been synthesized by free radical polymerization. The initiator, potassium persulfate, decomposed under heat and generated an anion radical of sulfate. The radical abstracts hydrogen from the OH groups of natural polymers to form alkoxy radicals on the backbones. Thus, this persulfate–natural polymers redox system results in active centers of the backbone that can initiate radical graft polymerization of acrylamide onto natural polymers. Meanwhile, the monomer simultaneously can be crosslinked in the presence of crosslinker agent, N,N-methylene-bis-acrylamide. The mechanism of graft polymerization of acrylamide onto natural polymers is shown in Scheme 7.

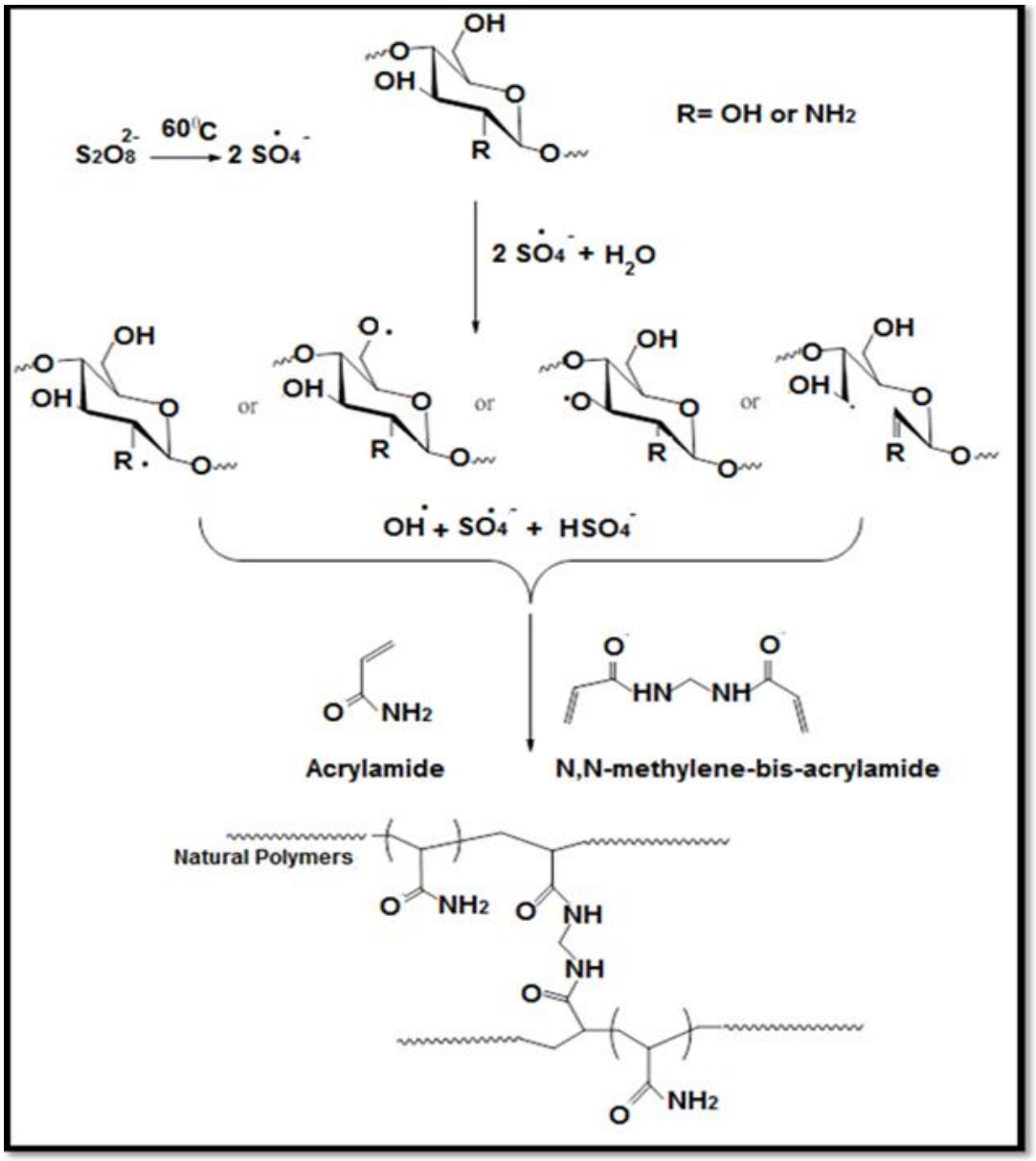

Scheme 8. Schematic illustration for the synthesis of hydrogels in the presence of potassium persulfate as an initiator

4.1.3 Synthesis of Pullulan-graft-polyacrylamide Porous Hydrogel

The porous hydrogel was synthesized via graft polymerization of acrylamide onto pullulan in the presence of calcium carbonate as a porogen (Scheme 8). Then, the synthesized hydrogel was immersed in a hydrochloric acid solution; as a result, bubble gases rose up and several pores appeared inside of the hydrogel. The porosity

of the synthesized hydrogel was calculated 87 % with ~190 μm in size that confirmed with the optical microscope images (Figure 4).

For further investigation of the synthesized hydrogel, polyacrylamide and pullulan were separately reacted with N,N'-methylene-bis-acrylamide, the crosslinker. The results showed that the acrylamide was crosslinked properly while pullulan could not be crosslinked and consequently, gelation was not observed in the related experiment. Overall, a mixture of crosslinked acrylamide and pullulan-graft-polyacrylamide with 96.5 % gelation generated a porous hydrogel containing pores due to the leaving of CO_2 gases (Scheme 8).

Figure 3. Images of pullulan-graft-polyacrylamide porous hydrogel and its optical microscope image

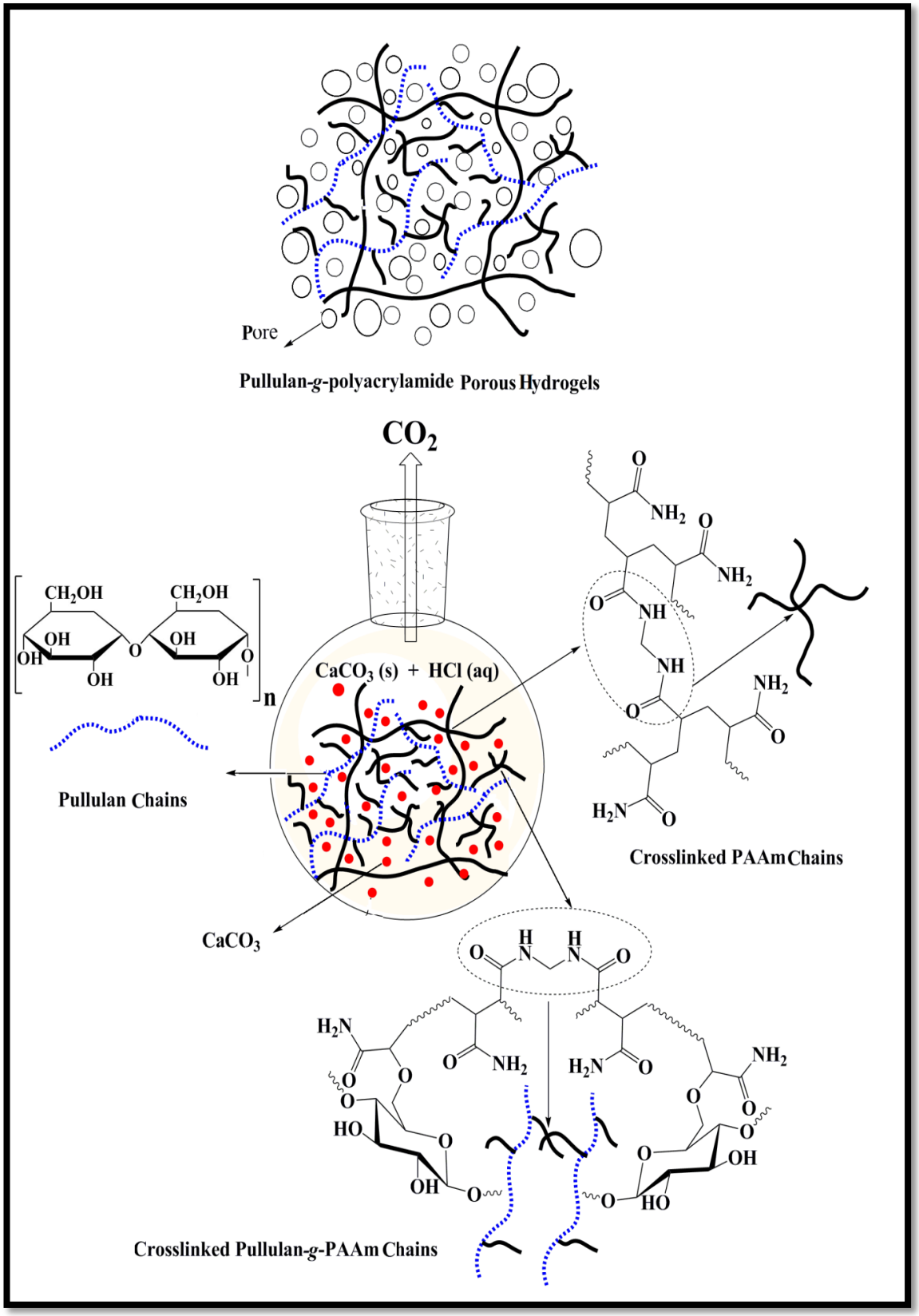

Scheme 9. Schematic illustration for the synthesis of pullulan-graft-polyacrylamide porous hydrogels

4.1.4 Synthesis of Cellulose-graft-polyacrylamide/hydroxyapatite Composite Hydrogel

The composite hydrogel was prepared via the suspension polymerization technique (Figure 5). The hydroxyapatite powder, which was synthesized with 66 % yield were embedded in the hydrogel matrix through ionic crosslinking of species OH^-, Ca^{2+}, PO_4^{3-} and amide groups of acrylamide and/or hydroxyl groups in the cellulose backbone (Scheme 9).

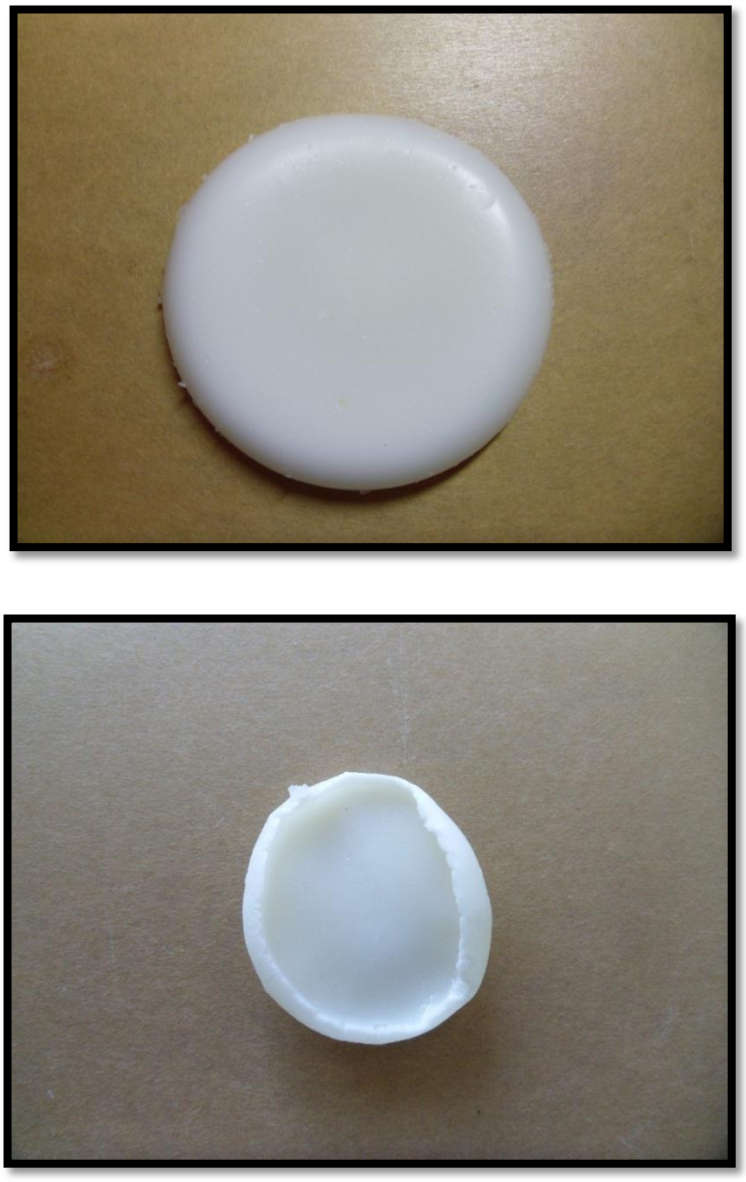

Figure 4. Images of cellulose-graft-polyacrylamide/hydroxyapatite composite hydrogel before and after drying

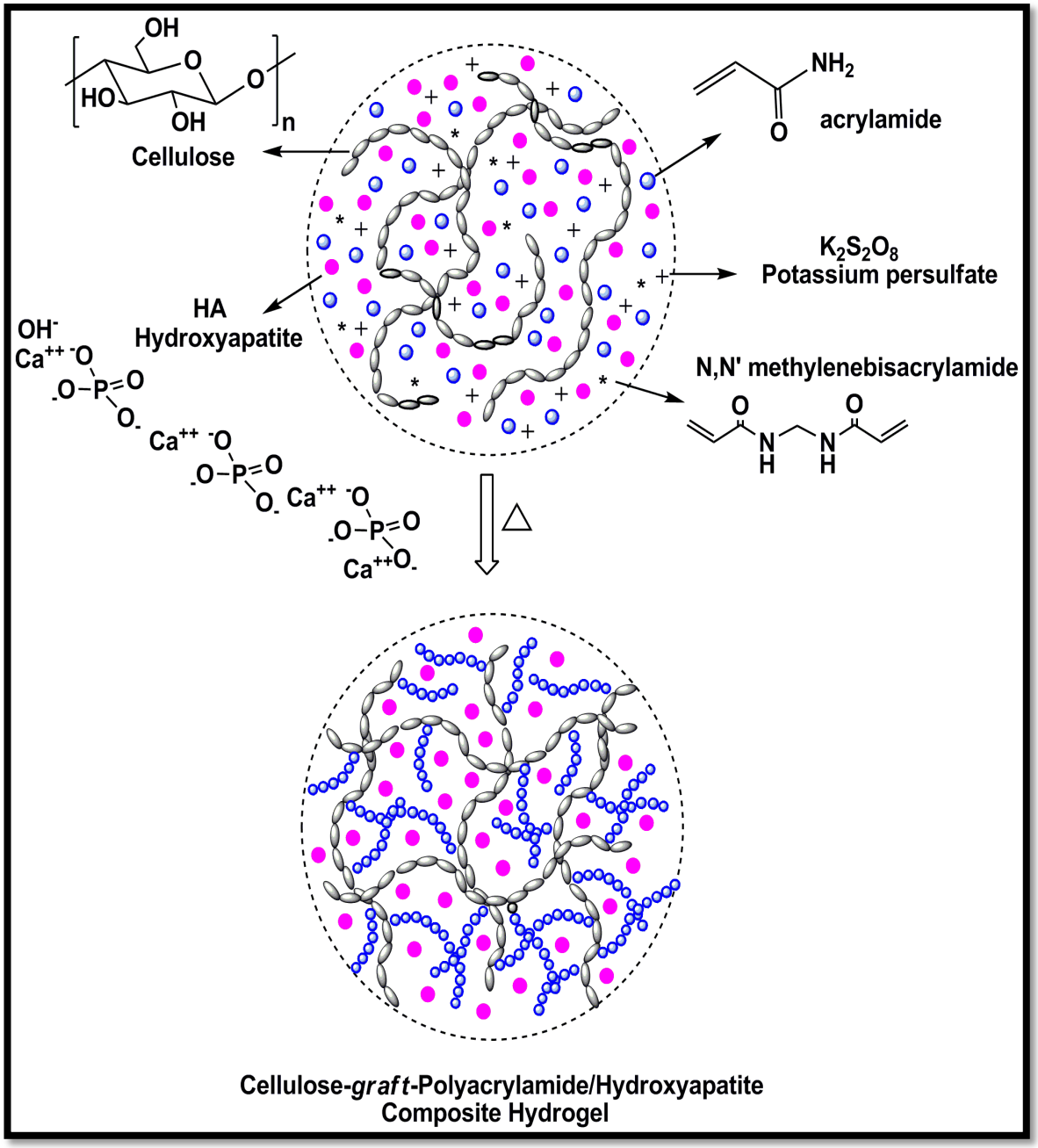

Scheme 10. Schematic illustration for the synthesis of cellulose-graft-polyacrylamide/hydroxyapatite composite hydrogels

4.2 Characterization of Hydrogels

4.2.1 Dynamic Laser Scattering (DLS) Analysis

Particle size distribution of the nano-hydroxyapatite particles that were produced via micro-emulsion was investigated by DLS. The synthesized nano-hydroxyapatites were found to have an average diameter of 254 nm, with a broad distribution with a single peak (Figure 6). The particles in the maximum mean volume, however, exhibited diameters as large as 122 nm. The broad distribution in diameter is attributed to the effect of the pH value during formation of nano-hydroxyapatite, which changed quickly. This hypothesis is consistent with the results reported in literature; the pH value of the reaction solution and the temperature of hydrothermal treatment are the most significant variables in nucleation and growth of the hydroxyapatite nano-crystallites during the synthesis process [96, 97].

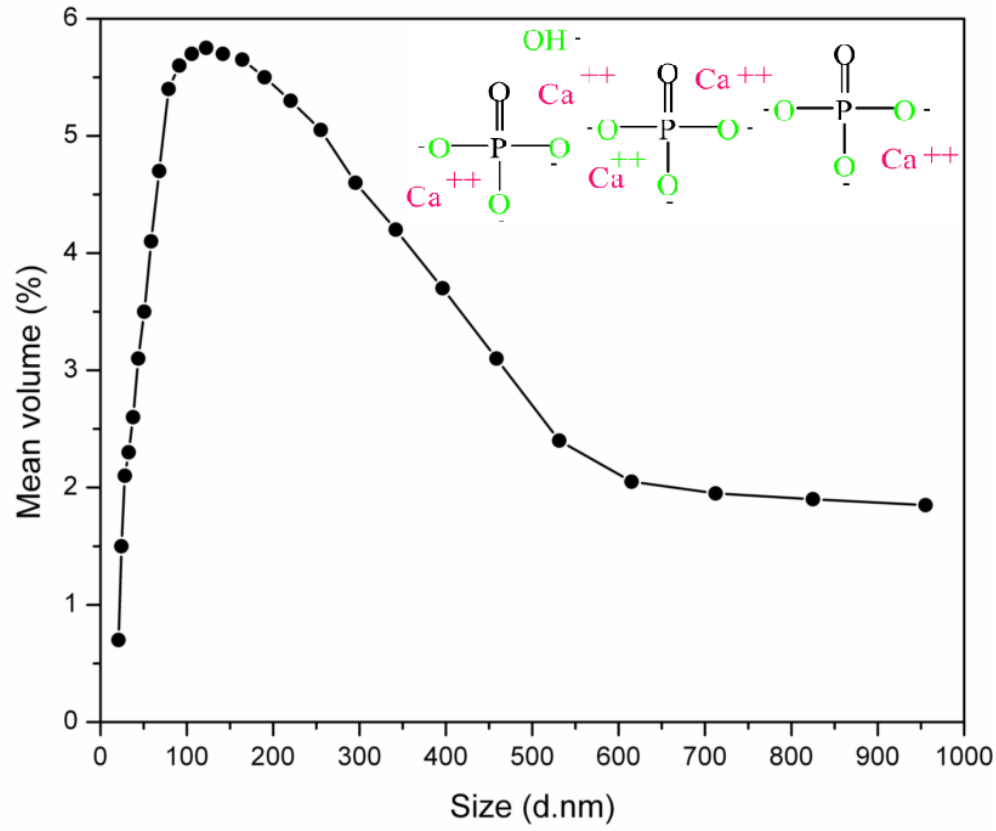

Figure 5. Size distribution curve of synthesized nano-hydroxyapatite, inset shows the nano-hydroxyapatite structure

4.2.2 Fourier Transform Infrared (FTIR) Analysis

The FTIR spectral analyses were performed to confirm the graft polymerization of acrylamide onto natural polymers to synthesis the chitosan, cellulose and pullulan-graft-polyacrylamide hydrogels.

The most typical absorption bands of chitosan situated at 1597 cm^{-1} and 1655 cm^{-1} corresponding to amine and amide I bands, have a minor shift and are stronger in the hydrogel spectrum due to the presence of more amide bonds (reconfirmed by a peak at 3206 cm^{-1}). In addition, the peak at 1406 cm^{-1} in the hydrogel spectrum related to C-N stretching can support the grafting of acrylamide onto chitosan. Moreover, the C–H and O–H bending vibrations are observed in the 1300–1400 cm^{-1} with a sharp peak at 1383 cm^{-1}. However, this sharp peak is related to the O-H group likes two very sharp peaks at 1159 and 1082 cm^{-1} (alcoholic and etheric C–O stretching vibrations, respectively), which are not present in the hydrogel spectrum. This implies that the hydroxyl group of chitosan is the preferred site for the reaction with the crosslinker and the grafting of acrylamide due to lower steric hindrance of the primary hydroxyl group.

The characteristic absorption bands at 2927, 2911 and 2902 cm^{-1} (C-H) and 1700, 1024 cm^{-1} ($C\text{-}OO^{-}$), which are related to the pyranoid rings of cellulose, were observed in cellulose grafted hydrogel spectra. By grafting acrylamide onto cellulose, new peaks of amide groups at 1666, 3200 cm^{-1} were seen. The sharp peaks at 1445, 1134 cm^{-1} (C-N in amide group) of acrylamide also observed.

As shown in Figure 7, the infrared spectrum of the pullulan and hydrogel displayed two strong absorption peaks at 3305 cm^{-1} due to OH stretching vibrations and 2923 cm^{-1} due to the sp^3 C–H bond. In addition, the absorption band located at 3187 cm^{-1} arises from the stretching vibration of the amide group, which confirmed the presence of acrylamide in the structure of the synthesized hydrogel. However, the most characteristic bands for acrylamide were observed in the spectra of the hydrogels with two strong and shoulder peaks at 1648 cm^{-1} (N-H) and 1604 cm^{-1} (C=O). In addition, only a single peak at 1636 cm^{-1} was assigned to the stretching vibration of O-C-O in pullulan. Other features of pullulan were also observed in the spectra including C-O-H bend (1354 cm^{-1}) and C-O-C stretch (1148 cm^{-1}) [98]. The typical absorption bands for the α-configuration of α-D-glucopyranose units in pullulan were observed at 851 cm^{-1}. In addition, the two main linkages of pullulan (i.e., α-(1, 4) and α-(1, 6)-D-glucosidic bonds) were observed at 738 and 918 cm^{-1} [99]. Finally, in a specific area (1500–1400 cm^{-1}) of the hydrogel spectrum, the absorption related to the stretching vibration of the C-N group at 1448 cm^{-1} and 1412 cm^{-1} confirmed the grafting of acrylamide onto pullulan [5].

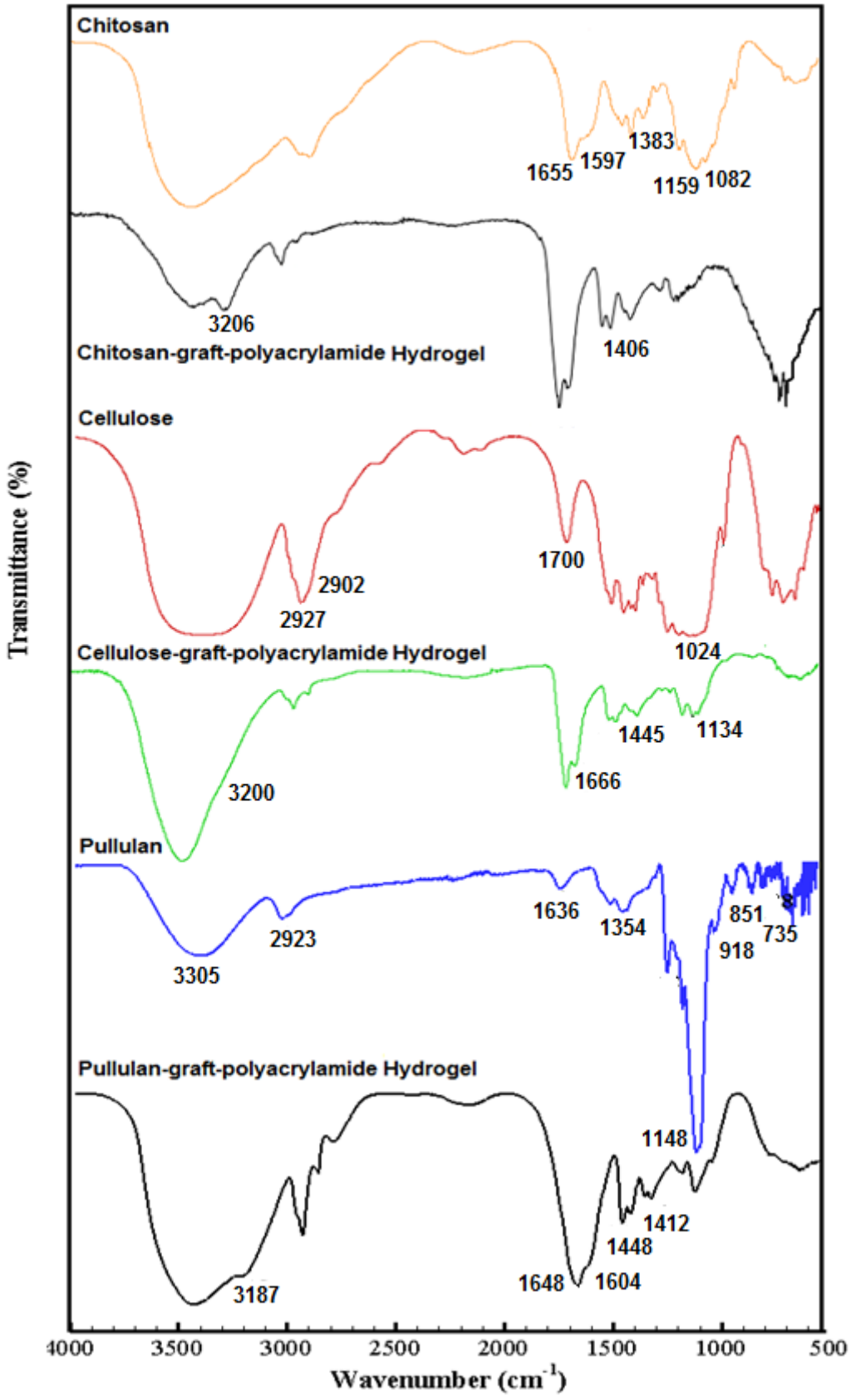

Figure 6. FTIR spectra of cellulose, chitosan and pullulan and its grafted polyacrylamide hydrogels in the range 500–4000 cm^{-1}

FTIR spectroscopy of the synthesized nano-hydroxyapatite in Figure 8 showed a clear hydroxyl vibration peak, at both 633 cm^{-1} and 3570 cm^{-1}. The second peak was located on a broad band between 2500 cm^{-1} and 3600 cm^{-1}, representing asymmetrical and symmetrical stretching vibrations of adsorbed water. The most intense absorption bands of hydroxyapatite were situated at 1029 cm^{-1} and 1092 cm^{-1}, corresponding to the asymmetric stretching modes of PO_4^{3-}, while the peaks at 961 derived from the symmetric stretching mode of PO_4^{3-}, respectively. The two very sharp and separated peaks at 602 and 566 cm^{-1} represent the bending mode of the phosphate group. Moisture adsorption gives a peak at 1658 cm^{-1} from the O–H bond in water. While, examining the FTIR spectrum of cellulose-graft-polyacrylamide composite hydrogel, in addition to the all peaks related to the cellulose and acrylamide which mentioned during interpretation of the spectra of cellulose grafted hydrogel, the sharper O-H stretching vibration peaks at 3400 cm^{-1} and 1029, 962 cm^{-1} related to the O-P-O bending vibration of nano-hydroxyapatite were traced.

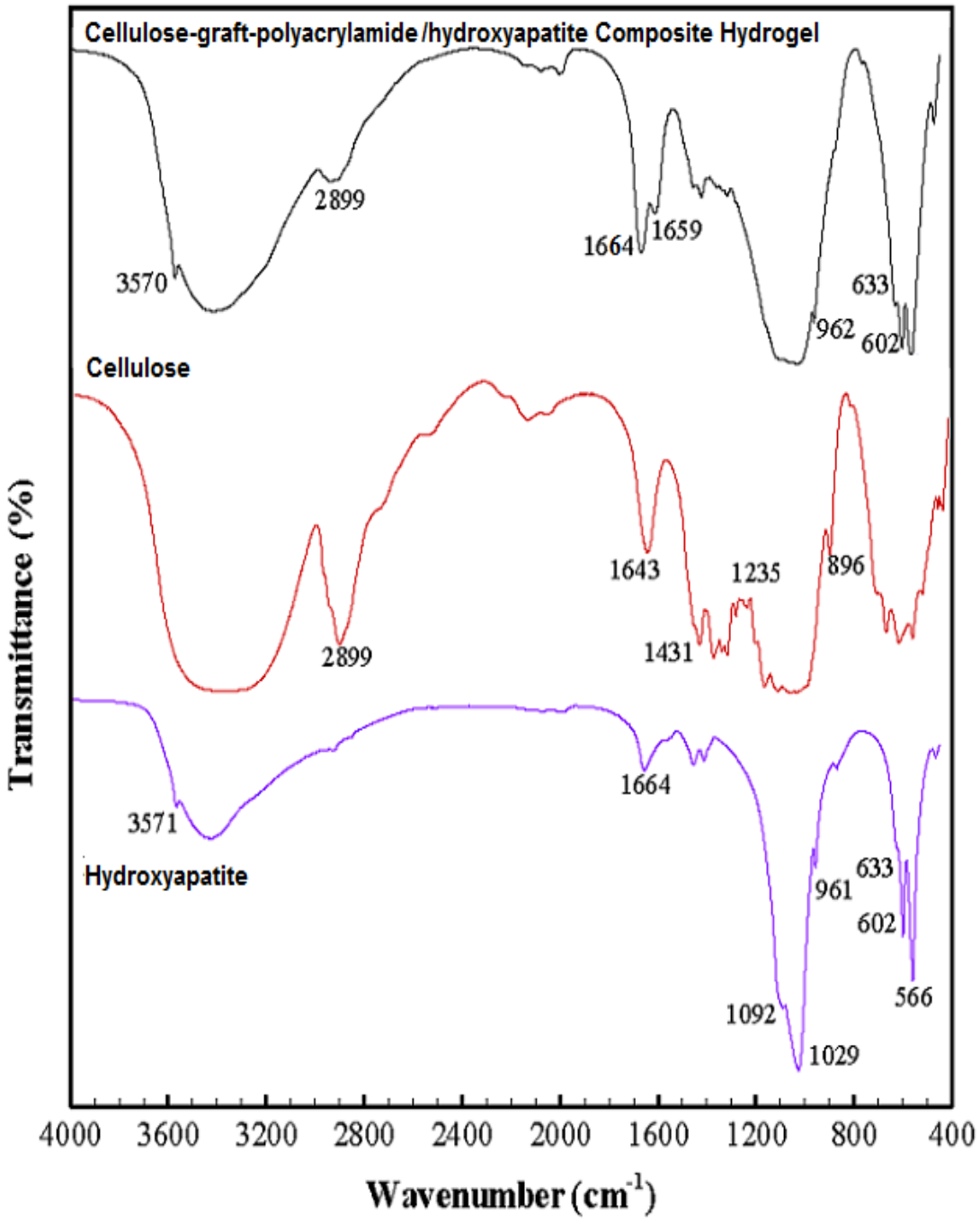

Figure 7. FTIR spectra of cellulose, hydroxyapatite and its grafted polyacrylamide composite hydrogel in the range 500–4000 cm^{-1}

4.2.3 Scanning Electron Microscopy (SEM) Analysis

The scanning electron microscopy (SEM) images of pure chitosan, cellulose and pullulan in the powder form before grafting and also their polyacrylamide grafted hydrogels reflect their surface morphology are shown in Figure 9-11. As can be seen, natural polymers have a rough surface, whereas the hydrogels exhibit a uniformly smooth surface but contains cracks and flaws. In addition, several white spots visible on the image are probably due to the non-optimal preparation and drying process. This distinguished change in the surface of natural polymers before and after grafting, is evidence of the graft polymerization of polyacrylamide. The new morphologies of natural polymers after grafting are convenient for more and easier penetration of water into the polymeric network, and can improve water absorbency of corresponding hydrogels. The morphology of the porous hydrogel and composite hydrogel also were examined with scanning electron microscopy (Figure 12). The SEM image of pullulan-graft-polyacrylamide porous hydrogel showed various pores in its textures. According to the magnification of image, hydrogels contains very crowded pores with ~190 μm in size.

The SEM image of composite hydrogels in comparison with the SEM image of cellulose-graft-polyacrylamide detected a coarser surface. This distinctive change in the SEM images affirms the presence of hydroxyapatite in the surface of composite hydrogel. It is worth to mention that the hydroxyapatite particles are almost uniformly embedded into the polymer chain of grafted cellulose. In addition, it shows dense microstructures without pores or cracks, implying that the addition of hydroxyapatite did not change significantly the dense nature of the cellulose grafted hydrogel layer.

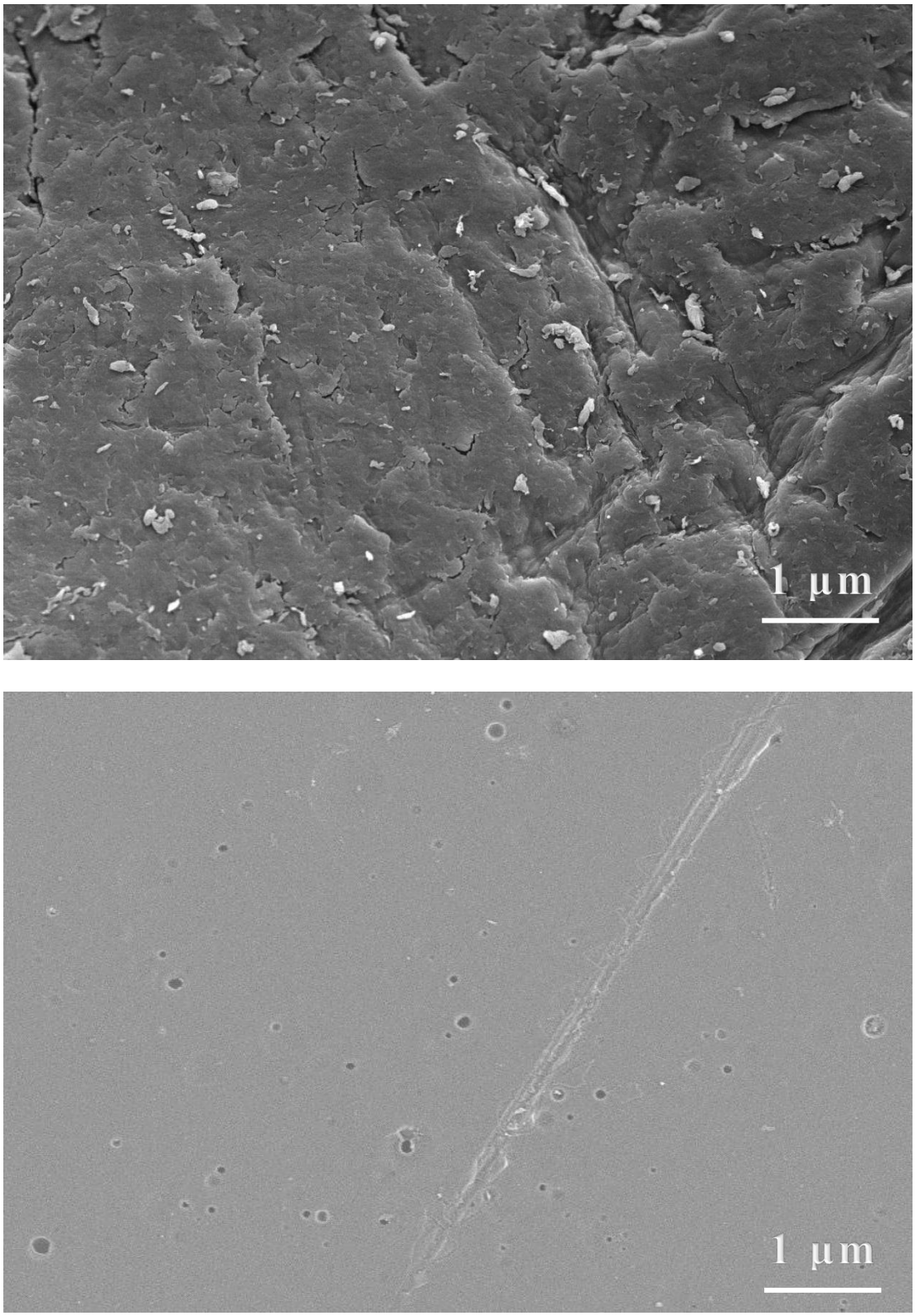

Figure 8. SEM images of cellulose powder (top) and cellulose-graft-polyacrylamide hydrogel (bottom)

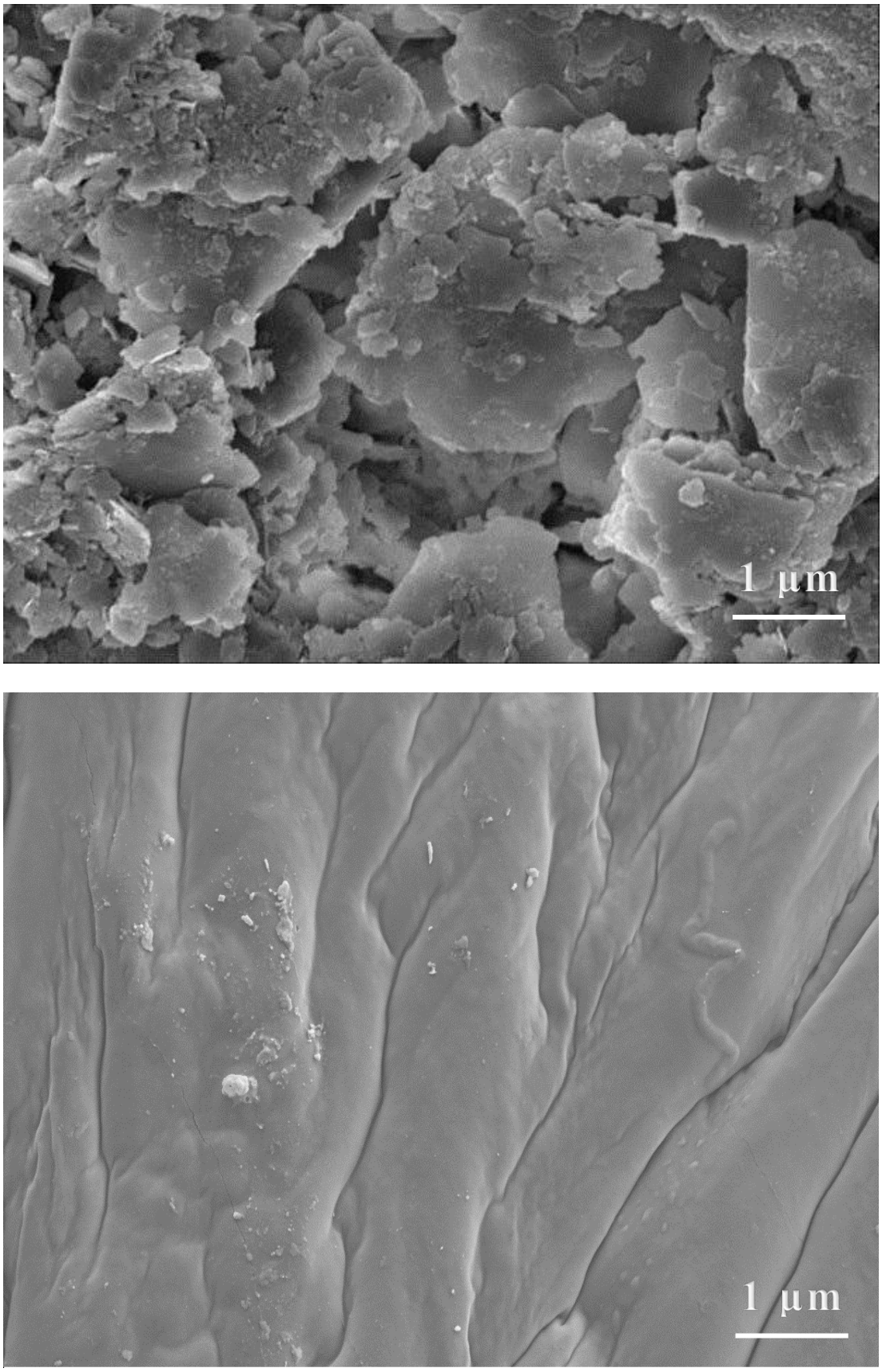

Figure 9. SEM images of chitosan powder (top) and chitosan-graft-polyacrylamide hydrogel (bottom)

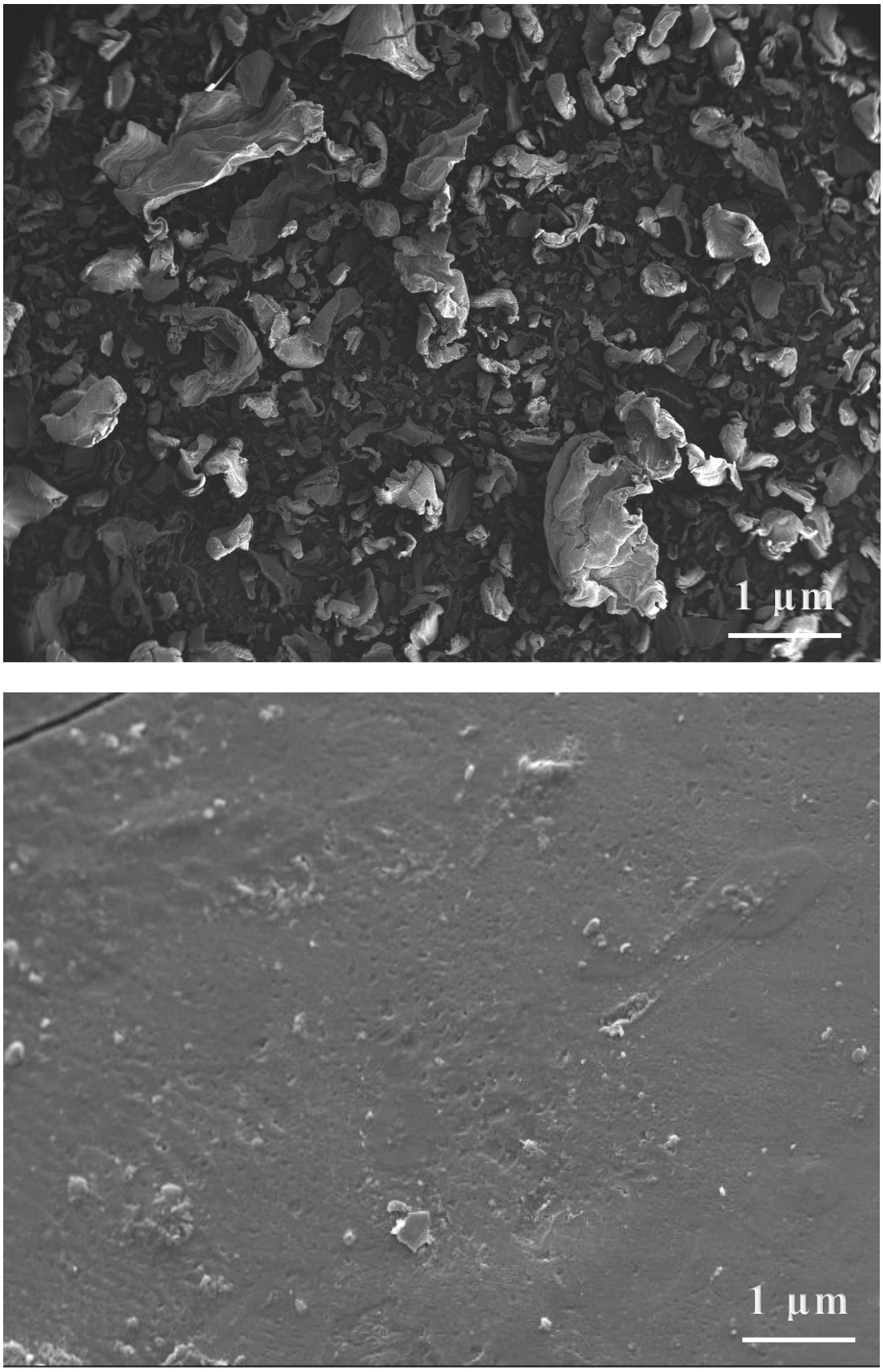

Figure 10. SEM images of pullulan powder (top) and pullulan-graft-polyacrylamide hydrogel (bottom)

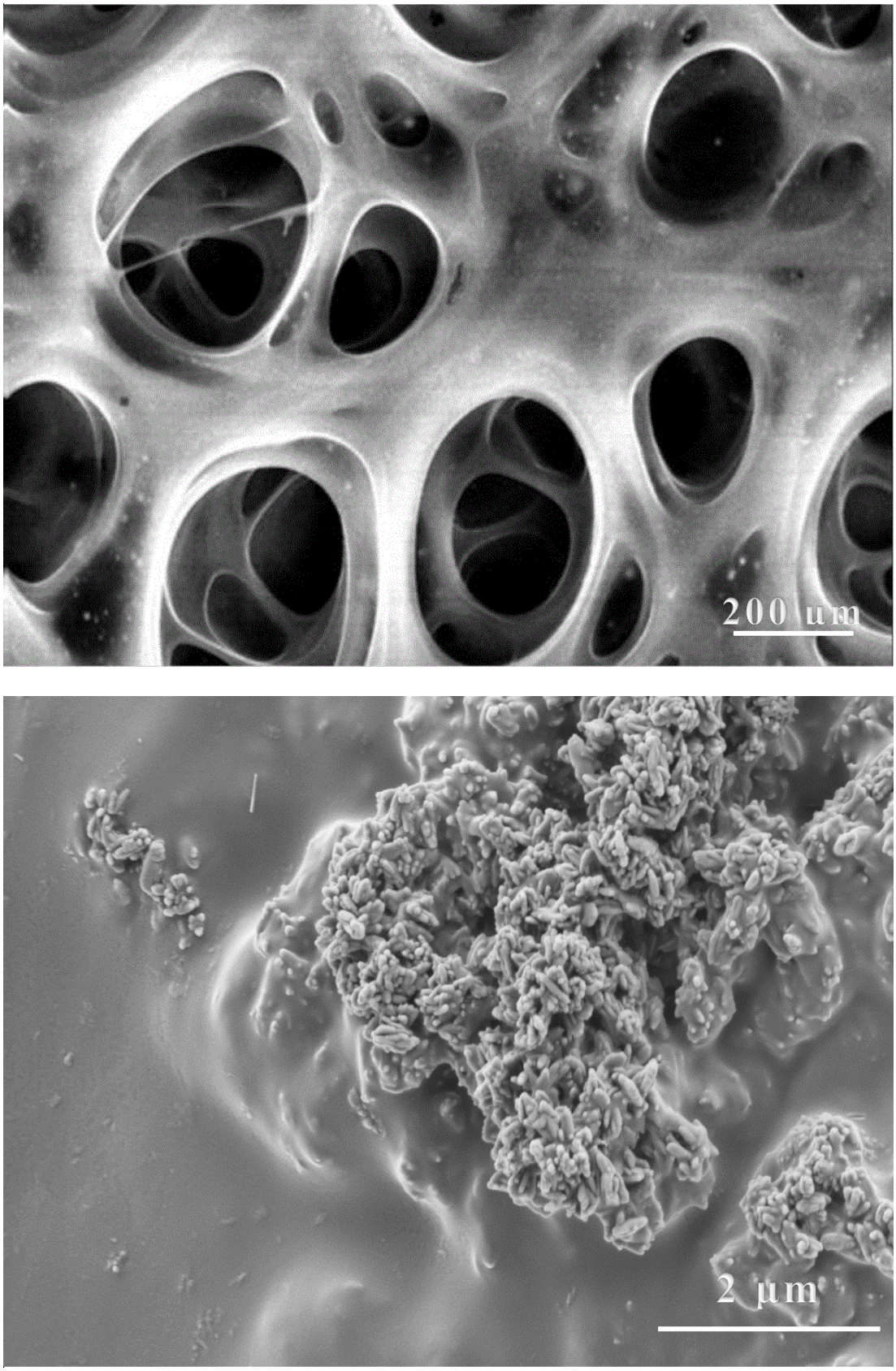

Figure 11. SEM images of pullulan-graft-polyacrylamide porous hydrogel (top) and cellulose-graft-polyacrylamide/hydroxyapatite hydrogel (bottom)

4.3 Swelling Properties of Hydrogels

4.3.1 Effect of Time on Swelling Behavior of Hydrogels

Figure 13 shows the effect of time on the swelling percentage of the natural polymers grafted hydrogels obtained in distilled water at room temperature. First, the swelling percentage increased, afterward, the big differences in water uptake were not observed with further increases in time until it reached a plateau. Initially, the water molecules are in contact with the hydrogel. Then, they attack to the surface of the hydrogel, which contains hydrophilic acrylamide chains due to the osmotic pressure difference between hydrogel and water. Therefore, water penetrates inside of the network and the hydrogel swells. Obviously, this swelling system cannot continue forever and by the increasing hydrogel-water interaction, the osmotic pressure difference will be reduced. Finally, at the equilibrium, the osmotic force will be balanced with an elasticity force. It should be noted that the elasticity force prevents the deformation of the hydrogel network by the stretching balance of the network.

According to the Figure 13, chitosan grafted polyacrylamide has the lowest swelling (%) after pullulan hydrogels. The maximum swelling percentage in equilibrium (5170 %) is belonged to cellulose-graft-polyacrylamide hydrogel, was achieved after immersing the hydrogel in water for 18 h. This swelling behavior of hydrogels can be attributed to the difference in water solubility of natural polymers. For instance, during the synthesis of pullulan-graft-polyacrylamide hydrogels, pullulan, monomer and crosslinker were dissolved in water completely. While, the chitosan was dissolved in acetic acid solution and cellulose was dissolved in the mixture of lithium chloride/N,N-dimethylformamide solution. Therefore, through synthesis of pullulan-graft-polyacrylamide hydrogel, the monomer was in contact with pullulan backbone

and crosslinker directly and easily, hence, the gelation (%) and simultaneously crosslinking was higher than other hydrogels. The high cross-linking inside the network of pullulan-graft-polyacrylamide reduces the amount of space in the chains for water preservation during swelling.

The high rate of water uptake capacity of pullulan-graft-polyacrylamide porous hydrogels compared to the bulky pullulan grafted hydrogel at the beginning of the contact with water was due to the presence of several pores in the structure of the hydrogel. Hence, it can enhance the contact area between the polymeric network and the external solution and speeding up the diffusion rate. The molecules of water inside the network engage in hydrogen bonding with the hydroxyl groups of pullulan and the amide groups of acrylamide.

The low water absorption capacity of cellulose-graft-polyacrylamide/hydroxyapatite composite hydrogel compared to the cellulose grafted hydrogel can be attributed to the presence of hydroxyapatite and its role as a physical crosslinker. The increased amount of hydroxyapatite results in the generation of more crosslink points in the polymeric network, which causes decreased elasticity of the polymer chains and a decrease in the amount of hydrophilic groups on the composite backbone [100].

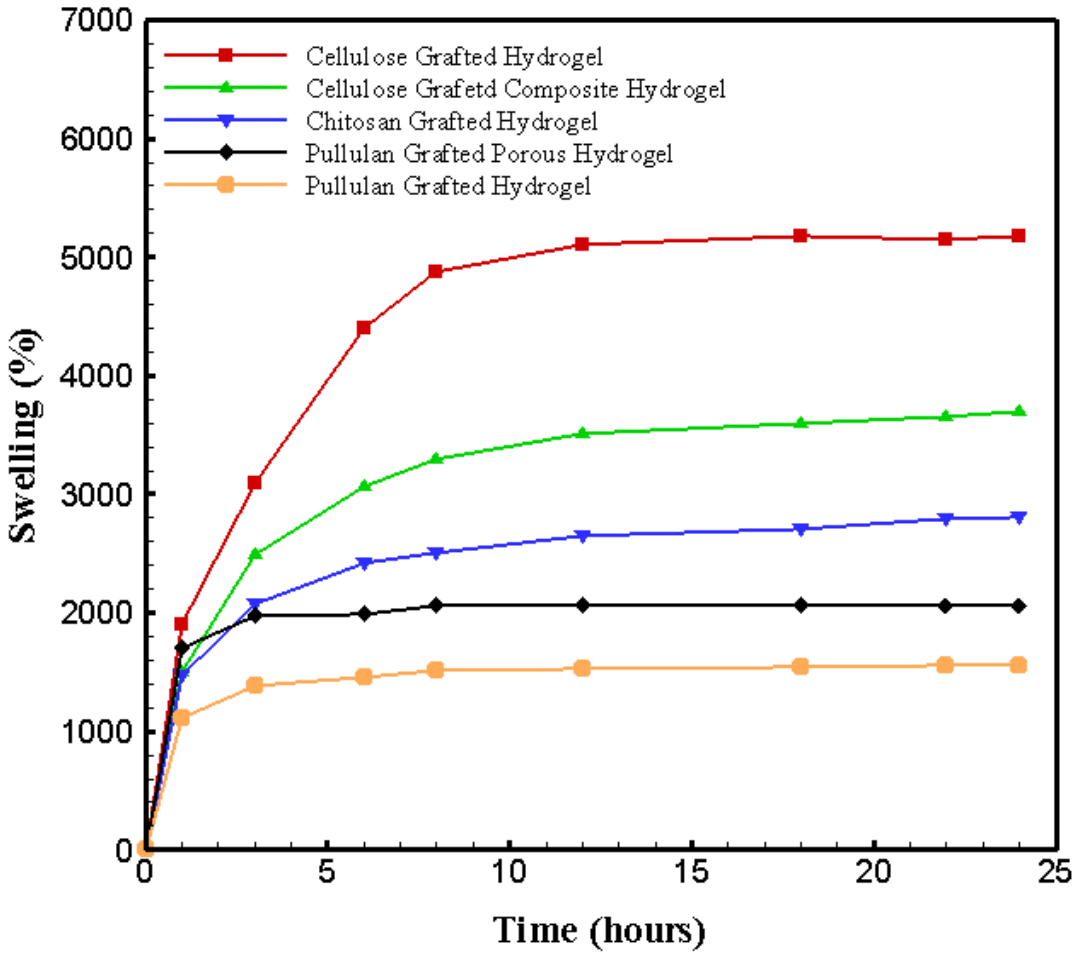

Figure 12. Effect of time on swelling behavior of cellulose, chitosan, and pullulan grafted hydrogels and porous and composite hydrogels

4.3.2 Swelling Kinetics of Hydrogels

To evaluate the swelling mechanism of chitosan, cellulose and pullulan-*graft*-polyacrylamide hydrogels, Schott's pseudo first-order and second-order kinetic models were studied. According to kinetic equations, if the swelling process of the hydrogel follows first-order kinetics, the plot of $\ln(W_e-W_t/W_e)$ vs. t should give a straight line. As is clear from Figure 14, the swelling kinetic of this synthesized hydrogels did not fit the first-order kinetic model because of the various polymer–solvent interactions that are occurring due to the large number of different chemical groups on the polymer chains of the hydrogels. Therefore, the swelling process conforms to the second-order kinetic model (Figure 14). According to Table 2, the theoretical W_e derived from the slope of plot t/W_t vs. t, for all hydrogels is very close to the W_e obtained from the experiments, with better correlation coefficient (R^2) values. It can therefore be concluded that the swelling kinetics of the hydrogels are best fitted with the second-order model.

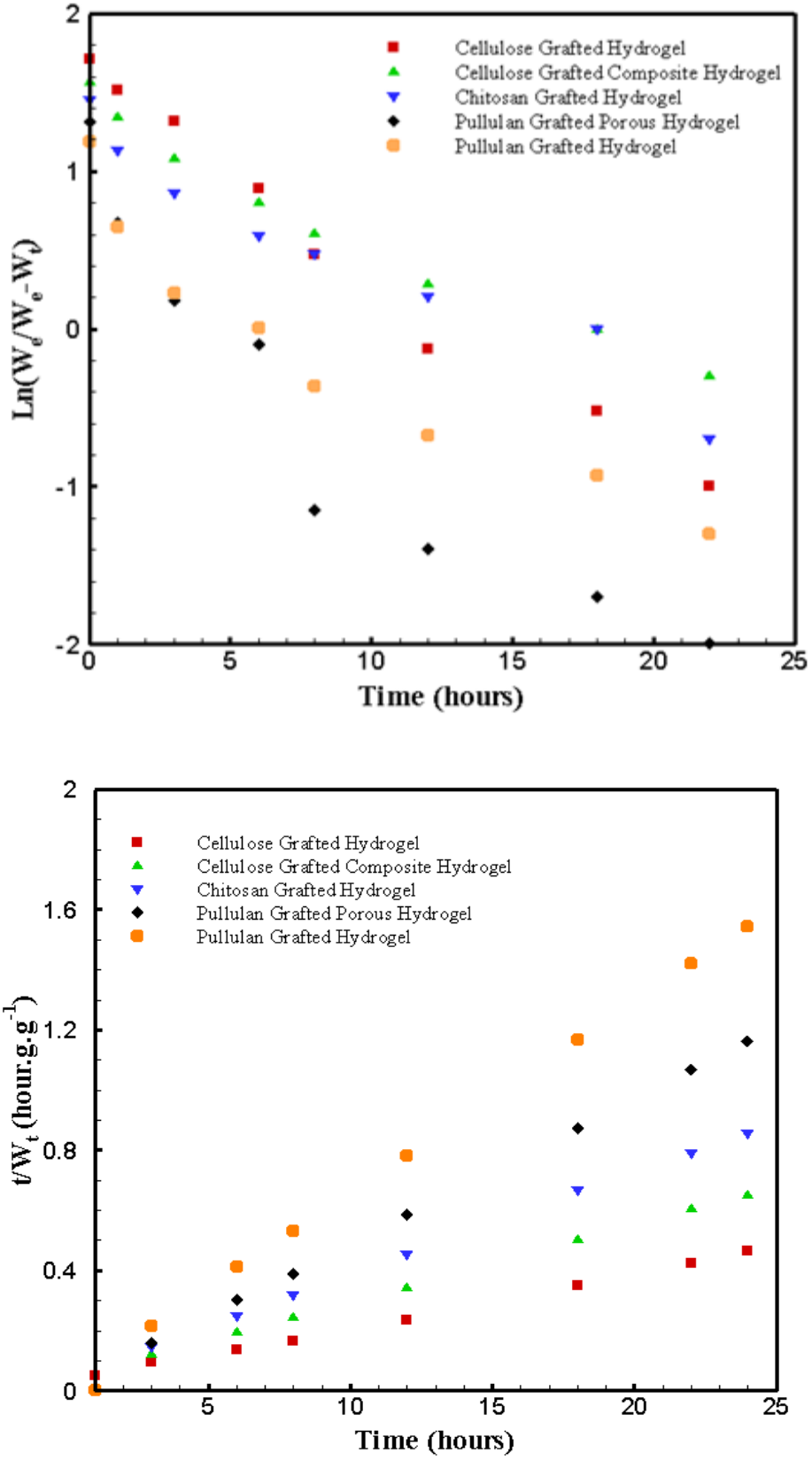

Figure 13. First-order (top) and second-order (bottom) plots of swelling kinetic of cellulose, chitosan, and pullulan grafted hydrogels and porous and composite hydrogels

Table 3. Swelling kinetic parameters of cellulose, chitosan, and pullulan grafted hydrogels and porous and composite hydrogels

Samples	First-Order-Kinetic				Second-Order-Kinetic		
	k_1 ($hour^{-1}$)	R^2	W_e (cal.) ($g.g^{-1}$)	W_e (exp.) ($g.g^{-1}$)	k_2 ($g.g^{-1}.hour^{-1}$)	R^2	W_e (cal.) ($g.g^{-1}$)
Cellulose Grafted Hydrogel	0.2851	0.9825	41.3	51.8	0.0145	0.9949	54.6
Cellulose Grafted Composite Hydrogel	0.1847	0.9679	23.7	37.1	0.0223	0.9971	38.46
Chitosan Grafted Hydrogel	0.1906	0.9454	16.6	28.0	0.0403	0.9982	28.73
Pullulan Grafted Porous Hydrogel	0.3245	0.8751	5.12	20.6	0.0771	0.9999	20.7
Pullulan Grafted Hydrogel	0.2277	0.9071	5.20	15.5	0.2060	0.9998	15.6

4.3.3 Effect of pH on Swelling Behavior of Hydrogels

The effects of pH values on the different hydrogels swelling behaviors were examined in 100 mL buffer solutions in the pH range of 2.0–11.0 at room temperature for 12 h. The results in Figure 15 indicate that the water absorbency of the synthesized hydrogels considerably increased with the increase in pH from 2.0 to 4.0, and decreased within pH ranges of 9.0–11.0. Two sharp swelling behaviors of the hydrogels were obtained at pH 4.0 and 9.0. The results can be attributed to the presence of the amide groups ($-CONH_2$) in the polymeric network. Under acidic conditions, the amide group can be protonated, and thus the charge density and the osmotic pressure inside the network increase due to the electrostatic repulsion of the NH_3^+ ions. Therefore, the osmotic pressure within the network neutralized with the uptake of water and the highest swelling ratio was observed around pH = 4.0. Under basic conditions, the amide groups undergo hydrolysis and convert into the carboxyl ($-COO^-$) groups. The swelling percentage will then be increased because of this anionic nature and mutual repulsion among carboxylate ions. However, under very acidic conditions (less than 4.0), the acrylamide converts to acrylic acid and the swelling is decreased. With a pH above 9.0, the network structure began to collapse and the swelling ratio decreased sharply.

In the above paragraph, the swelling behavior of hydrogels in the buffer solutions with different pHs were regarded to the presence of acrylamide in the synthesized hydrogels. It is worth to mention that the different natural polymers in the structure of hydrogels can affect the swelling behavior of hydrogels. This effect can be obvious by the difference in the swelling amount of hydrogels that explained extensively in the Section 4.3.1.

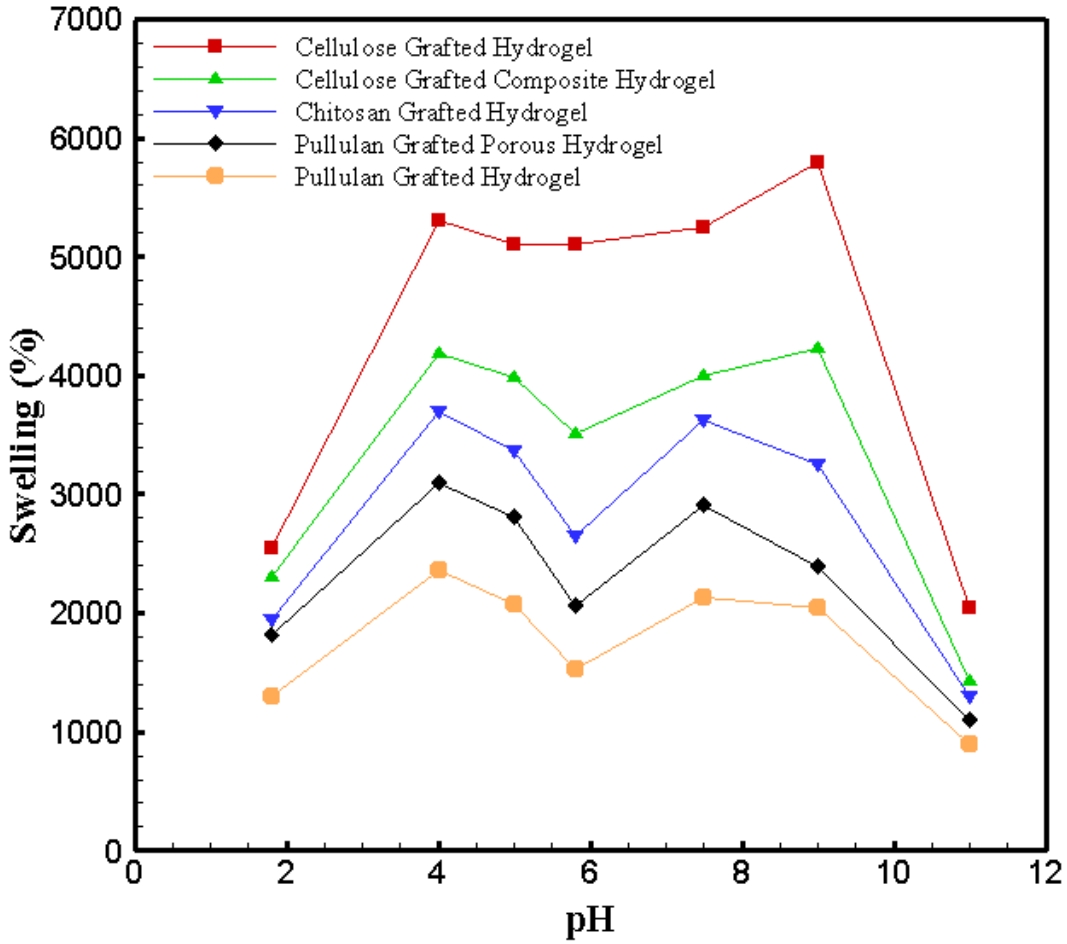

Figure 14. Effect of pH on swelling behavior of cellulose, chitosan, and pullulan grafted hydrogels and porous and composite hydrogels

4.3.4 Effect of Temperature on Swelling Behavior of Hydrogels

To study the influence of temperature on the water uptake capacity of hydrogels, the swelling studies were performed over 12 h at temperatures ranging from 20 to 60 °C. As shown in Figure 16, swelling percentage gradually increases with increases in temperature up to 45 °C. The maximum swelling percentage (6123 %) at 45 °C like effect of time on swelling was achieved by the cellulose-graft-polyacrylamide hydrogel. Further increase of temperature leads to a decrease in water uptake capacity of hydrogels. This well-known phenomenon can be attributed to the greater activation of backbone radicals, with increased temperature opening up the network structure, thereby increasing water accessibility [49]. However, increasing

temperature beyond the optimum level causes the matrix to collapse and leads to desorption of water.

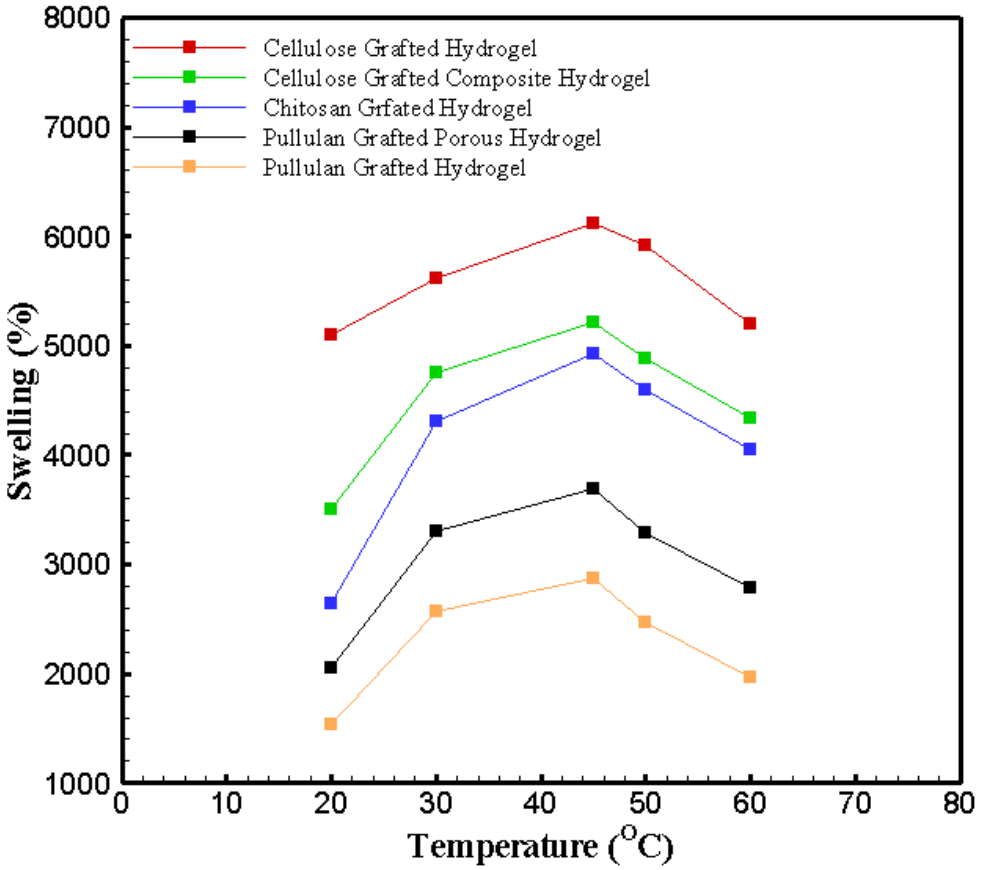

Figure 15. Effect of temperature on swelling behavior of cellulose, chitosan, and pullulan grafted hydrogels and porous and composite hydrogels

4.3.5 Deswelling Behavior of Hydrogels

The water retention ability of hydrogels is one of its most important features regarding its practical applications. Figure 17 illustrates this ability of swollen hydrogels at 80 °C, and shows that the rate percentage of retained water in the hydrogel decrease as time passes. As Pourjavadi and Hosseinzadeh reported, water inside of the swollen hydrogel can be classified into free water, bound water and half-bound water [101]. It is obvious that free water has the higher mobility compared to the other and therefore can be removed easily. However, the bound water and half-bound water may have some hydrogen bonds with the hydrophilic

groups in the structure of the hydrogels (such as -OH, -NH_2, -$CONH_2$, -COOH in this study). As can be seen from the Figure 17, the cellulose grafted hydrogel and composite hydrogel with the largest amount of swelling lost around 75 % of their free and partly half-bound adsorbed water after 12 h. In addition, the swollen pullulan grafted porous hydrogel has the highest and most quick retention (%) during the three hours, and then its rate decreased. Furthermore, it can be concluded from the Figure 17 that the pullulan and chitosan grafted hydrogels can be applied in dry and desert regions due to their ablility to save 30-35 % of adsorbed water, even after 24 hours.

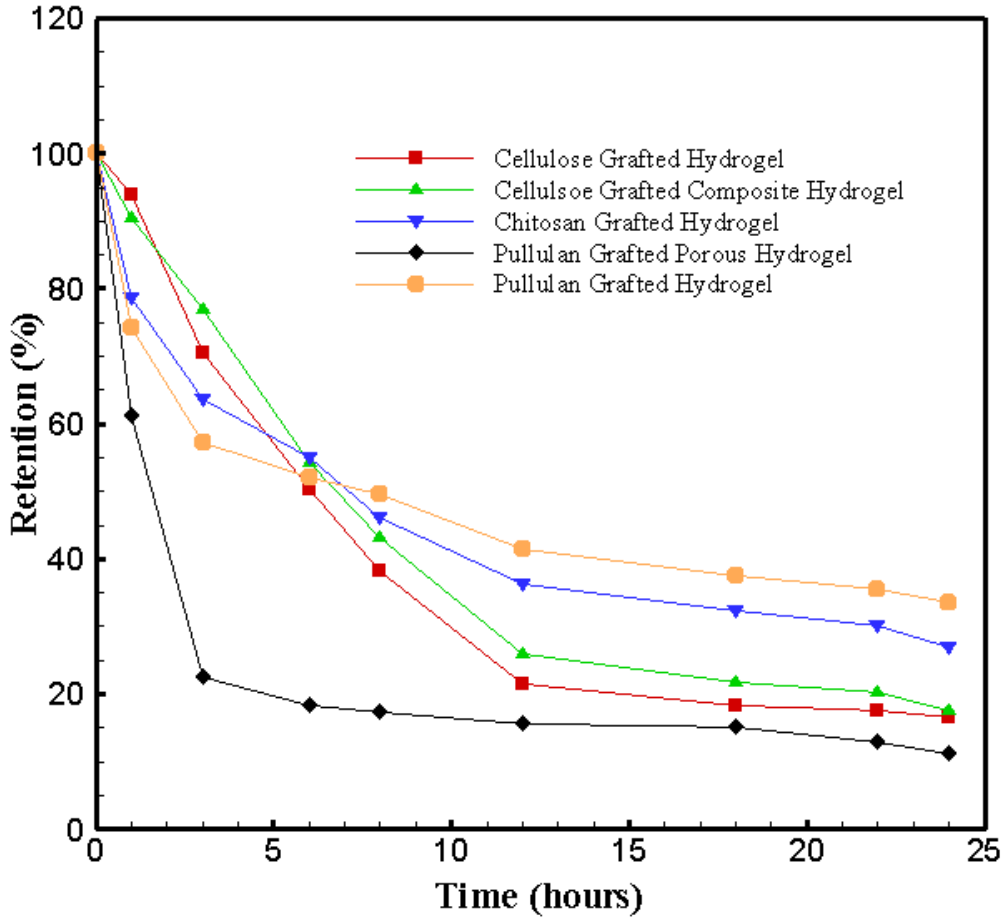

Figure 16. Effect of time on deswelling behavior of cellulose, chitosan, and pullulan grafted hydrogels and porous and composite hydrogels

4.4 Removal of Mercury(II) Ions by Hydrogels

4.4.1 Effect of Time on Adsorption

The Hg(II) adsorption performance of the synthesized hydrogels was evaluated by a batch equilibration technique as a function of time at room temperature. As shown in Figure 18, initially, the adsorption of mercury ions by the hydrogels was rapid, and then, the uptake speed gradually decreased until it remained steady as time progressed and finally adsorption equilibrium was achieved. This behavior can be attributed to the free charge groups in surface area of the hydrogels at the initial stage of the adsorption process. Subsequently, as the surface sites became saturated, adsorption did not increase significantly with further contact time. This increase in the rate of Hg(II) ions uptake at the first stage can be attributed to the presence of plenty active sites on the adsorbent, which were occupied by the adsorbate molecules. As time passes, the aggregation of Hg(II) ions around the saturated hydrogels may hinder the migration and consequently diffusion of adsorbate molecules inside the adsorbents [102].

The maximum adsorption by cellulose-graft-polyacrylamide hydrogel (1.93 $g.g^{-1}$), cellulose-graft-polyacrylamide composite hydrogel (1.99 $g.g^{-1}$), chitosan-graft-polyacrylamide hydrogel (1.87 $g.g^{-1}$), pullulan-graft-polyacrylamide hydrogel (1.75 $g.g^{-1}$), and pullulan-graft-polyacrylamide porous hydrogel (1.78 $g.g^{-1}$) were attained after 24 h. Although, a similar behavior was expected for cellulose, chitosan and pullulan grafted hydrogels consistent with their swelling behaviors, the rate and efficiency of adsorption by the porous and composite hydrogels are considerable. The maximum adsorption of Hg(II) which were attained using a cellulose grafted composite hydrogel, is attributed to the presence of hydroxyapatite with ionic species

such as calcium, hydroxyl and phosphate in the structure of composite. The mechanism most often cited for heavy metal capture by hydroxyapatite is the ion-exchange process, in which the metal attaches to the hydroxyapatite surface or diffuses inside and provokes calcium release by pushing out the more soluble endogenous calcium ions [103]. In addition, the presence of anionic species (i.e., hydroxyl and phosphate ions) and their ionic dipole interaction with mercury can increase the adsorption efficiency of composite compare to the grafted hydrogel.

Although, the adsorption (%) of pullulan-graft-polyacrylamide hydrogel in porous and bulk shape did not show the big difference but the rate of adsorption in the porous hydrogel is much more than the bulky gel. The pullulan grafted porous hydrogel can reach to the equilibrium of adsorption just in 3 hours after interaction with mercury solution. This porous hydrogel adsorption behavior can be due to the presence of several pores in its structure, which gives the vast surface area. Therefore, this structural property of porous hydrogel can assist the mercury solution to contact with the surface of hydrogel easily and adsorbed by porous hydrogel in an early and short contact time. In conclusion, the synthesized composite hydrogel containing hydroxyapatite with greater uptake capacity is a promising and versatile adsorbent for mercury ions.

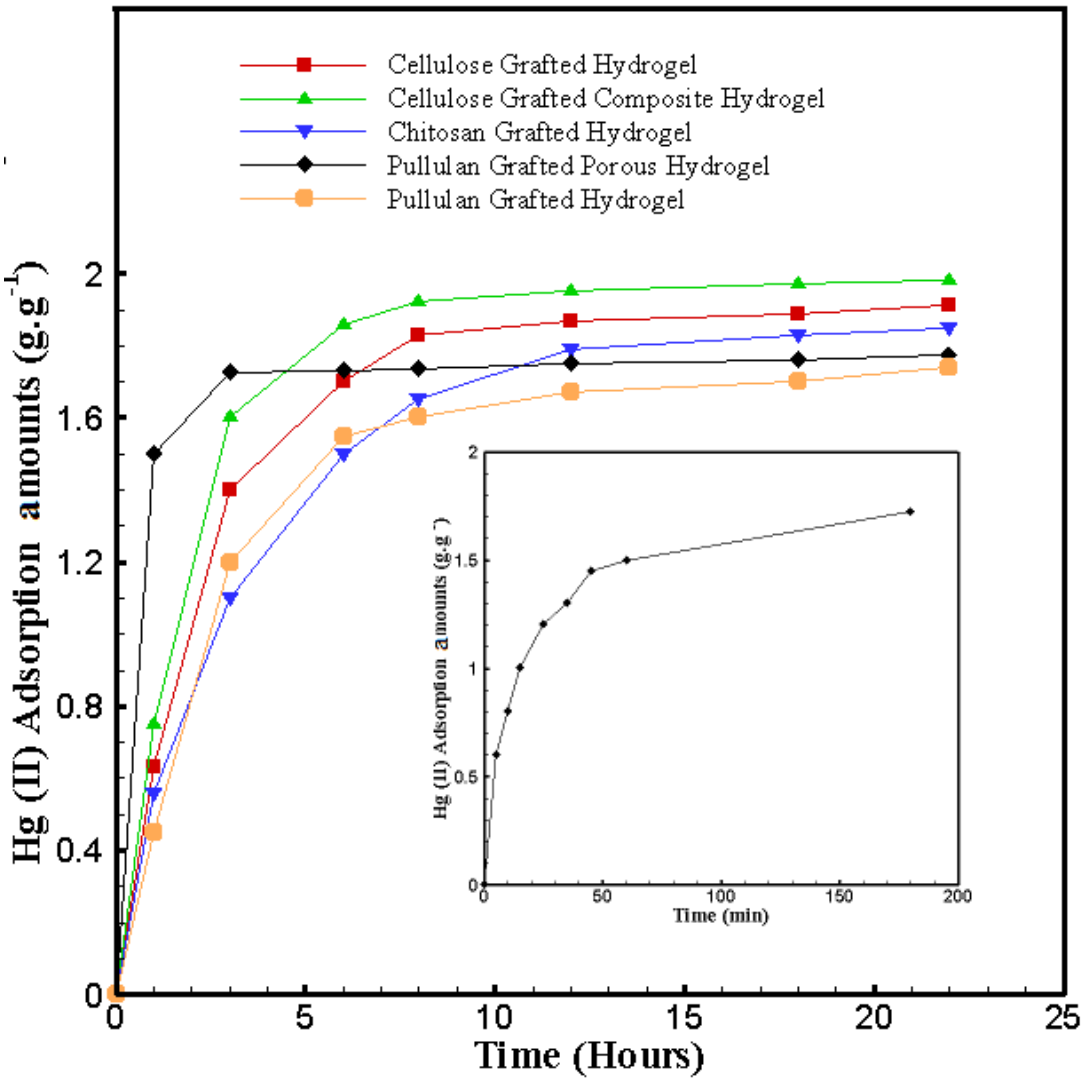

Figure 17. Effect of time on Hg(II) adsorption behavior by cellulose, chitosan, and pullulan grafted hydrogels and porous and composite hydrogels, inset shows the high rate adsorption of porous hydrogel

4.4.2 Kinetics of Adsorption

In order to investigate the possibility of using an adsorbent for a particular separation task and to determine the adsorption efficiency as well as the adsorption rate, the kinetics of the adsorption process was considered. The adsorption kinetics of the Hg(II) ions with the synthesized hydrogels was investigated using three kinetic models: pseudo-first-order, pseudo-second-order, and intra-particle diffusion. The output of these models are shown in Figure 19-20 and listed in Table 4.

As shown in Figure 19 and 20, the plot of (t/q_t) versus t in the pseudo-second-order model presented a linear relationship with better R^2 value in comparison with plot of pseudo-first-order. Moreover, the theoretical equilibrium adsorption capacity for all hydrogels, which can be determined from the slope of the plot are very close to the experimental data (Table 4). It can be concluded that the adsorption of mercury ions by synthesized hydrogels is best fitted by pseudo-second-order model.

Sorption kinetics can be controlled by different steps including solute transfer to the sorbent particle surface, transfer from the sorbent particle surface to the intraparticle active sites, retention on these sites via sorption and intraparticle precipitation phenomena [104, 105]. The adsorbate species are typically transferred from the solution to the solid phase via an intraparticle diffusion mechanism, which corresponds to the rate-limiting step in many adsorption processes occurring on an adsorbent, especially in a rapidly stirred batch reactor [55].

According to Equation 14, if the intra-particle diffusion is the main rate-controlling step, the plot of q_t versus $t^{0.5}$ should be linear and pass through the origin. However, the plot shown in Figure 20 did not pass through the origin and presented multilinearity, indicating the presence of two steps in the adsorption process. The first linear segments can be attributed to the Hg(II) ions transfer from the solution onto the external surface or boundary layer of the hydrogels (the boundary layer diffusion effects). The second less sloping linear portion indicates the gradual adsorption stage leading to the equilibrium (intra-particle diffusion) [106]. This indicates that the overall kinetics of the adsorption process is probably controlled by the surface adsorption and intra-particle diffusion [107]. As seen from the data in

Table 3, the intra-particle diffusion constants of the two linear segments are not similar and the first step comprises the bigger $K_3(1)$ value and the higher correlation coefficient for all samples. This observation indicates that the adsorption of mercury ions onto the synthesized hydrogels in this thesis at the first section occurs more rapidly due to the availability of adsorption centers; this, is then followed by the slow diffusion, which takes up to twelve hours.

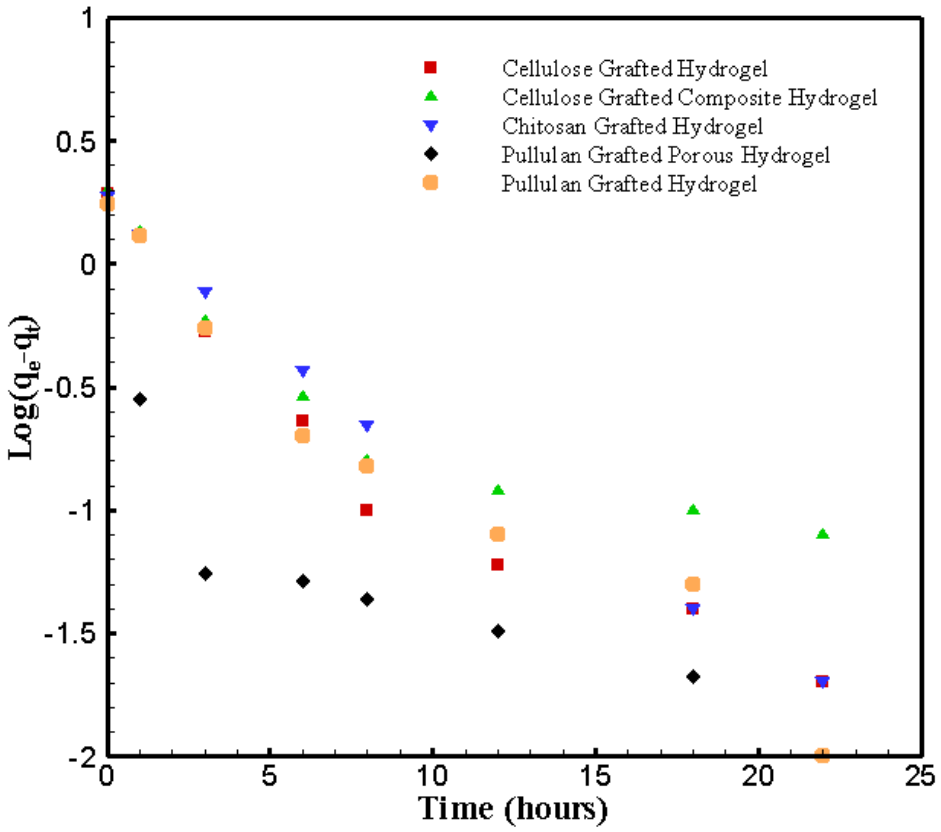

Figure 18. Pseudo-first-order plot for adsorption of Hg(II) ions by cellulose, chitosan, and pullulan grafted hydrogels and porous and composite hydrogels

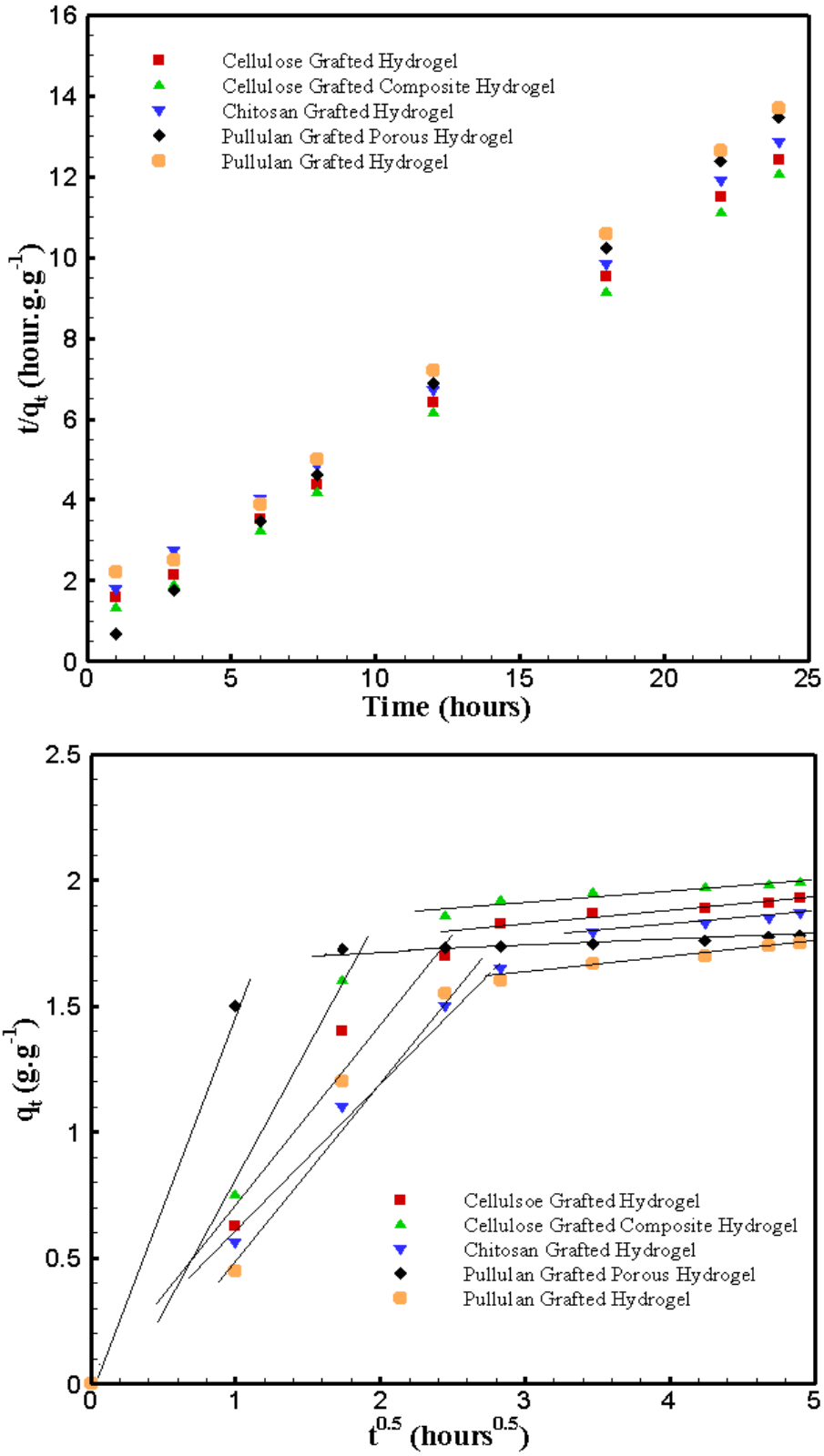

Figure 19. Pseudo-second-order (top) and intraparticle diffusion (bottom) plots for adsorption of Hg(II) ions by cellulose, chitosan, and pullulan grafted hydrogels and porous and composite hydrogels

Table 4. Hg(II) ions adsorption kinetic parameters by cellulose, chitosan, and pullulan grafted hydrogels and porous and composite hydrogel

Samples	Pseudo-first order			Pseudo-second order				Intraparticle diffusion					
	K_1 ($hour^{-1}$)	R^2	q_e (cal.) ($g.g^{-1}$)	q_e (exp.) ($g.g^{-1}$)	K_2 ($g.g^{-1}.hour^{-1}$)	R^2	q_e (cal.) ($g.g^{-1}$)	$K_3(1)$ ($g.g^{-1}.hours^{-0.5}$)	C_1 ($g.g^{-1}$)	R^2	$K_3(2)$ ($g.g^{-1}.hours^{-0.5}$)	C_2 ($g.g^{-1}$)	R^2
Cellulose Grafted Hydrogel	0.1982	0.9110	1.0575	1.93	0.3203	0.9980	2.0597	0.7261	0.008	0.9800	0.0438	1.709	0.9703
Cellulose Grafted Composite Hydrogel	0.1384	0.8201	1.0178	1.99	0.4502	0.9984	2.0894	0.7980	0.018	0.9734	0.0317	1.834	0.9702
Chitosan Grafted Hydrogel	0.2047	0.9790	1.4187	1.87	0.2041	0.9988	2.0678	0.6000	0.008	0.9955	0.0534	1.603	0.9884
Pullulan Grafted Porous Hydrogel	0.2042	0.7671	2.9046	1.78	0.2734	0.9999	1.7895	1.5000	0	1.0000	0.0181	1.687	0.9605
Pullulan Grafted Hydrogel	0.2104	0.9470	1.1795	1.75	0.2539	0.9956	1.9135	0.0833	0.058	0.9733	0.0689	1.414	0.9709

4.4.3 Effect of Adsorbent Amounts on Adsorption

In order to find the influence of synthesized hydrogel amount on the Hg(II) uptake capacity, the adsorption of 100 mL mercury solutions (1 $g.L^{-1}$) was examined by five different hydrogel doses ranging from 0.005 to 0.2 g for 24 h in atmospheric conditions. As shown in Figure 21, with an increase in the amount of hydrogels, their mercury adsorption capacity increases. This could be a result of an increase in the number of available sites due to the increase in the mass of the adsorbent. Any further increase in mass will not alter the adsorption efficiency. At this stage, almost all the mercury (II) ions may uptaked, thus any further increase in adsorbent dosage, which is denominator of fraction of equation 10 will lead to an appreciable decrease in adsorption amounts.

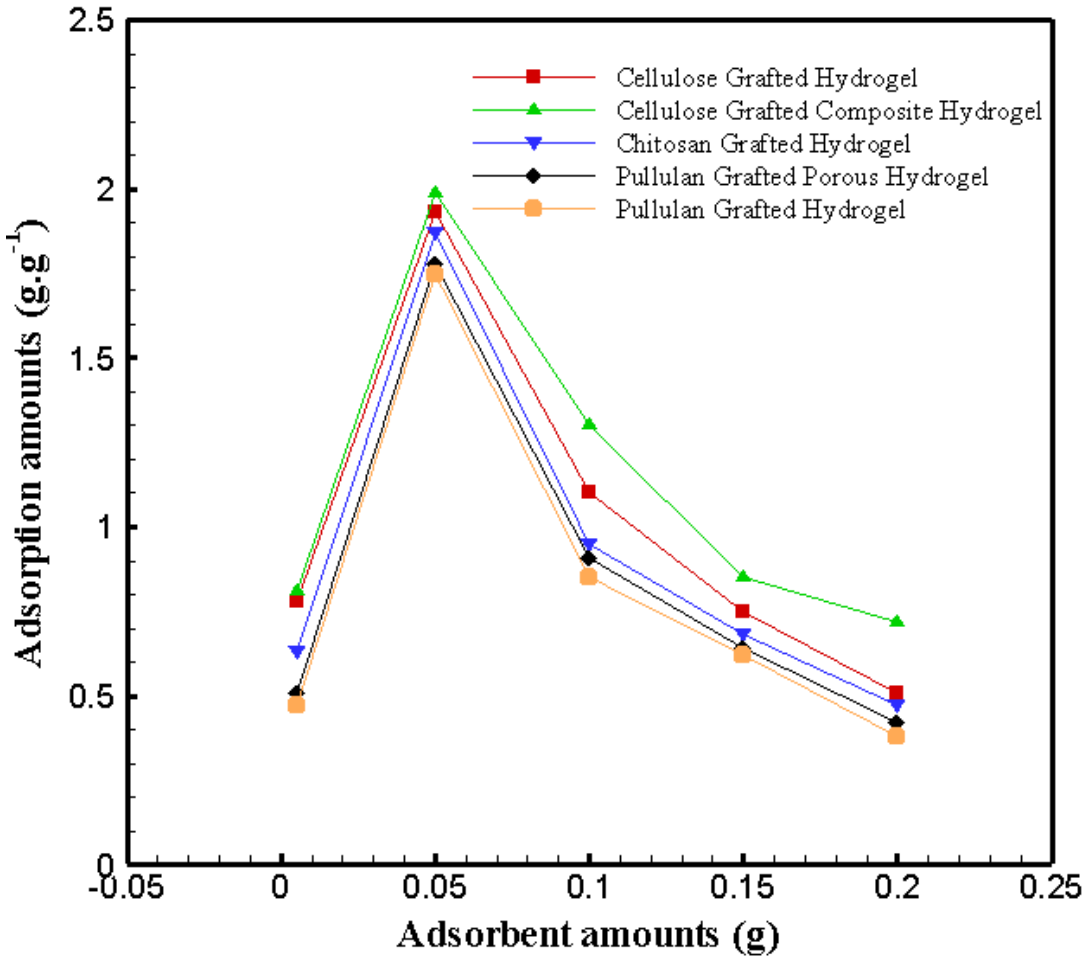

Figure 20. Effect of adsorbent amounts on Hg(II) adsorption behavior by cellulose, chitosan, and pullulan grafted hydrogels and porous and composite hydrogels

4.4.4 Effect of Initial Adsorbate Concentrations

Figure 22 shows the maximum capacities of synthesized hydrogels in adsorption of Hg(II), using adsorbent–adsorbate solutions with different initial concentrations (1-4 $g.L^{-1}$). It is clear that the mercury ions adsorption capacity of hydrogels increases with increasing initial concentration of solution. The maximum adsorption by 0.05 g cellulose-graft-polyacrylamide/hydroxyapatite composite hydrogel from 100 ml of mercury solution (4 $g.L^{-1}$) was observed as 6.9 $g.g^{-1}$ at ~20 °C in pH=5.8. This was most likely due to a greater availability of Hg(II) ions in the vicinity of the adsorbent and a high driving force for mass transfer prior to reaching the adsorption–desorption equilibrium. According to Equation 9, the adsorption capacity is proportional to the initial mercury concentration. It is worth mentioning that, increasing the concentration of Hg(II) solution does not have a significant effect on the maximum adsorption efficiency of the hydrogels. Therefore, it can be concluded that the hydrogels are concentration-sensitive and with an increase in solution concentration, adsorption will increase.

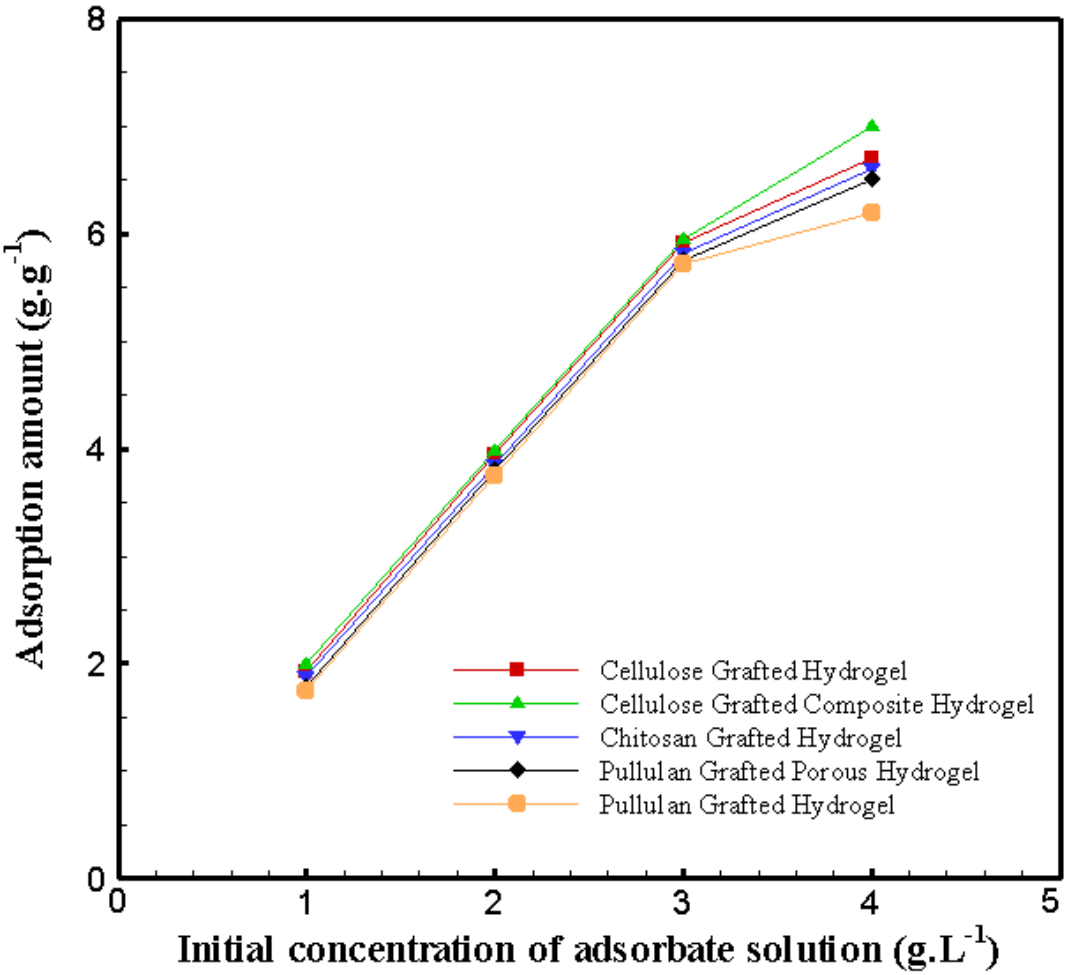

Figure 21. Effect of initial concentration of adsorbate solution on Hg(II) adsorption behavior by cellulose, chitosan, and pullulan grafted hydrogels and porous and composite hydrogels

4.4.5 Isotherm of Adsorption

The adsorption isotherms generally illustrate the interaction of adsorbate with the adsorbent and they can give an idea of the adsorption capacity of the adsorbent. In this study, two isotherm models, those of Langmuir and Freundlich were investigated to find which one is more suitable model for the design process.

As shown in Figure 23 and 24, the linear plot of C_e/q_e versus C_e demonstrates the validity of applying Langmuir isotherm models comparing to the plot of $\log q_e$ versus $\log C_e$, which represents the Freundlich isotherm model. In addition, the results of the

experimental data fitted to the Equations of these adsorption isotherms and their parameters are shown in Figure 23 and 24 and Table 5. According to the values of correlation coefficients (R^2) in Table 5 and the calculated values of q_{max} belong to the Langmuir model compared to the experimental data, the Langmuir model is more suitable for describing the adsorption. As it is clear from the data in Table, based on the Langmuir model, the q_{max} of Hg(II) ions by composite hydrogel is the highest and the pullulan based hydrogel has the lowest maximum adsorption which are parallel with the experimental data. Also, the favorability of the adsorption was evaluated from equilibrium parameters (R_L), which is a dimensionless constant and calculated using Equation 16 [102]. For favorable adsorption process, the value of R_L should lie in the range of 0-1. As shown in Table 5, for all kinds of synthesized adsorbents, the values of R_L are less than 1, indicating favorable homogeneous and monolayer adsorption of Hg(II) ions. It is worth mentioning that the lower amount of R_L for composite hydrogel show that their interaction with Hg(II) ions might be relatively stronger compared to the other hydrogels.

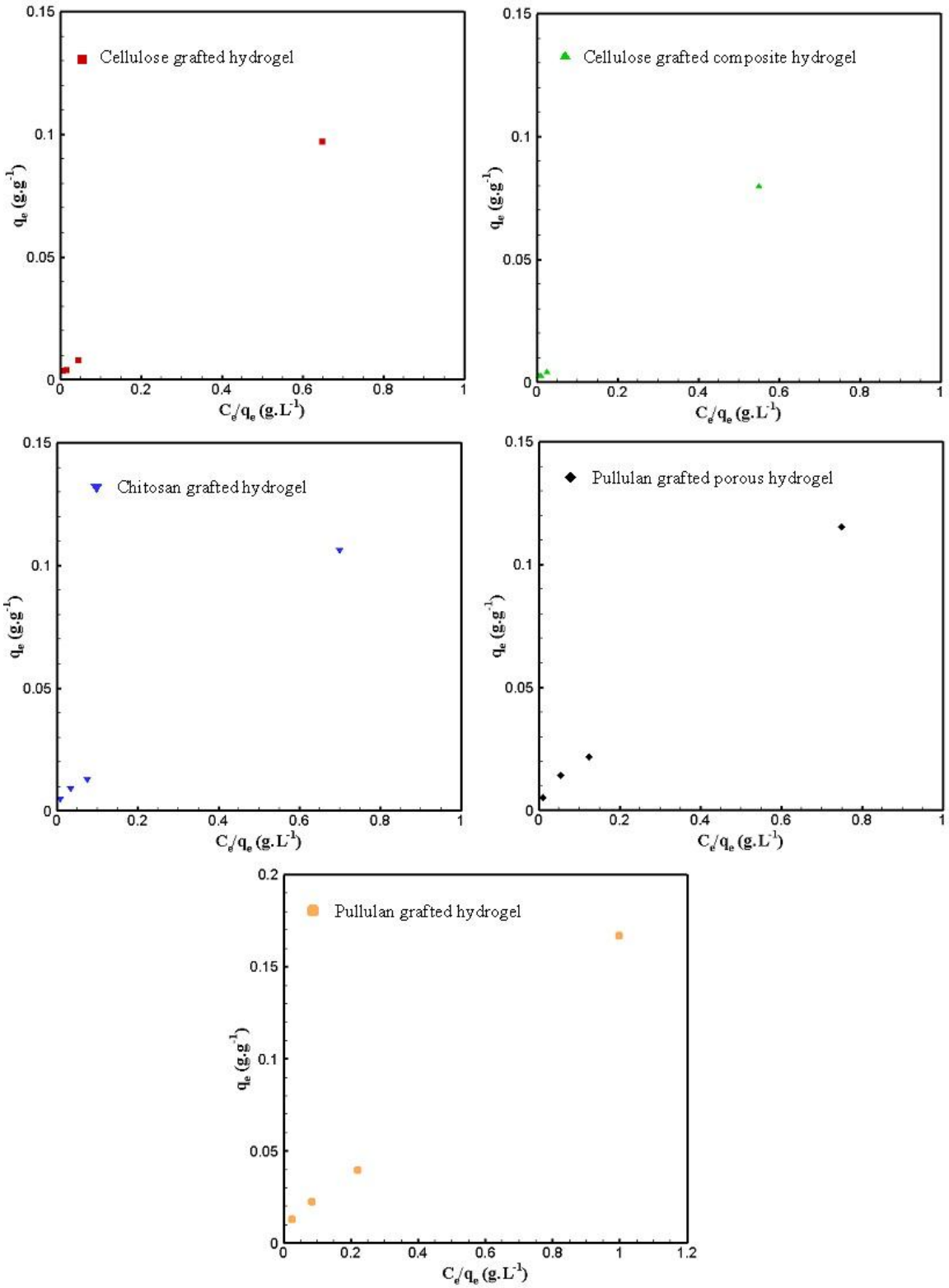

Figure 22. Langmuir isotherm plot for adsorption of Hg(II) ions by cellulose, chitosan, and pullulan grafted hydrogels and porous and composite hydrogels

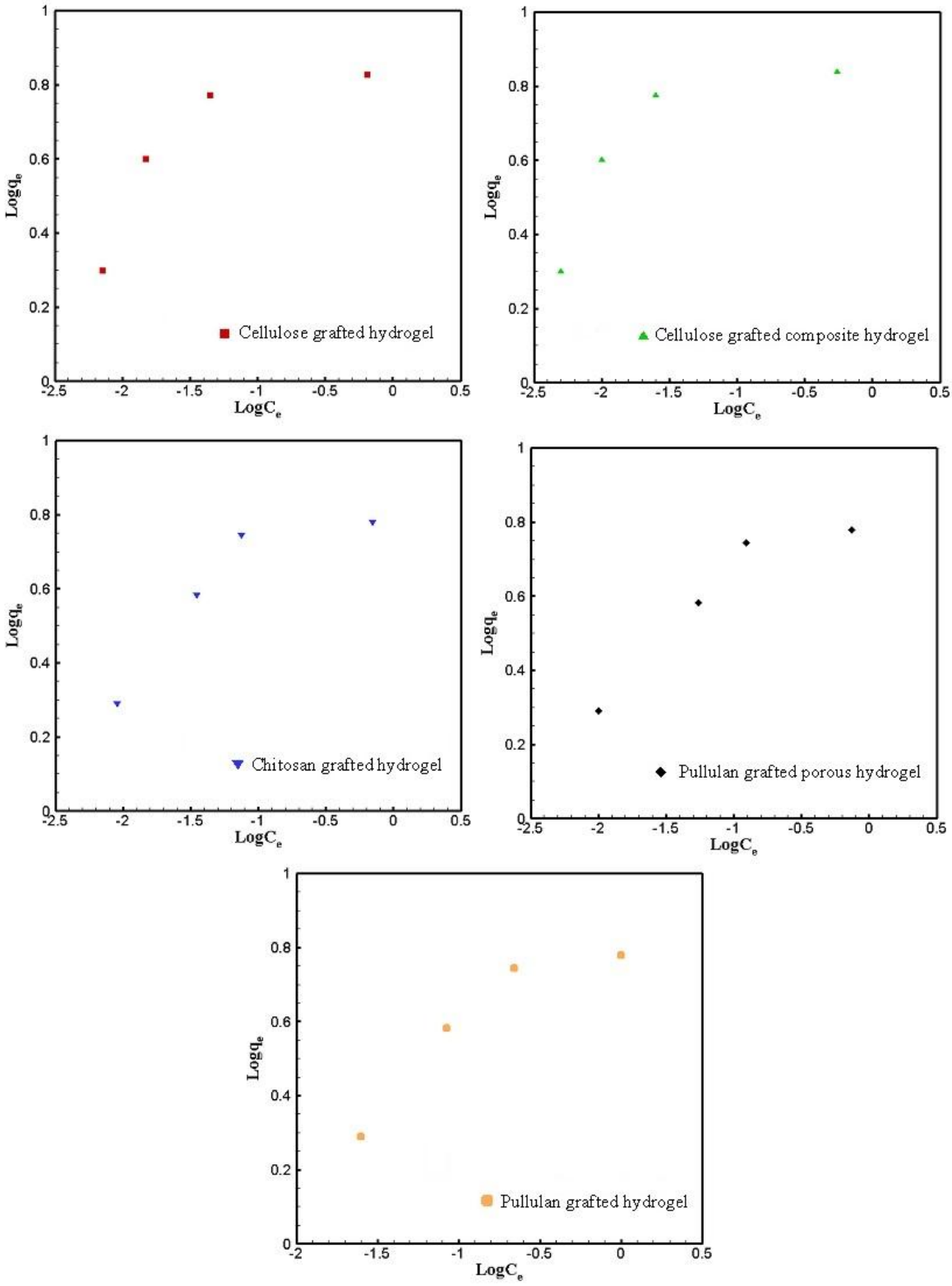

Figure 23. Freundlich isotherm plot for adsorption of Hg(II) ions by cellulose, chitosan, and pullulan grafted hydrogels and porous and composite hydrogels

Table 5. Hg(II) ions adsorption isotherm parameters by cellulose, chitosan, and pullulan grafted hydrogels and porous and composite hydrogels

Samples	Langmuir					Freundlich		
	q_{max} (Exp.) ($g.g^{-1}$)	K_L ($L.g^{-1}$)	R^2	q_{max} (Cal.) ($g.g^{-1}$)	R_L range	K_F ($L.g^{-1}$)	R^2	n ($g.g^{-1}$)
Cellulose Grafted Hydrogel	6.71	86.17	0.9998	6.82	0.002-0.01	8.6996	0.6862	4.3554
Cellulose Grafted Composite Hydrogel	6.95	118.9	0.9998	7.00	0.002-0.008	9.1180	0.6452	4.6425
Chitosan Grafted Hydrogel	6.67	50.75	0.9997	6.79	0.004-0.02	8.6536	0.7974	3.7622
Pullulan Grafted Porous Hydrogel	6.52	34.44	0.9994	6.75	0.007-0.03	8.2413	0.8878	3.5587
Pullulan Grafted Hydrogel	6.01	20.86	0.9993	6.30	0.01-0.04	7.1055	0.8463	3.2981

4.4.6 Effect of pH on Adsorption

The effect of initial pH on Hg (II) removal efficiency by 0.05 g hydrogels was examined in 100 ml buffer solutions in the pH range of 2-10 at room temperature for 24 h. Maximum adsorption (1.99 $g.g^{-1}$) of Hg(II) ions was achieved in pH=6.9 by using cellulose-graft-polyacryalmide/hydroxyapatite composite hydrogel. Although, in highly acidic and basic conditions the mercury ions adsorption by all of the synthesized hydrogels was negligible (Figure 25). The minimum mercury adsorption (> 0.1 $g.g^{-1}$) was obtained at pH=10 with pullulan-graft-polyacrylamide hydrogel. This was attributed to the fact that three main species $HgCl_2$, Hg(OH)Cl and HgO are present in the solution depending on the pH range. Under acidic conditions, $HgCl_2$ exists and the protons compete with mercury ions to occupy active sites. Therefore, $HgCl_2$ will reduce uptake of the mercury ions and, can be useful for regeneration of bonded mercury from hydrogels, as illustrated in the next section. Furthermore, an increase in pH (4-6) the species Hg(OH)Cl was produced, which increases mercury uptake. With further increases in pH to basic conditions, the red mercury oxide will precipitate with the most thermodynamically stable species achieved at high pH. Observation from similar researches shows that a clear precipitation of red mercury oxide was obtained at higher concentrations of mercury, above 1000 $mg.L^{-1}$ [90].

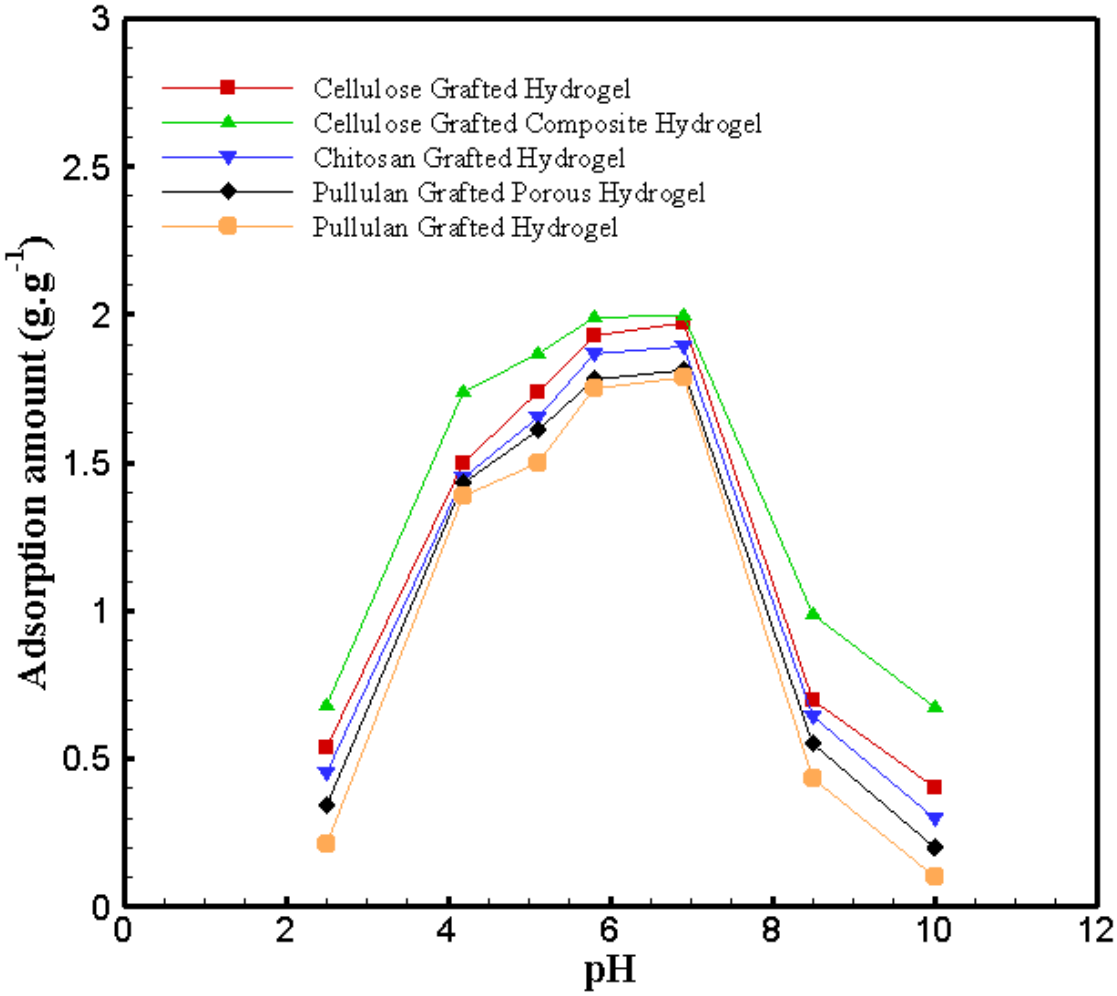

Figure 24. Effect of pH on Hg(II) adsorption behavior by cellulose, chitosan, and pullulan grafted hydrogels and porous and composite hydrogels

4.4.7 Effect of Temperature on Adsorption

To study the effect of temperature on mercury (II) adsorption, the adsorption from 1 $g.L^{-1}$ Hg(II) solutions was examined at four different temperatures 20 °C, 30 °C, 45 °C and 60 ºC for 24 h in the atmospheric conditions. It was found that the adsorption capacity increased by increasing the temperature. As can be seen from Figure 26, the pullulan grafted hydrogels are more temperature sensitive hydrogel compared to the others. The cellulose grafted composite hydrogel is the least sensitive due to the high adsorption capacity even at room temperature. This increase in mercury ion adsorption capacity of the synthesized hydrogels comes from the positive influence of temperature in increasing the mobility of adsorbate molecules and providing the necessary activation energy to open up the network structure and make it more accessible to adsorbate [55].

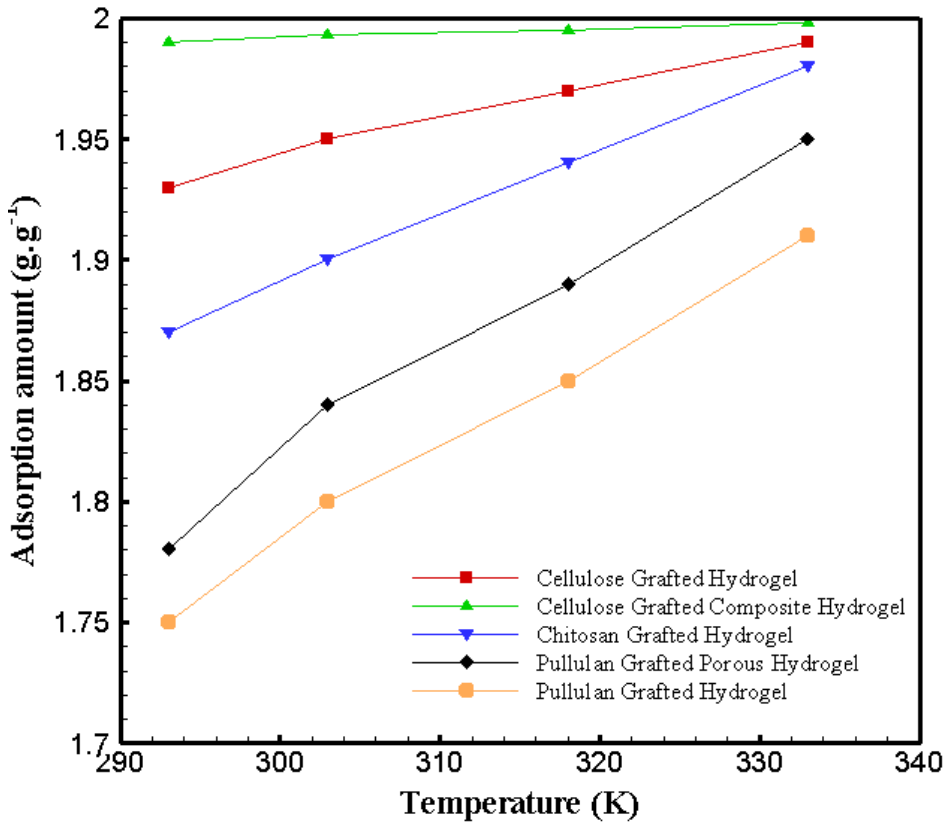

Figure 25. Effect of temperature on Hg(II) adsorption behavior by cellulose, chitosan, and pullulan grafted hydrogels and porous and composite hydrogels

4.4.8 Thermodynamics of Adsorption

In order to investigate whether the adsorption of mercury ions by synthesized hydrogels is an exothermic or endothermic process, the thermodynamic parameters including standard enthalpy change (ΔHº), the Gibbs free energy change (ΔGº) and standard entropy change (ΔSº) have been determined. Table 5 presents the thermodynamic parameters of Hg(II) adsorption by the synthesized hydrogels in different contact temperatures. It is clear to see that the values of free energy (ΔGº) at all of the tested temperatures were negative. This confirms that the adsorptions are spontaneous and thermodynamically favorable. The positive value of ΔHº confirms the endothermic nature of sorption, which is supported by the increase in the adsorption capacity of the hydrogels [108]. Besides, the positive value of ΔSº shows the freedom of adsorbate ions during adsorption and the high degree of randomness at the solid-liquid interface during the adsorption of Hg(II) ions onto hydrogels.

Table 6. Hg(II) adsorption thermodynamic parameters by cellulose, chitosan, and pullulan grafted hydrogels and porous and composite hydrogels

Temperature (K)	Cellulose Grafted Hydrogel	Cellulose Grafted Composite Hydrogel	Chitosan Grafted Hydrogel	Pullulan Grafted Porous Hydrogel	Pullulan Grafted Hydrogel
			ΔG° (kJ.mol^{-1})		
293	-46.65	-43.83	- 44.28	-35.71	-26.53
303	-48.25	-45.33	- 45.80	-36.93	-27.43
318	-50.64	-47.57	-48.07	-38.76	-28.79
333	-53.03	-49.82	-50.34	-40.59	-30.15
ΔH° (kJ.mol^{-1})	39.93	31.15	38.21	30.80	21.91
ΔS° (J.mol^{-1}.K^{-1})	159.37	149.71	151.29	121.99	90.63

4.4.9 Desorption of Mercury (II) Ions

Desorption studies are significant to elucidate the nature of the adsorption process, to regenerate the adsorbent and to recover the adsorbate ions. Regeneration of synthesized hydrogels, which act as a mercury (II) ions adsorbents in this thesis was carried out in low pH by using hydrochloric acid because the adsorbents contained amino groups. The Hg(II) adsorbed hydrogels (0.05 g) were regenerated with 50 mL hydrochloric acid solution (0.1 mol.L^{-1}) at room temperature, and then used again for adsorption of mercury ions from an aqueous solution. As can be seen in Table 7, adsorption/desorption cycles can be repeated several times, the data shows three cycles. The regeneration results indicate that the percentage of desorption for all synthesized hydrogels was high for the three cycles with a very small decrease in the adsorption and desorption capacities over the course of several cycles. The desorption behavior of adsorbed hydrogels is consistent with their adsorption and swelling behaviors. The pullulan hydrogels with the lowest swelling capacity has the lowest adsorption-desorption efficiency. While, the desorption of adsorbed Hg(II) ions from the porous hydrogels was rapid, the presence of hydroxyapatite in the structure of composite hydrogel lead to the slower desorption of loaded mercury ions. This result was expected due to the presence of hydroxyapatite and its role as the physical crosslinker. Finally, it can be concluded that the synthesized hydrogels qualified for practical application since they can be used repeatedly with negligible loss of adsorption capacity for the representative heavy metal.

Table 7. Hg(II) desorption by cellulose, chitosan, and pullulan grafted hydrogels and porous and composite hydrogels for three adsorption-desorption cycles

Samples	Cycles								
	1			2			3		
	Adsorption ($g.g^{-1}$)	Desorption ($g.g^{-1}$)	Regeneration (%)	Adsorption ($g.g^{-1}$)	Desorption ($g.g^{-1}$)	Regeneration (%)	Adsorption ($g.g^{-1}$)	Desorption ($g.g^{-1}$)	Regeneration (%)
Cellulose Grafted Hydrogel	1.93	1.37	71.1	1.91	1.31	68.6	1.90	1.20	63.5
Cellulose Grafted Composite Hydrogel	1.99	1.30	65.4	1.97	1.27	64.9	1.94	1.20	62.2
Chitosan Grafted Hydrogel	1.87	1.20	64.4	1.83	1.14	62.4	1.80	1.07	59.4
Pullulan Grafted Porous Hydrogel	1.78	1.19	67.2	1.73	1.06	61.2	1.71	1.12	56.8
Pullulan Grafted Hydrogel	1.75	0.91	52.5	1.72	0.82	48.1	1.70	0.80	47.1

Chapter 5

CONCLUSIONS

In this thesis five different hydrogels, cellulose-graft-polyacrylamide, chitosan-graft-polyacrylamide and pullulan-graft-polyacrylamide, cellulose-graft-polyacrylamide/hydroxyapatite composite hydrogel and pullulan-graft-polyacrylamide porous hydrogel were synthesized.

The main method for the synthesis of all hydrogels was free radicalic polymerization by using potassium persulfate as initiator. The monomer, acrylamide, accompanied with N,N-methylene-bis-acrylamide as a crosslinker was added to the natural polymer (i.e. cellulose, chitosan and pullulan) solutions. By comparing the FTIR spectra of natural polymers before grafting in pure state with synthesized grafted hydrogels and also the surface morphology of them before and after grafting, the preparation of grafted hydrogels was confirmed.

For the synthesis of porous hydrogel, acrylamide was grafted onto pullulan in the presence of calcium carbonate as a porogen. Then, by immersing the synthesized hydrogel in a hydrochloric acid solution and removing bubble gases of carbon dioxide, several pores with ~190 μm in size appeared in the structure of the porous hydrogel with 87 % porosity. The pullulan-graft-polyacrylamide hydrogel shows the highest gelation amount (%) due to the high water solubility of pullulan in

comparison with chitosan and cellulose accompanied by high water solubility of acrylamide and N,N-methylene-bis-acrylamide during the synthesis.

Before preparation of the composite hydrogel, nano-hydroxyapatite with 66 % yield was synthesized through micro-emulsion method by using disodium hydrogen phosphate and calcium chloride solutions. The average size of nano powder was determined as 122 nm using dynamic light scattering analysis. Then, the synthesized hydroxyapatite powder was embedded in the cellulose-graft-polyacrylamide hydrogel during the synthesis of hydrogel. The nano-hydroxyapatite acts as a physical crosslinker in the structure of composite hydrogel.

The minimum and maximum swelling percentages in equilibrium (1554 and 5170 %) belonged to pullulan-graft-polyacrylamide and cellulose-graft-polyacrylamide hydrogel, respectively. The high rate of water uptake capacity of pullulan-graft-polyacrylamide porous hydrogels compared to the bulky pullulan grafted hydrogel at the beginning of the contact with water was due to the presence of several pores in the structure of the hydrogel. The low water absorption capacity of cellulose-graft-polyacrylamide/hydroxyapatite composite hydrogel compared to the cellulose grafted hydrogel can be attributed to the presence of hydroxyapatite and its role as a physical crosslinker which leads to the decrease in elasticity of polymer chains. The swelling of all synthesized hydrogels best fitted with the second-order kinetic model. In addition, the synthesized hydrogels immersed in different buffer solutions showed different swelling behavior. They have maximum swelling amount (%) in the solution with pH=4.0 and 9.0 due to the presence of various ionic species in their structure. By increasing the temperature of medium, the swelling (%) of synthesized

hydrogels increased and the maximum swelling was observed at 45 °C. Further increase of temperature leads to a decrease in water uptake capacity of hydrogels. Finally, the water retention ability of swollen hydrogels was investigated and the results showed that the pullulan and chitosan grafted hydrogels can be applied in dry and desert regions due to their ability to save 30-35 % of adsorbed water, even after 24 hours.

The main aim of this thesis was the synthesis of different hydrogels for applying in water treatment area and compare their ability in adsorption of mercury (Hg(II)) ion from aqueous solutions. The effect of several variables such as time, adsorbate and adsorbent amounts, temperature and pH was on adsorption capacity of hydrogels was examined.

As time passed, the adsorption of mercury ions by the hydrogels was rapid, and then, the uptake speed gradually decreased until it remained unchanged as time progressed and finally adsorption equilibrium was achieved. The maximum adsorption from 100 mL mercury ions solution (1 $g.L^{-1}$) by 0.05 g of cellulose-graft-polyacrylamide hydrogel (1.93 $g.g^{-1}$), cellulose-graft-polyacrylamide composite hydrogel (1.99 $g.g^{-1}$), chitosan-graft-polyacrylamide hydrogel (1.87 $g.g^{-1}$), pullulan-graft-polyacrylamide hydrogel (1.75 $g.g^{-1}$), and pullulan-graft-polyacrylamide porous hydrogel (1.78 $g.g^{-1}$) were attained after 24 h. The maximum adsorption of Hg(II) which were attained using a cellulose grafted composite hydrogel, is attributed to the presence of hydroxyapatite with ionic species such as calcium, hydroxyl and phosphate in the structure of composite. The pullulan grafted porous hydrogel can reach to the equilibrium of adsorption just in 3 hours after interaction with mercury solution. This

porous hydrogel adsorption behavior can be due to the presence of several pores in its structure, which gives the vast surface area. According to the results of two kinetic models, pseudo-first-order and pseudo-second-order, investigation, the adsorption of Hg(II) ions by all hydrogels, pseudo-second-order kinetic model is more suitable for describing the adsorption. In addition, the plot of intra-particle diffusion kinetic model for all hydrogels did not pass through the origin and presented multilinearity, indicating the presence of two steps in the adsorption process.

In the other step of adsorption behavior investigation, the impact of the amount of hydrogels from 0.005 g to 0.2 g was examined. The mercury adsorption capacity of hydrogels increased due to the increase in their amounts. This could be a result of an increase in the number of available sites due to the increase in the mass of the adsorbent. In addition, the adsorption of mercury ions by synthesized hydrogels is pH sensitive. They can uptake Hg(II) ions from the solution with pH range between 4-7. Under very acidic conditions, $HgCl_2$ exists and the protons compete with mercury ions to occupy active sites. With further increases in pH (more than 8) to basic conditions, the red mercury oxide will precipitate.

Then, the effect of initial concentration of mercury solution on adsorption capacity of hydrogels was tested. The results showed that the mercury ions adsorption capacity of hydrogels increases with increasing initial concentration of solution due to a greater availability of Hg(II) ions in the vicinity of the adsorbent. The maximum adsorption by 0.05 g cellulose-graft-polyacrylamide/nano-hydroxyapatite composite hydrogel from 100 ml of mercury solution (4 $g.L^{-1}$) was observed 6.9 $g.g^{-1}$ at ~20 °C

in pH=5.8. Then, the Hg(II) adsorption isotherms of synthesized hydrogels by Langmuir and Freundlich models were examined to understand the interaction of adsorbate with the adsorbent and to give an idea about the adsorption capacity of the adsorbent. According to the values of correlation coefficients (R^2) and the calculated values of q_{max} belong to the Langmuir model compared to the experimental data and Freundlich model, it can be concluded that the Langmuir model is the best-fitted model. Based on the data of Langmuir model, the q_{max} of Hg(II) ions by composite hydrogel is the highest and the pullulan based hydrogel has the lowest maximum adsorption which are parallel with the experimental data. In addition, for all kinds of synthesized adsorbents, the values of R_L are less than one, indicating favorable homogeneous and monolayer adsorption of Hg(II) ions. The lower amount of R_L for cellulose-graft-polyacrylamide/hydroxyapatite composite hydrogel show that their interaction with Hg(II) ions might be relatively stronger compared to the other hydrogels.

The last variable which was effective for adsorption of Hg(II) ions by synthesized hydrogels was temperature. The pullulan-grafted hydrogels were more temperature sensitive hydrogel compared to the others. The cellulose grafted composite hydrogel is the least sensitive due to the high adsorption capacity even at room temperature. According to the thermodynamic data of adsorption, the values of free energy (ΔG^o) at all of the tested temperatures were negative while ΔH^o and ΔS^o were positive. This confirms that the adsorptions are spontaneous, thermodynamically favorable and endothermic and adsorbate ions are free during adsorption.

Finally, after desorption studies through three adsorption/desorption cycles of hydrogels, the results indicate that the percentage of desorption for all synthesized hydrogels was high for the three cycles with a very small decrease in the adsorption and desorption capacities over the course of several cycles. The desorption behavior of adsorbed hydrogels is consistent with their adsorption and swelling behaviors. It can be concluded that the synthesized hydrogels qualified for practical application since they can be used repeatedly with negligible loss of adsorption capacity for the mercury ions.

REFERENCES

[1] Saber-Samandari, S., et al., *Efficient removal of anionic and cationic dyes from an aqueous solution using pullulan-graft-polyacrylamide porous hydrogel.* Water Air. Soil. Pollut., 2014. **225**: p. 2177.

[2] Mahdavinia, G.R. and R. Zhalebaghy, *Removal kinetic of cationic dye using poly (sodium acrylate)-carrageenan/Namontmorillonite nanocomposite superabsorbents.* J. Mater. Environ. Sci., 2012. **3**: p. 895.

[3] Mahajan, R. and M. Bali, *Analytical studies on metal speciation studies of river sutlej.* Int. J. Emerg. Technol. Adv. Engin., 2012. **2**: p. 551.

[4] Uludag, Y., H.M. Ozbelge, and L.J. Yilmaz, *Removal of mercury from aqueous solutions via polymer-enhanced ultrafiltration.* J. Membr. Sci., 1997. **129**: p. 93.

[5] Saber-Samandari, S. and M. Gazi, *Removal of mercury (ii) from aqueous solution using chitosan-graft-polyacrylamide semi-ipn hydrogels.* Separ. Sci. Technol., 2013. **48**: p. 1382.

[6] Miretzky, P. and A.F. Cirelli, *Hg (II) removal from water by chitosan and chitosan derivatives: A review.* J. Hazard. Mater., 2009. **167**: p. 10.

[7] Jüttner, K., U. Galla, and H. Schmieder, *Electrochemical approaches to environmental problems in the process industry*. Electrochimica Acta, 2000. **45**: p. 2575.

[8] Bose, P., M.A. Bose, and S. Kumar, *Critical evaluation of treatment strategies involving adsorption and chelation for wastewater containing copper, zinc, and cyanide.* Adv. Environ. Res., 2002. **7**: p. 179.

[9] Metcalf and Eddy, *Wastewater Engineering: Treatment and Reuse*. 2003: McGraw Hill International Edition, New York.

[10] Semerjian, L. and G.M. Ayoub, *High-pH-magnesium coagulation-flocculation in wastewater treatment.* Adv. Environ. Res., 2003. **7**: p. 389.

[11] Zabel, T., *Flotation in water treatment in The Scientific Basis of Flotation*. 1984: Martinus Nijhoff Publishers, The Hague.

[12] Ardejani, F.D., et al., *Adsorption of direct red 80 dye from aqueous solution onto almond shells: effect of pH, initial concentration and shell type.* J. Hazard. Mater., 2008. **151**: p. 730.

[13] Saber-Samandari, S., et al., *Efficient removal of lead (II) ions and methylene blue from aqueous solution using chitosan/Fe-hydroxyapatite nanocomposite beads.* J. Environ. Manag., 2014. **146**: p. 481.

[14] Shafaei, A., F.Z. Ashtiani, and T. Kaghazchi, *Equilibrium studies of the sorption of Hg (II) ions onto chitosan.* Chem. Eng. J., 2007. **133**: p. 311

[15] Guibal, E., E. Touraud, and J. Roussy, *Chitosan interactions with metal ions and dyes: Aissolved-state vs solid-state application.* World J. Microb. Biot., 2005. **21**: p. 913.

[16] Li, N., R.B. Bai, and C.K. Liu, Enhanced and selective adsorption of mercury ions on chitosan beads grafted with polyacrylamide via surface-initiated atom transfer radical polymerization. Langmuir, 2005. 21: p. 11780.

[17] Jeon, C. and K.H. Park, *Adsorption and desorption characteristics of mercury(II) ions using aminated chitosan bead.* Water Res., 2005. **39:** p. 3938.

[18] Kyzas, G.Z. and E.A. Deliyanni, *Mercury(II) removal with modified magnetic chitosan adsorbents.* Molecules, 2013. **18:** p. 6193.

[19] Rabelo, R.B., et al., *Adsorption of copper(II) and mercury(II) ions onto chemically-modified chitosan membranes: equilibrium and kinetic properties.* Adsorp. Sci..Technol., 2012. **30:** p. 1.

[20] Kushwaha, S. and P.P. Sudhakar, *Adsorption of mercury(II), methyl mercury(II) and phenyl mercury(II) on chitosan cross-linked with a barbital derivative.* Carbohydr. Polym., 2011. **86:** p. 1055.

[21] Vieira, R. and M. Beppu, *Dynamic and static adsorption of Hg (II) ions on chitosan membranes and spheres.* Water Res., 2006. **40**: p. 1726.

[22] Jeon, C. and W.H. Holl, *Chemical modification of chitosan and equilibrium study for mercury ion removal.* Water Res., 2003. **37**: p. 4770.

[23] Son, B.C., et al., *Selective biosorption of mixed heavy metal ions using polysaccharides.* Korean J. Chem. Eng., 2004. **21**: p. 1168.

[24] Shawky, H.A., A.H.M. El-Aassar, and D.E. Abo-Zeid, *Chitosan/carbon nanotube composite beads: Preparation, characterization, and cost evaluation for mercury removal from wastewater of some industrial cities in Egypt.* J. Appl. Polym. Sci., 2012. **125:** p. 93.

[25] Wang, X.H., et al., *Selective removal of mercury ions using a chitosan-poly(vinyl alcohol) hydrogel adsorbent with three-dimensional network structure.* Chem. Eng. J., 2013. **228:** p. 232.

[26] Wang, X. and A. Wang, *Adsorption characteristics of chitosan-g-poly(acrylic acid)/attapulgite hydrogel composite for Hg(II) ions from aqueous solution.* Separ. Sci. Technol., 2010. **45**: p. 2086.

[27] Zhou, L.M., S.R. Liu, and Q.W. Huang, *Adsorption of mercury and uranyl onto poly(ethyleneimine) grafted chitosan microspheres.* Mod. Chem. Ind., 2007. **27**: p. 175.

[28] Yang, Z., Y. Yuan, and Y. Wang, *Synthesis and evaluation of chitosan aryl azacrown ethers as adsorbents for metal ions.* J. Appl. Polym. Sci., 2000. **77**: p. 3093.

[29] Li, N., R. Bai, and C. Liu, *Enhanced and selective adsorption of mercury ions on chitosan beads grafted with polyacrylamide via surfaceinitiated atom transfer radical polymerization.* Langmuir, 2005. **21**: p. 11780.

[30] Zhou, L., et al., *Characteristics of equilibrium, kinetics studies for adsorption of Hg(II), Cu(II), and Ni(II) ions by thiourea-modified magnetic chitosan microspheres.* J. Hazard. Mater., 2009. **161**: p. 995.

[31] Bicak, N., D.C. Sherrington, and B.F. Senkal, *Graft copolymer of acrylamide onto cellulose as mercury selective sorbent.* React. Funct. Polym., 1999. **41**: p. 69

[32] Navarro, R.R., et al., *Mercury removal from wastewater using porous cellulose carrier modified with polyethyleneimine.* Wat. Res., 1996. **30**: p. 2488.

[33] Takagai, Y., et al., *Synthesis and evaluation of different thio-modified cellulose resins for the removal of mercury (II) ion from highly acidic aqueous solutions.* J. Colloid Interf. Sci., 2011. **353**: p. 593.

[34] Gonte, R.R., K. Balasubramanian, and J.D. Mumbrekar, *Porous and cross-linked cellulose beads for toxic metal ion removal: hg(ii) ions.* J. Polym., 2013. **2013:** 309136.

[35] Cekli, S., E. Yavuz, and B.F. Senka, *Preparation of sulfonamide containing cellulose based sorbent for removal of mercury ions.* Separ. Sci. Technol., 2012. **47**: p. 1350.

[36] Yavuz, E., B.S. Senkal, and N. Bicak, Poly (acrylamide) grafts on spherical polyvinyl pyridine Resin for removal of mercury from aqueous solutions. React. Funct. Polym., 2005. 65: p. 121.

[37] Sonmez, H.B., et al., *Atom transfer radical graft polymerization of acrylamide from N-chlorosulfonamidated polystyrene resin, and use of the resin in selective mercury removal.* React. Function. Polym., 2003. **55:** p:1.

[38] Sreedhar, M. K. and T. S. Anirudhan, *Preparation of an adsorbent by graft polymerization of acrylamide onto coconut husk for mercury(II) removal from aqueous solution and chloralkali industry wastewater.* J. Appl. Polym. Sci., 2000. **75:** p. 1261.

[39] Senkal, B. F., E.Yavuz and and N. Bicak, *Poly(acrylamide) grafts on spherical polymeric sulfonamide based resin for selective removal of mercury ions from aqueous solutions.* Macromol. Symp., 2004. **217:** p. 169.

[40] Sinha, V.R., et al., *Chitosan microspheres as a potential carrier for drugs.* Intern. J. Pharm., 2004. **274**: p. 1.

[41] Vinsova, J.V., *Recent advances in drugs and prodrugs design of chitosan* Curr. Pharm. Design, 2008. **14**: p. 1311.

[42] Mourya, V.K. and N. Nazma, *Chitosan-modifications and applications: opportunities galore.* React. Funct. Polym., 2008. **68**: p. 1013.

[43] Meifang, H.X., S. Yuan, and F. Yue'e, *Study of graft copolymerization of n-maleamic acid-chitosan and butyl acrylate by γ-ray irradiation.* International J. Biol. Macromol., 2005. **36**: p. 98.

[44] Jayakumar, R., R.L. Reis, and J.F. Mano, *Graft copolymerized chitosan-present status and applications.* Carbohydr. Polym., 2005. **62**: p. 142.

[45] Saber-Samandari, S., O. Yilmaz, and E. Yilmaz, *Photoinduced graft copolymerization onto chitosan under heterogeneous conditions.* J. Macromol. Sci., A, 2012. **49**: p. 591.

[46] Fras-Zemljic, L., V. Kokol, and D. Cakara, *Antimicrobial and antioxidant properties of chitosan-based viscose fibres enzymatically functionalized with flavonoids.* Text. Res. J., 2011. **81**: p. 1532.

[47] Tripathi, S., G.K. Mehrotra, and P.K. Dutta, *Preparation and physicochemical evaluation of chitosan/poly(vinyl alcohol)/pectin ternary film for food-packaging applications.* Carbohydr. Polym., 2010. **79**: p. 711.

[48] Pourjavadi, A., S. Barzegar, and G.R. Mahdavinia, *Modified chitosan, 7-graft copolymerization of methacrylonitrile onto chitosan using ammonium persulfate initiator.* E-Polymers, 2004: p. 053.

[49] Saber-Samandari, S., M. Gazi, and E. Yilmaz, *UV-induced synthesis of chitosan-g-polyacrylamide semi-IPN superabsorbent hydrogels.* Polym. Bull., 2012. **68**: p. 1623.

[50] Huang, X.Y., et al., *Cross-linked succinyl chitosan as an adsorbent for the removal of Methylene Blue from aqueous solution.* Int. J. Biol. Macromol., 2011. **49**: p. 643.

[51] Wu, F.C., R.L. Tseng, and R.S. Juang, *Comparative adsorption of metal and dye on flake and bead-types of chitosans prepared from fishery wastes.* J. Hazard. Mater., 2000. **B73**: p. 63.

[52] Onsoyen, E. and O. Skaugrud, *Metal recovery using chitosan.* J. Chem. Technol. Biotechnol., 1990. **49**: p. 395.

[53] Bhat, V., et al., *Miscibility and thermal behavior of pullulan/polyacrylamide blends.* J. Macromol. Sci. A., 2011. **48**: p. 920.

[54] Rekha, M.R. and C.P. Sharma, *Pullulan as a promising biomaterial for biomedical applications: a perspective.* Trends Biomater Art. Org., 2007. **20**: p. 116.

[55] Constantin, M., et al., *Removal of anionic dyes from aqueous solutions by an ion-exchanger based on pullulan microspheres.* Carbohydr. Polym., 2013. **91**: p. 74.

[56] Talasaz, E., *Synthesis and characterization of pullulan/poly(acrylamide) based semi-ipn hydrogels*. 2013, Eastern Mediterranean University.

[57] Yamada H, K.M., *Nitrile hydratase and its application to industrial production of acrylamide.* Biosci. Biotechnol. Biochem., 1996. **60**(9): p. 1391.

[58] Vandana, S., K. Premlata, and S. Ajit, *microwave accelerated synthesis and characterization of poly(acrylamide).* J. Appl. Polym. Sci., 2007. **104**: p. 3702.

[59] Saber-Samandari, S., *UV-radiation induced graft copolymerization onto chitosan*. 2010, Eastern Mediterranean University.

[60] Saber-Samandari, S., et al., *Synthesis, characterization and application of cellulose based nano-biocomposite hydrogels.* J. Macromol. Sci., .A., 2013. **50**: p. 1133.

[61] Bajpai, A.K. and H. Bundela, *γ-radiation assisted fabrication of hydroxyapatite-polyacrylamide nanocomposites with possible application in bone implantology*. J. Compos. Mater., 2010. **44**: p. 757.

[62] Lee, W.G., U. Demirci, and A. Khademhosseini, *Microscale electroporation: Challenges and perspectives for clinical applications.* Integr. Biol., 2009. **1**: p. 242.

[63] Batchelar, D.L., et al., *Bone-composition imaging using coherent-scatter computed tomography: Assessing bone health beyond bone mineral density.* Med. Phys., 2006. **33**: p. 904.

[64] Chen, F., et al., *Magnetic nanocomposite of hydroxyapatite ultrathin nanosheets/Fe3O4 nanoparticles: Microwave-assisted rapid synthesis and application in pH-responsive drug release.* Biomater. Sci., 2013. **1**: p. 1074.

[65] Roy, I., et al., *Calcium phosphate nanoparticles as novel non-viral vectors for targeted gene delivery.* Int. J. Pharm., 2003. **250**: p. 25.

[66] Legeros, R.Z., *Crystallographic studies of the carbonate substitution in the apatite structure*. 1967, New York University.

[67] Holmes, R.E., *Bone regeneration within a coralline hydroxyapatite implant.* Plast. Reconstr. Surg., 1979. **63**: p. 626.

[68] Kokubo, T., *Bioceramics and their clinical applications*. 2008: Woodhead publishing limited.

[69] Legeros, R.Z., *Calcium phosphates in oral biology and medicine*. Monogr. Oral Sci., 1991. **15:** Karger: Basel.

[70] Legeros, R.Z. and M.S. Tung, *Chemical stability of carbonate- and fluoride containing apatites.* Caries. Research, 1983. **17**: p. 419.

[71] Kokubo, T. and H. Takadama, *How useful is SBF in predicting in vivo bone bioactivity?* Biomaterials, 2006. **27**: p. 2907.

[72] Habibovic, P., et al., *Comparative in vivo study of six hydroxyapatite-based bone graft substitutes.* J. Orthop. Res., 2008. **26**: p. 1363.

[73] Prego, C., et al., *Transmucosal macromolecular drug delivery*. J., Control. Release, 2005. **101**: p. 151.

[74] Luo, D. and W. Saltzman, *Synthetic DNA delivery systems.* Nature Biotechnol., 2000. **18**: p. 33.

[75] Slosarczyk, A., J. Szymura-Oleksiak, and B. Mycek, *The kinetics of pentoxifylline release from drug-loaded hydroxyapatite implants.* Biomaterials 2000. **21**: p. 1215.

[76] Suzuki, T., T. Hatsushika, and Y. Hayakawa, S*ynthetic hydroxyapatites employed as inorganic cation-exchangers.* J. Chem. Soc. Faraday Trans., 1981. **77**: p. 1059.

[77] Daniels, Y. and S.D. Alexandratos, *Design and Synthesis of Hydroxyapatite with Organic Modifiers for Environmental Remediation.* Waste Biomass. Valor. 1, 2010: p. 157.

[78] Saber-Samandari, S., S. Saber-Samandari, and M. Gazi, *Cellulose-graft-polyacrylamide/hydroxyapatite composite hydrogel with possible application in removal of Cu (II) ions.* React. Funct. Polym., 2013. **73**: p. 1523.

[79] Rosskopfova, O., et al., *Study of sorption processes of copper on synthetic hydroxyapatite.* J. Radioanal. Nucl. Chem., 2012. **293**: p. 641.

[80] Feng, Y., et al., *Adsorption of Cd (II) and Zn (II) from aqueous solutions using magnetic hydroxyapatite.* Chem. Eng. J. , 2010. **162**: p. 487.

[81] Kramer, E.R., et al., *Synthesis and characterization of iron-substituted hydroxyapatite via a simple ion-exchange procedure.* J. Mater. Sci., 2013. **48**: p. 665.

[82] Available from: http://carlkarm.com/index_eng.php and http://chemtoworld.en.ec21.com/Liquid_Mercury--6980934_6980973.html.

[83] Shah, R. and S. Devi, *Preconcentration of mercury(II) on dithizone anchored poly(vinyl pyridine) support.* React. Func. Polym., 1996. **31**: p. 1.

[84] F., H., *Ion Exchange*. New York: McGraw-Hill

[85] Sonmez, H.B. and N. Bicak, *Quaternization of poly(4-vinyl pyridine) beads with 2-chloroacetamide for selective mercury extraction.* React. Func. Polym., 2002. **51**: p. 55.

[86] Sonmez, H.B., B.F. Senkal, and N. Bicak, *Poly(acrylamide) grafts on spherical bead polymers for extremely selective removal of mercuric ions from aqueous solutions.* J. Polym. Sci. A, 2002. **40**: p. 3068.

[87] Ley, H. and H. Kissel, *Berichte der deutschen chemischen Gesellschaft.* Chemische Berichte 1899. **32**: p. 1358.

[88] Wu, S. and R.A. Shanks, *Solubility study of polyacrylamide in polar solvents.* J. Appl. Poly. Sci., 2004. **93**: p. 1493.

[89] El-Moselhya, M.M., A.K. Sengupta, and R. Smith, *Carminic acid modified anion exchanger for the removal and preconcentration of Mo(VI) from wastewater*. J. Hazard. Mater., 2011. **185**: p. 442.

[90] Pourjavadi, A. and G.R. Mahdavinia, *Superabsorbency, pH-sensitivity and swelling kinetics of partially hydrolyzed chitosan-g-poly(acrylamide) hydrogels.* Turk. J. Chem., 2006. **30**: p. 595.

[91] Salleh, M.A.M., et al., *Cationic and anionic dye adsorption by agricultural solid wastes: a comprehensive review.* Desalination, 2011. **280**: p. 1.

[92] Bajpai, S.K., N. Chand, and M. Mahendra, *The adsorptive removal of cationic dye from aqueous solution using poly (methacrylic acid) hydrogels: part-I. equilibrium studies.* Inter. J. Environ. Sci., 2012. **2**: p. 1609.

[93] Mahmoodi, N.M., et al., *The effect of pH on the removal of anionic dyes from colored textile wastewater using a biosorbent.* J. Appl. Polym. Sci., 2011. **120**: p. 2996.

[94] Srivastava, V. and Y.C. Sharma, *Synthesis and characterization of Fe3O4@n-SiO2 nanoparticles from an agrowaste material and its application for the removal of Cr(VI) from aqueous solutions.* Water Air Soil Pollut., 2013. **225**: p. 1776.

[95] Hobzova, R., et al., *Methacrylate hydrogels reinforced with bacterial cellulose.* Polym. Int., 2011. **61**: p. 1193.

[96] Jiang, F.X., et al., *Regulating Size, Morphology and Dispersion of Nano-Crystallites of Hydroxyapatite by pH Value and Temperature in Microemulsion System.* Key Eng. Mat., 2008. **361-363**: p. 195.

[97] Liu, J.B., et al., *Osteopenic bone cell response to synthesized by hydrothermal method.* Ceram. Int. 2003. **29**: p. 629.

[98] Cheng, K.C., A. Demirci, and J.M. Catchmark, *Effects of plastic composite support and pH profiles on pullulan production in a biofilm reactor.* Appl Microbiol. Biotechnol., 2010. **86**: p. 853.

[99] Trovatti, E., et al., *Sustainable nanocomposite films based on bacterial cellulose and pullulan.* Cellulose 2012. **19**: p. 729.

[100] Wang, J.L., Y.A. Zheng, and A.Q. Wang, Adv. Mat. Res., 2010. **96**: p. 227.

[101] Pourjavadi, A. and H. Hosseinzadeh, *Synthesis and properties of partially hydrolyzed acrylonitrile-co-acrylamide superabsorbent hydrogel.* Bull. Korean Chem. Soc., 2010. **31**: p. 3163.

[102] Ramesh, S.T., et al., *Adsorptive removal of Pb (II) from aqueous solution using nano-sized hydroxyapatite.* Appl. Water Sci., 2013. **3**: p. 105.

[103] Nzihou, A. and P. Sharrock, *Role of phosphate in the remediation and reuse of heavy metal polluted wastes and sites.* Waste Biomass Valor. 1 2010: p. 163.

[104] Itodo, A.U., et al., *Intraparticle diffusion and intraparticulate diffusivities of herbicide on derived activated carbon.* Researcher, 2010. **2**: p. 74.

[105] Ratnamala, G.M., K.V. Shetty, and G. Srinikethan, *Removal of remazol brilliant blue dye from dyecontaminated water by adsorption using red mud: equilibrium, kinetic, and thermodynamic studies.* Water Air Soil Pollut., 2012. **223**: p. 6187.

[106] Ansari, R., et al., *Adsorption of cationic dyes from aqueous solutions using polyaniline conducting polymer as a novel adsorbent.* J. Adv. Sci. Res., 2011. **2**: p. 27.

[107] Wang, W., et al., *A simple hydrothermal approach to modify palygorskite for high-efficient adsorption of Methylene blue and Cu(II) ions.* Chem. Eng. J., 2015. **265:** p. 228.

[108] Chen, J.J., A.L. Ahmad, and B.S. Ooi, *Poly(Nisopropylacrylamide-co-acrylic acid) hydrogels for copper ion adsorption: equilibrium isotherms, kinetic and thermodynamic studies.* J. Environ. Chem. Engin., 2013. **1**: p. 339.